UNIVERSITY OF GENOVA

PHD PROGRAM IN BIOENGINEERING AND ROBOTICS

Organic FET-based transistor arrays for metabolic and electrophysiological measurements

by

Laura Martines

Thesis submitted for the degree of *Doctor of Philosophy* (33° cycle)

9^{th} June 2021

Supervisors — prof. Sergio Martinoia
prof. Annalisa Bonfiglio
prof. Andrea Spanu

Head of the PhD program — prof. Giorgio Cannata

Dibris

Department of Informatics, Bioengineering, Robotics and Systems Engineering

Acknowledgements

I put all my efforts and dedication into this work, but without the guidance of my tutors and the priceless help of the special people I worked with, I would never have reached this result.
I am very grateful firstly to my tutors prof. Martinoia, prof. Bonfiglio and prof. Spanu, for their support and because during these years I have learned so much. A special thanks to prof. Spanu, that has been always willing to discuss and guide me.
Thank you Giorgio and Filippo for the support and creativity in helping to solve all the technical issues. Thank you Brunella, for your time, for the beautiful cultures and for your precious advises.
Thank you to all the people I have worked with in this time. Thank you Martina for your genuine friendship, for cheering me up in the darkest moments and because of Spike (the best companion and company in these years). Thank you Stefania, for your kind and smiling presence. Thank you Stefano for all your suggestions and teachings, and because you always take care of the laboratory for all of us. Thank you Giulia because you have always a kind word. Thank you Mimo, for the interesting talks and for your suggestions; you are a good friend. Thank you Marietta, Pietro, Lorenzo, Donatella, Federica, Nello, Piero, Nicola and all the other people both of the University of Cagliari and Genova, because to work with you made these years lighter and enjoyable. I have wonderful memories with each of you, and I hope that is the same also for you.
Thank you to all my friends, the oldest and the newest, because I can be completely myself with you, and you are always with me anyway. I am so thankful to have all of you.
I want to thank my parents, my love Stefano, and Rossana because you all always supported me and trusted in me and in my capabilities even when I could do not it either. You have always so genuinely spurred me to do my best; I would not be who I am without you. I am not good in reveal and describe my feelings and emotions, but I really want you to know that these years signified very much to me, and they would not have been the same without each of you.

Table of contents

List of figures

Nomenclature

Acronyms / Abbreviations

AP Action Potential

APS Active Pixel Sensor

CMOS Complementary Metal-Oxide-Semiconductor

CP Conducting Polymer

CVD Chemical Vapour Deposition

EDL Electric Double Layer

EGOFET Electrolyte Gated Organic Field Effect Transistor

iPSC induced Pluripotent Stem Cell

ISFET Ion Sensitive Field Effect Transistor

ITO Indium Tin Oxide

LOD Limit of Detection

MEA Micro Electrodes Array

MOA Micro OCMFET Array

MOSFET Metal Oxide Semiconductor Field Effect Transistor

OCMFET Organic Charge Modulated Field Effect Transistor

OECT Organic ElectroChemical Transistor

OSC Organic Semiconductor

OSFET Oxide Semiconductor Field Effect Transistor

PEN Polyethylene naphthalate

SiN Silicon Nitride

SNR Signal to Noise Ratio

TFT Thin Film Transistor

TIA Transimpedance Amplifier

TiN Titanium Nitride

Introduction

Behind each scientific discovery there is the technological progress that allows to gain a better insight into the question under analysis. This is valid in particular when the topic relates to the understanding of our body and its functioning principle: the desire to understand how the human body works is innate in man since its origins, but the transition from theories and hypotheses to scientific evidences is possible only with the creation of a technology suitable for observing the phenomena of interest. In addition, when a new objective is reached, the next became immediately visible a little beyond and the technology must evolve in order to match the scientific requirements and help to reach always more complex goals. In the last decades, several groups of researchers have investigated the behaviour, both in healthy or pathological conditions, of various types of living cells (from epithelial to muscular or neuronal ones) for different purposes, ranging from toxicology to pharmacology to the understanding of their ways to communicate with each other. At the same time, different devices based on passive electrodes or on active elements (such as transistors, both inorganic or organic) have been developed to make these studies possible by recording the cells' detachment or their electrophysiological activity, for example. Now, more complex analyses should be performed to add details to the current knowledge; consequently, the effort is focused on finding new approaches to analyse more complicated systems such as three-dimensional networks of cells or organoids (i.e. conglomerates of cells that can be also be formed by different cell types), thus mimicking in a more physiological manner the real conditions in which living cells operate. A second approach to collect new information about living systems is to acquire different kinds of information, in order to connect a precise behaviour with the variation of different parameters; indeed, monitoring the highest number possible of parameters in a parallel and non-invasive manner can help to better interpret the cells response to different stimuli. In particular, very few examples of devices able to monitor more than one feature have been presented in the last decades, principally due to the difficulties linked to the integration of different kinds of sensors in the same substrate.

In this context this PhD thesis is inserted, since its main ambition has been to design a sensors array capable of measuring simultaneously two parameters of the *in vitro* cell cultures; in particular, this device has been designed for electrogenic cells and can measure the electrophysiological and the metabolic activity. To this purpose, the properties of a peculiar kind of organic field effect transistor, called *organic charge modulated field effect transistor* or OCMFET, have been exploited to create two different sensors whose structures are quite similar (and thus can be easily integrated in a single array), that can be operated simultaneously to monitor different aspects of the cells culture. Starting from the OCMFET-based sensors, the array called *Multi OMCFET array* or MOA has been fabricated at the University of Cagliari, while the tests with the cells have been performed at the University of Genova.

In the next chapters, firstly a brief state of the art regarding the kind of electrodes employed for these purposes in literature is showed; follows a brief history of the OCMFET, its working principle along with its previous applications. After that, we will enter in the heart of this work by describing the modifications on the MOA's structures investigated during these years and the obtained experimental results. The fabrication of the MOA, along with more details regarding the electronics readout used to perform the experiments and the mathematical description of the equivalent electrical model of the sensor, developed as support for the data analysis, have been illustrated in the appendixes.

Part I

Section One

Chapter 1

1. Standard techniques for *in vitro* cellular interfacing

The endless advancement of knowledge in the field of electrophysiology causes and in turn is caused by the continuous progress of the technologies that become available to scientists to carry out their experiments. As we will see in this chapter, the first experiments in the field of electrophysiology were focused on understanding how electricity is generated inside the cells and how it propagates along the nerves, questions related to the study of the single cell and the changes in electrical potential across its membrane. To this end, the so called intracellular techniques, like the patch clamp, had been developed. Besides that, when scientists started to study also the dynamics of a network of excitable cells, were developed new techniques based on the recording of extracellular field potentials, i.e. the variations of potential induced outside the cell membrane by the ions exchange between the cell and the extracellular environment. These techniques are non-invasive and allow to long-term recording with respect to the intracellular methods; in addition, more electrodes can be placed in a smaller area to guarantee simultaneous measurements at different points of the cellular network. On the other hand, they can record signals with a smaller amplitude and are less sensitive to sub-threshold signals. This chapter, after a brief digest of the main events that left a mark on the history of electrophysiology, will present the very first technique for electrophysiological recordings, i.e. the patch clamp. Subsequently, the more established devices for extracellular recordings in the scientific community, and also available on the market will be introduced. These are based both on passive (i.e. the micro-electrodes array or MEA) and active (Field Effect Transistor-based device such as ISFET and CMOS-MEA) technologies.

1.1 Introduction to electrophysiology

The attempt to understand how human body works and how to heal it from diseases has grabbed the attention of many philosophers and scientists of all eras, and since several centuries before Christ, there were many hypothesis regarding body motion and functioning. Indeed, it is well known that in the 5th century BC Empedocles and Democritus theorized the presence of different kinds of particles that form the four elements (earth, water, fire and air), adding that the lightest and fastest moving of these particles compose also psyche and soul. The concept of nerve excitation and conduction came out between 2nd and 3rd centuries AC, when Galen harked back to the Aristotelian concept of "vital pneuma" to introduce a "psychic pneuma" that moves through the nerves thus producing actions and sensations. Although also Descartes - that in his *Treatise on Man* speculated that the finest particles of a so called *animal spirit* reaches the brain and can flow into the nerves triggering visible motion - and Sir Isaac Newton - that was probably the first to suggest the electrical nature of nerve signals - made their contribution to the rise of electrophysiology, its birth conventionally coincides with the activity of Luigi Galvani. In 1780, with the help probably of his wife Lucia Galeazzi, Galvani started his experiments involving the frog neuromuscular preparation to find out whether electricity could be the cause of muscle movement. He exploited different energy sources (i.e. a lancet connected to a Leyden jar, or the atmospheric electricity both in stormy and in sunny days) to trigger muscle's contraction to conclude that animals' muscles intrinsically accumulate electricity and that external conductors are capable of inducing contractions. He hypothesized that the electricity results from accumulation of positive and negative charges in nerve or muscle fibers, in analogy with the internal and external plates of the Leyden jar, i.e. the first proposed capacitor; moreover, he also speculated the presence of channels which penetrate the surface of nerve fibers, thus foreseeing the presence of the ion channels. In 1791, Galvani published its memories, *De viribus electricitatis in motu musculari. Commentarius* (Galvani, 1791), that were read and greatly admired through Europe. Lastly - to answer to the Volta's retorts, that hypothesized that the muscles' electricity was actually produced by putting in contact two different metals with the frog's leg - Galvani also elicited the contraction using a mono-metallic arc or no metallic arc at all (putting the frog's leg in a container and the cut end of the sciatic nerve in another one, the contraction is triggered when the two containers are put in contact), in addition he repeated the experiment by eliciting the contraction putting in contact two prepared sciatic nerves. With his discoveries, Galvani opened the way for the experimental proof of the theories of propagation of the action potential. After the Galvani's death, his work had been

carried on by his nephew Giovanni Aldini, that performed also electrical stimulation on body parts of executed criminals. Several years would pass, new instrumentation would be created, and several scientists followed Galvani's footsteps continuing investigating the nervous conduction process. Just to give the reader a short summary of the most interesting discoveries, in 1825 Leopoldo Nobili developed an electromagnetic *astatic* galvanometer and with it recorded for the very first time electrical activity from the neuromuscular preparation (Nobili, 1828); unfortunately, he completely misinterpreted his results. A decade later, Carlo Matteucci clearly demonstrated that the animal electricity existed by putting in series a heap of *rheoscopic frog* and founding that the electric current measured by the galvanometer was proportional to the number of frogs in series (Matteucci and Savi, 1844). After that, Emil du Bois-Reymond directly measured the action potential from both the muscle and the nerve (Du Bois-Reymond, 1884) and Herman Ludwig Ferdinand von Helmholtz discovered the propagation speed of nerve impulse by measuring the delay between the application of the stimulus and the contraction of muscle (Helmholtz, 1850), (Helmholtz, 1852). Subsequently, both the rest and the action potentials were recorded for the first time (Bernstein, 1868), and also a membrane excitation theory that linked the resting potential to its selective K^+ permeability had been proposed (Bernstein, 1912). Overton demonstrated that, in addition to K^+, also Na^+ ions are required to produce the potential variation (Overton, 1902); in addition he also found that lipid-soluble dyes enter into cells easier than water-soluble ones, and so proposed a "*lipoidal membrane*" model (Overton, 1899). The lipid bi-layer membrane model was proposed subsequently (Gorter and Grendel, 1925) and finally, in 1935 the model was improved by James Frederic Danielli and Hugh Davson, that proposed a lipid bi-layer membrane covered with proteins and water-filled channels that allow the passage of lipid-insoluble molecules, such as ions (Danielli and Davson, 1935). But the turning point started in 1949 when Cole (Cole, 1949) and Marmont (Marmont, 1949) proposed the *voltage clamp* technique [1]: adopting this innovative approach, Hodgking and Huxley studied how the AP is generated and propagated inside an axon of giant squid - research that earned them the Nobel prize in medicine and physiology in 1963 - thus partially confirming the Galvani's theories. In fact, they found an imbalance in the concentration of electrically charged ions between the inner and outer side of the membrane, which being a lipid bi-layer is also impermeable to ions. Consequently, these ions can only cross it through specific protein pores, and since these pores are largely closed at rest, electricity is stored. Ion channel opens only when the resting potential moves toward more positive values (i.e. when the membrane is depolarized,

[1] The voltage clamp technique allows for recording of ion currents through the cell membrane while the membrane voltage is kept constant

according to modern terminology), and their openings cause an additional depolarization that in turn leads to a further channels' openings and so on, until a full nerve impulse is released (Hodgkin and Huxley, 1952b), (Hodgkin et al., 1952) (Hodgkin and Huxley, 1952a). In this way, in the time frame between the 1780 and the 1950, the science evolved, getting rid of the "animal spirit" while the electrophysiology arose (Piccolino, 2006), (Cajavilca et al., 2009), (Verkhratsky and Parpura, 2014).

1.2 The patch clamp

The patch clamp is a technique that allow to measure the currents flowing through ion channels and the membrane potential of electrically active cells by clamping the voltage of an isolated piece of cell membrane (a membrane patch) or of the whole cell; consequently, this method permits to record very small currents, i.e. in the picoAmpere range. The definition of the patch-clamp technique was the result of a complicated process, paved by the efforts of many groups of scientists (Verkhratsky et al., 2006). The first big progress in this direction was the development, in 1949, of micro-electrodes (Ling and Gerard, 1949) obtained by pulling glass pipettes which tips are so thin to be suitable for low-invasive measurements of individual cells: very soon they became the most commonly used devices for electrophysiological recordings. A second huge step forward the patch clamp was carried out in 1976, when Neher and Sakmann, following up a previous work by Neher and Lux (Neher and Lux, 1969), managed to electrically isolate a patch of membrane by pressing on it the smooth tip of a microelectrode; in this way, if the area of the membrane patch under analysis is adequately small, the background noise can be reduced enough to make the picoAmpere currents that flow through a single ion channel measurable (Neher and Sakmann, 1976). But the real turning point happened with the discovery in 1980 of the so called "gigaseal", i.e. a very high resistance (in the order of tens $G\Omega$) seal that can be obtained between the electrode's tip and the cell's membrane. The gigaseal reduced the background noise of an order of magnitude, and can be achieved both by taking some precautions to keep the pipette surface clean, and by applying suction to pipette interior (Sigworth and Neher, 1980). With the application of the gigaseal to the patch-clamp technique previously developed, it became applicable to a huge variety of electrophysiological problems, thus revolutionizing the field of electrophysiology as demonstrated by the work by Sakmann and Neher, for which they were awarded the Nobel prize in medicine and physiology in 1991. In their 1981 paper (Hamill et al., 1981), they explained how to set up the experiments, together with the kind of recording performed. In particular, they demonstrated that the

greater difference with the previous versions of this technique is the suction: when the pipette was pressed against the clear surface of a muscular cell, the seal resistance is 150MΩ; while when a slight negative pressure is applied to the pipette, the seal resistance immediately increases up to 60GΩ, as shown in figure 1.1.

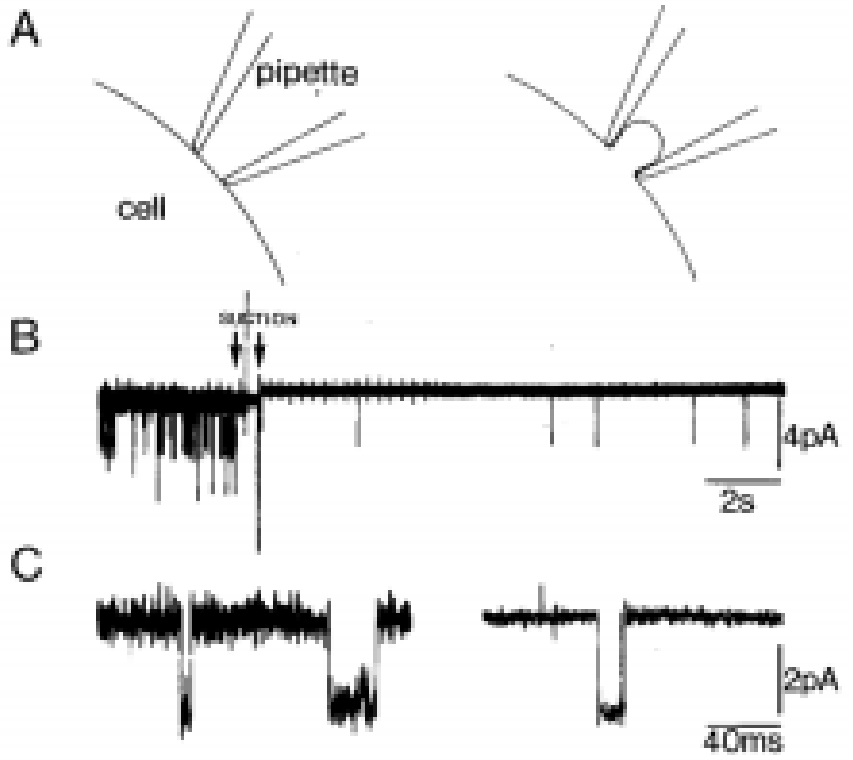

Figure 1.1 Gigaseal formation. A) schematic showing a pipette pressed against a cell membrane (seal resistance 50-100MΩ) (*left*), and after the formation of gigaseal (seal resistance 60GΩ (*right*). B) continuous recording of current before, during and after the suction and C) single channel current recorded before (*left*) and after (*right*) gigaseal formation. Figure taken from (Hamill et al., 1981)

The first suggested explanation for this phenomenon was that the suction makes the membrane at the pipette tip form an Ω-shaped protrusion, thus provoking an increase of the contact area between the glass and the membrane - fact that has been supported by measures of patch capacitance after the gigaseal formation - but the effect of this increasing contact can't cause such a boost of seal resistance. It was also demonstrated that small molecules can't diffuse through the seal area, and this can imply that the increase of seal resistance is ascribable to a tight contact between membrane and pipette. In addition, the high seal resistance allow to change the potential of the patch membrane without evoking noisy leakage currents: this permits to - for example - measure the variations of a single channel current in adult muscle fibers over a wide range of potentials, resulting that the underling relation is

linear. Finally, the gigaseal is not only electrically tight but also mechanically stable, and this allow for the withdrawal of the pipette after its formation without damaging it. Indeed, in the same work in which the patch clamp is presented, the authors noticed that, withdrawing the pipette after the gigaseal formation, a vesicle of lipid bi-layer is formed inside the tip of the pipette itself, as also shown in figure 1.2.

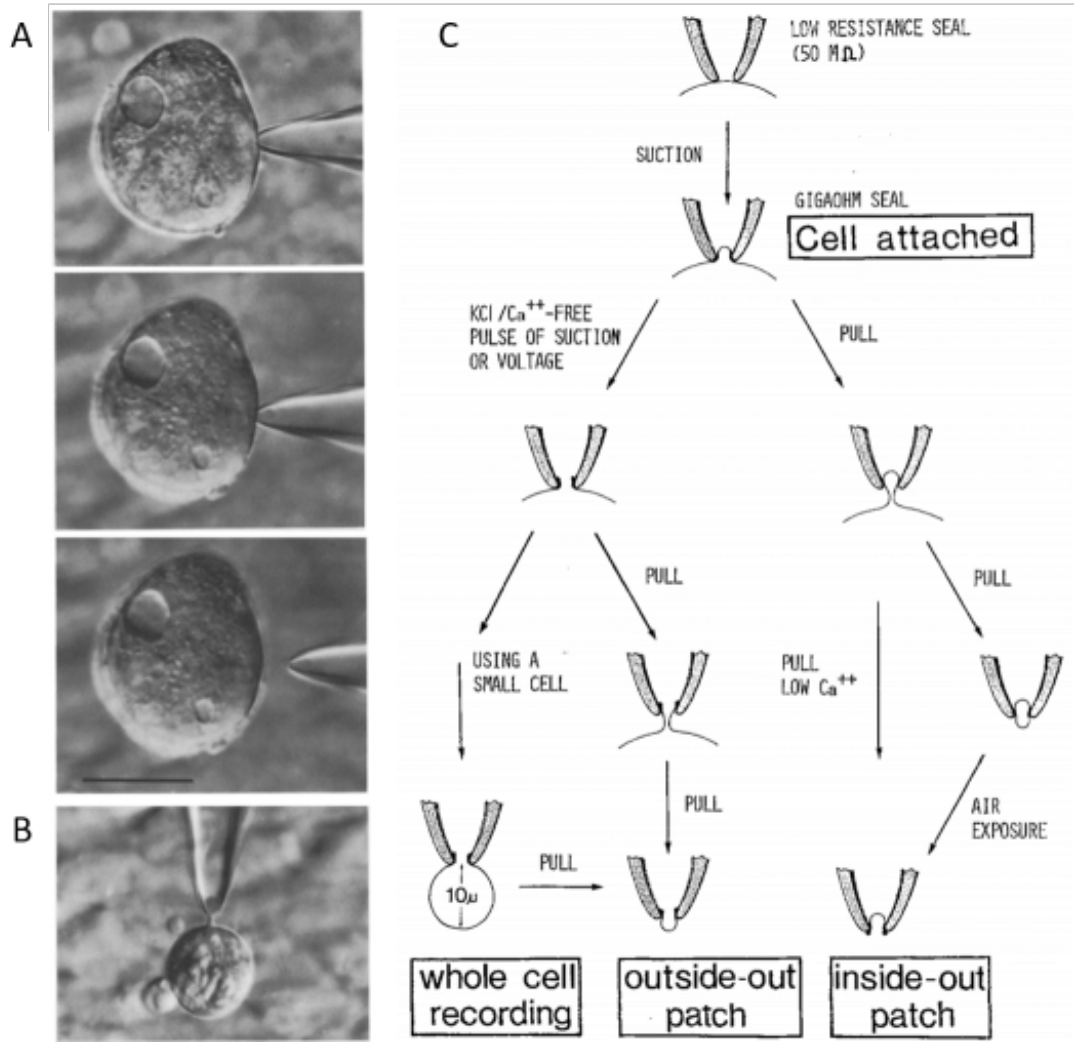

Figure 1.2 Formation of the membrane vesicle and patch configuration. A) Images of the vesicle formation; the pipette is pressed against the membrane (*upper image*), when the suction is applied, an Ω shaped vesicle is formed inside the pipette tips (*middle image*), and finally after the pipette withdrawal, the patch separates itself from the cytoplasmic membrane and the vesicle is formed (*lower image*). B) shows the cytoplasmic bridge between the cell membrane and the vesicle inside the pipette. C) sketch of the procedure that leads to different configurations. Figure taken from (Hamill et al., 1981)

The so formed vesicle is partly exposed to the solution inside the pipette (let's call *inner membrane* the part exposed to the pipette solution) and partly to the solution in the bath (*outer membrane*). Starting from the creation of the vesicle, it is possible to selectively break either the inner or the outer membrane; in particular, when the outer membrane has been disrupted, the cytoplasmic face of the inner membrane is exposed to the bath solution, while the extracellular face is exposed to the solution inside the pipette: this configuration is called *inside-out*. On the other hand, when the inner membrane is destroyed, the cytoplasmic face of the outer membrane is exposed to the pipette solution, and its extracellular face to the bath solution, in the so called *outside-out* configuration. These configurations have been broadly exploited to study the key properties of the most important ion channels, i.e. to measure the current signal of single ion channels in cell-free patches when both the bath solution and the pipette solution can be managed by the experimenter. Another recording possibility is the *whole-cell*: indeed, it has been demonstrated also the stability of the stage in which the membrane patch inside the pipette is broken without damage the gigaseal, and so the pipette communicate with the cytoplasm without damaging the cell membrane. Even if this configuration is suitable only for small cells, i.e. cells with a diameter smaller than 30 μm, it can be used to analyze the total ionic currents inside the cell, but also to alter its ionic content, since it has been shown that the intracellular solution exchanges quickly with the pipette interior. The patch clamp is suitable for analyze a bunch of different kinds of cells, as reported in this first work in which the authors obtained the gigaseal on a lot of preparation, including cell lines in tissue culture (like mouse neuroblastoma), primary tissue cultures such as rat fibroblasts or dorsal root ganglion cells, but also single cells (human and avian erythrocytes for example), and enzymatically dispersed or treated cells; and this is one of the properties that made it one of the most common electrophysiological techniques, extremely diffused also at the present days. On the other hand, this powerful tool has also some crucial limitations: firstly, it is a complex technique that necessitates to intricate skills to be performed; secondly, it is an invasive procedure that allow only for short term recordings (patched cells last only up to a few hours) and finally the patch-clamp set up is very bulky, and this limits the possibility to investigate more cells at the same time. This means that patch-clamp doesn't allow to analyze cells networks dynamics.

1.3 Micro electrodes

Conventional Micro electrodes arrays (*MEAs*) consist of arrays of passive (i.e. elements that have no gain or rectifying function), polarizable electrodes with fixed wiring: this

means that each electrode is connected through a wire to a signal pad usually situated on the edge of the substrate, and pads are in turn connected to external instrumentation for signal conditioning. Passive MEAs are easy to fabricate and many materials can be used for both substrate and electrodes. In particular, the latter are commonly made of Pt, Au, Indium Tin Oxide (ITO), or Titanium nitride (TiN), while the former can be for example glass, plastic or printed circuits board; wires are then passivated through a layer of silicon nitride (SiN), EPON SU-8 (a polymeric solid epoxy novolac resin) or polymide. The onset of thin film technology leads in 1970's to the development of the MEAs; in particular, in 1972 Thomas and coworkers (Thomas Jr et al., 1972) described the first MEA consisting in 30 gold-plated nickel electrodes deposited onto glass coverslips and passivated by a photopolymeric layer. These electrodes were arranged in two rows (the rows were distanced 50 μm from each other, while the distance between electrodes in the same row was 100 μm) and had exposed areas of $\approx 50 \mu m^2$, that were electrochemically covered by platinum black to reduce their impedance. They used it to record activity from a network of cultured chick heart cells. Shortly after, other groups started to use MEAs for *in vitro* electrophysiology with several kinds of cells, starting from an isolated snail ganglion (Gross et al., 1977), to a 3-weeks-old neuronal (i.e., superior cervical ganglion neurons dissociated from rat) networks (Pine, 1980). Since then, always more scientists began to use MEAs, and currently they are the gold standard for the extracellular recording of excitable cells, thanks to their ease of use, to their well known principle of transduction (Bove et al., 1995) and to the possibility to use them both to record signal or to stimulate cells across spatially separated regions in a network. In addition, as highlighted in the introduction of this chapter, MEAs are suitable for long-term recordings, allowing the researchers to study also the dynamics of the networks during their growth and development. Indeed, in the last decades MEAs have been used to analyse cultures' activity for several purposes, ranging from the investigation of basic mechanisms of cellulars' functioning and communication, to cytotoxicity studies, or to drug testing on human diseases in vitro; thus being applied on various kinds of excitable cells, starting from those harvested from rodents, chicks or cell lines[2], like cardiomyocytes (Law et al., 2009), (Wells et al., 2019), or neuronal networks (Pimashkin et al., 2013), (Kuang et al., 2015), and arriving to the cells derived from human induced pluripotent stem cell, also called *human iPSC*[3] that can be differentiated also in cardiomyocytes (Zwartsen et al., 2019),

[2]cells belonging to cell lines derive from tumors and therefore are highly able to proliferate, easier to culture, handle and eventually transfect.

[3]human iPSC are pluripotent stem cells generated directly from human somatic cells through a technology initially reported in 2006 by Shinya Yamanaka's group (Kazutoshi and Yamanaka, 2006) that, since can be made postnatally, guarantee greater availability of cells; in addition, they are generated starting from human

or neurons (Odawara et al., 2018). Thanks to their great diffusion in electrophysiology, also companies like Multi Channel Systems (www.multichannelsystems.com), Axion Biosystems (www.axionbiosystems.com) and Alpha MED Scientific (www.med64.com) have developed and placed on the market different MEAs, that differ to each other for electrodes' layout, number of electrodes, materials and so on, completed with the readout electronics and the software needed to see in real time the recorded signal and to stimulate the cultures. Anyhow, micro electrodes arrays have also several drawbacks regarding, as an example, the need of an external and usually bulky reference electrode (as an Ag/AgCl electrode) that limit the miniaturization of the device. Other drawbacks concern the high fabrication costs and the difficulty to obtain high densities of electrodes due to the external wiring.

1.4 Field Effect Transistor for cellular interfacing

The first Field Effect Transistor was presented in the late 1940s (Bardeen and Brattain, 1948), and since then FETs have gained an important role in the electronics field but not only: in the next years, several different FETs structures, adapted to many applications, have been obtained from the first version, and even now new FET architectures are periodically introduced. Between the various fields of application, FETs brought a new approach also to extracellular measurements and to cellular interfaces in general. Indeed, starting from some peculiar FET structures it is possible to obtain biosensors that can also help to get more information about living cells by measuring other parameters in addition to electrophysiological activity. These parameters can be monitored with the aim of both detecting changes in cellular behaviour in response to some treatment, and controlling the environmental conditions in the measurement chamber to maintain them as physiological as possible. One of the most important parameters to monitor is cellular metabolism, as it is sensitive to several stimuli, ranging from drug administration to electrical stimulation, and its variations can represent a clue of some change in the culture state. A measure of cells' metabolic activity can be deduced evaluating several phenomena, such as oxygen uptake due to cellular respiration, glucose consumption, lactate production or extracellular pH variation caused by the accumulation of acidic byproducts in the culture medium. In figure 1.3 a scheme of metabolic processes that leads to the acidification of the culture medium is shown.

In particular, the latter can be a convenient and easily applicable approach in *in vitro* cultures in real time. The acidification rate is linked with the physiological state of the

cells, thus pledging a better approximation of the human diseases and also lay the foundations for personalized medicine.

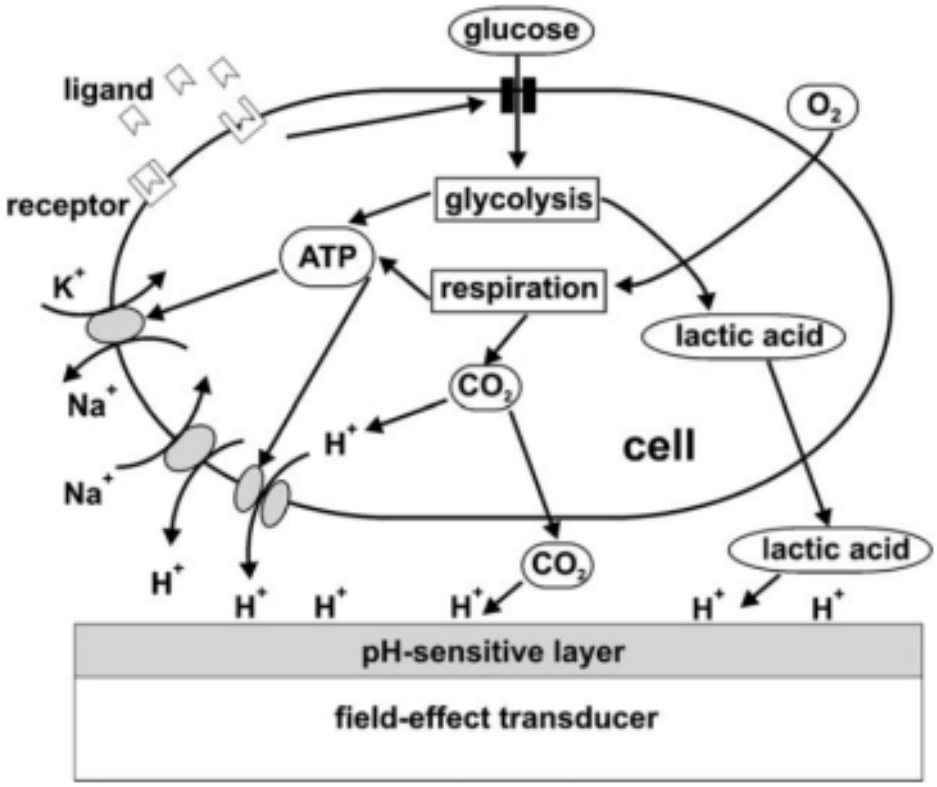

Figure 1.3 Scheme of metabolism of a cell onto a field-effect transistor. Briefly, ATP (adenosine trihposfate) consumption is compensated by increased uptake of glucose, leading to an augmented excretion of acidic byproducts (ΔpH). Figure taken from (Schöning and Poghossian, 2006).

cell: at steady state, a single cell produce $\approx 10^8 H^+ s^{-1}$, but following an external receptor stimulation, this quantity can raise from 10 to 100% depending on the kind of cell, the receptor and the coupling pathway (Owicki, 1992), (Poghossian et al., 2009). In addition, with the advent of semiconductor microsensors fabrication process, FET-based device can be integrated in the same substrate with other sensors (both FET-based or not) in order to obtain more complex monitoring systems (Baumann et al., 1999).

1.4.1 FET's working principle

Field Effect Transistors are four-terminal devices made of a semiconductor material, usually silicon, that can have different configurations depending on the majority charge carriers: in *p-type* transistors, the current is made by holes, while in *n-type* transistors, the majority charge carriers are electrons. A transistor is made of a doped silicon substrate, called also *body* that is partially covered by an insulating layer, typically silicon dioxide (SiO_2), covered in turn by an electrode of a low-resistivity material such as Aluminium, called *Gate* electrode,

to form a capacitor. Assuming to have an n-type transistor, the body is made of p-doped silicon i.e. with an higher density of holes, and on each side of the capacitor there are two areas heavily doped of electrons, i.e. n^+-doped, that are named *Source* and *Drain*, while the area underneath the gate capacitor is the channel of the transistor. A sketch of the structure is shown in figure 1.4.

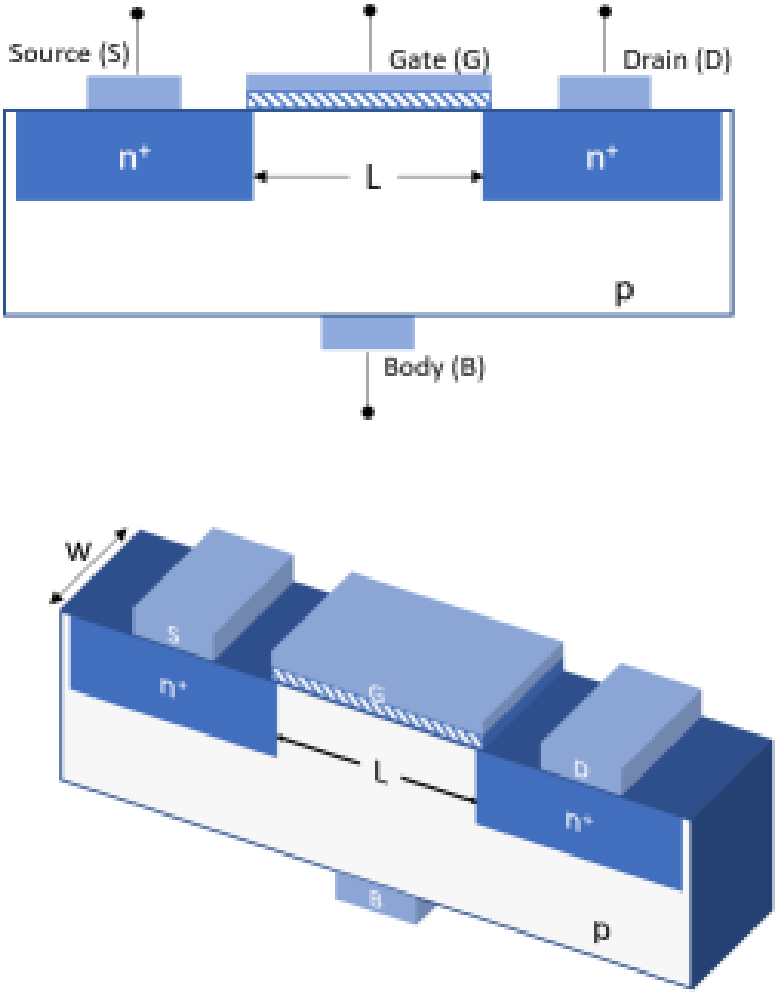

Figure 1.4 MOSFET sketch, in which electrodes and the principal physical parameters are highlighted. Frontal (*up*) and rotated (*down*) view.

Before to briefly recall the transistor's working principle, it is necessary to highlight that the source and the bulk electrodes must be connected to the same voltage (that is usually the mass), in order to analyse its behaviour as a function of the voltage V_{GS} applied to the gate electrode with respect to the source. When V_{GS} is a positive voltage, the charge density it induces is balanced by an accumulation of negative charges at the substrate/oxide interface. Consequently, if the voltage is positive enough to overcome the threshold voltage V_{TH}, an

inversion layer of charge carriers occurs, i.e. the electron density at the surface exceeds the hole density, and the surface from p-type becomes n-type: the so called transistor channel is formed. At this point, if a potential difference V_{DS} is applied between the drain and the source, a current I_{DS} will flow that depends on both voltages V_{DS} and V_{GS}. Indeed, while the gate voltage modulates the channel (the larger is the V_{GS} applied, the thicker is the inversion layer and bigger is the section of the channel), the drain voltage modifies the quantity of current that flows between source and drain, thus provoking a voltage gradient along the channel if $V_{DS} < (V_{GS} - V_{TH})$ that results in the pinch-off when $V_{DS} = (V_{GS} - V_{TH})$; from then on, the transistor is in its saturation region and the output current is independent on the drain voltage. Their general expression in triode [4] region is the following:

$$I_{DS} = \mu_n C_{ox} \frac{W}{L} [(v_{GS} - V_{TH}) v_{DS} - \frac{1}{2} v_{DS}^2] \tag{1.1}$$

While in saturation [5], the equation became:

$$I_{DS} = \frac{1}{2} \mu_n C_{ox} \frac{W}{L} [(v_{GS} - V_{TH})^2] \tag{1.2}$$

where

- μ_n is the electron mobility;
- C_{ox} is the oxide capacitance per unit area (F/cm^2);
- W is the channel width;
- L is the channel length;
- V_{TH} is the threshold voltage.

1.4.2 ISFET

The Ion Sensitive Field Effect Transistor (ISFET), is a MOSFET in which the gate electrode is replaced by a series of an electrolyte and a reference electrode, as shown in figure 1.5.

Consequently, its working principle is very similar to that of MOSFET itself (and such it is the general expression for the output current I_{DS}, that is similar to 1.1). The main difference

[4] also called *linear*, because for $V_{DS} < V_{GS} - V_{TH}$ the output current linearly depends on the drain voltage

[5] region in which I_{DS} does not depend anymore on V_{DS} because the point of pinch-off has been reached.

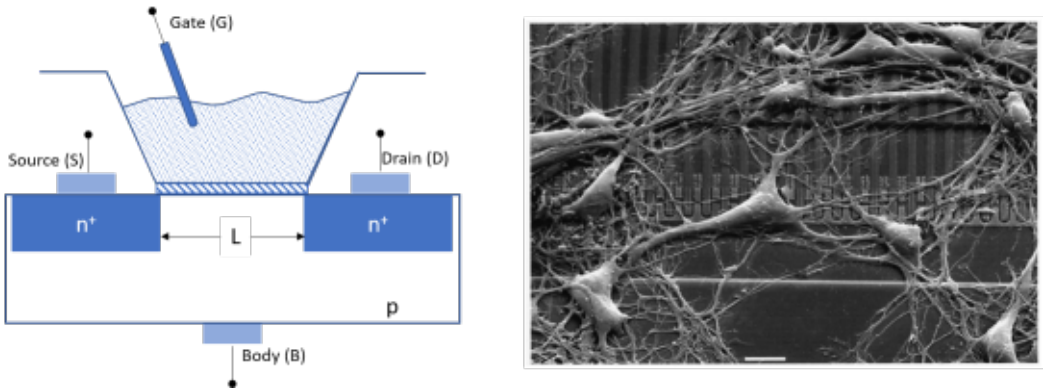

Figure 1.5 ISFET sketch, in which electrodes and the principal physical parameters are highlighted *left*. Cells are plated directly onto the transistor channel, as shown in the photograph on the *right*. Figure on the right taken from (Vassanelli and Fromherz, 1999).

between MOSFET and ISFET rely in the threshold voltage: while for the MOSFET V_{TH} is constant, its modulation is responsible for the ion sensitivity of ISFET. The first version of ISFET, specifically created for neurophysiological applications and has been presented for the first time in a short letter by Bergveld in 1970 (Bergveld, 1970), and described in more details in the following full paper in 1972 (Bergveld, 1972). ISFET is described by its inventor as "a MOSFET in which the gate metal is replaced by aqueous solution", and was operated without an externally applied gate voltage. In this first work, the authors noticed as, when the ISFET was kept in aqueous solution for some days, its oxide appeared to be less isolating; they associated this phenomenon with an hydration of the oxide, similarly to what happen to glass membrane in glass electrodes. With this first version of ISFET they record, as a proof of concept, the electrophysiological activity of a smooth muscle of Guinea pig taenia coli (chosen because it is spontaneously active and doesn't need to an external stimulation) placed on top of the transistor oxide layer. A few years later, the same group proposed another work linked to ISFET (Bergveld et al., 1976); in this case the oxide surface is treated in order to not be hydrated and so the device takes the name of *OSFET* (i.e. Oxide Semiconductor FET) and behaves almost exactly as a MOSFET; in this work, Bergveld was able to record electrical activity from the flexor tibialis muscle of the hind leg of a locust *in vivo*. However, after the pioneering work of Bergveld, several groups followed his footsteps and an astonishing number of papers regarding ISFET and ISFET-based devices appeared in many journals on several fields including bio-electronics, sensors/biosensors and actuators. Indeed, thanks to their versatility, mainly due to the possibility of introducing a functionalization of the oxide surface by bounding recognition molecules on it, ISFETs can be made sensitive to a lot of different substances. In the specific case of extracellular

recording, ISFET presented several advantages with respect to conventional MEAs; firstly, an intrinsic amplification of the recorded signal is guaranteed by ISFETs, since they are active devices, thus enhancing the signal to noise ratio; and the possibility to address ISFETs in a matrix configuration, thus reducing the wiring complexity. In the following, an overview of the first proposed ISFET-based devices for both electrophysiological and metabolic activities monitoring has been presented, for further information on their evolution, please refer to the following reviews (Schöning and Poghossian, 2006), (Poghossian et al., 2009), (Sakata, 2019).

ISFET-based devices for electrophysiology

Regarding the electrophysiology, the most breakthrough works are substantially two. The first is of the group of Fromherz, that in early 1990s proposed a very interesting study (Fromherz et al., 1991) in which the coupling between a leech neuron and an n-type, ISFET-based silicon FET has been investigated also through the comparison between the intracellular and extracellular signals, since the neuron's activity was recorded simultaneously from both the transistor and an intracellular pipette. This work was followed by a series of other, in which the same group continued to study the coupling between neuron and FET (Vassanelli and Fromherz, 1999), (Kaul et al., 2004), (Hutzler and Fromherz, 2004),(Fromherz, 2008); noteworthy, in one of these (Fromherz and Stett, 1995), the authors developed a silicon microstructure of p-doped electrodes that can be used to stimulate neurons through the application of a voltage step between silicon and electrolyte. The second one, is from Offenhauser and colleagues that, some years later, presented an array of 16 p-type FETs with different gate (without metallization) areas (Offenhäusser et al., 1997). For experiments, they used hippocampal neurons, that were stimulated through a patch-clamp pipette in order to allow the FETs to record the following response.

ISFET-based devices for metabolic activity monitoring

As previously mentioned in 1.4, in addition to electrophysiology, another interesting application of ISFET-based devices interfaced with living cells concerns the monitoring of metabolic activity of cells cultures. In 1998, a device with 4 pH-sensitive ISFETs adapted to measure extracellular acidification of cell cultures was presented (Baumann et al., 1999), with the prospect of a future integration in a more complex system for cell monitoring. Authors made several trials on this device, with different kinds of cell's types and drugs such as triton-X to kill the cells, and the cytostatic agent chloroacetaldehyde (CAA) to slow down

cells' metabolic activity and so their acidification rate, and they were able to record for up to 12 days with promising results. In addition, a first experiment in which authors recorded simultaneously from a pH-sensitive ISFET and an interdigitated structure for impedance measurement was presented. This group continued working to this ISFET-based acidification sensor (Lehmann et al., 2000) and two years later proposed also a single ISFET that can measure both the acidification of the medium and the oxygen consumption (Lehmann et al., 2001), by placing a palladium electrode around an ISFET sensor. In this way, the pH-ISFET measures the acidification rate, while the combination of the ISFET and the palladium electrodes measure the oxygen consumption. Obtained results showed the feasibility of measuring simultaneously the two parameters in a real time manner, even if further studies were needed. In 2001, the group of Martinoia (Martinoia et al., 2001) proposed a completely automated microsystem for cellular metabolism monitoring, containing 12 ISFETs to measure the pH variations in the culture medium caused by the cellular metabolic activity. In addition, there were 2 temperature sensors to verify the temperature of the culture medium, and a conductivity sensor that checks the cell adhesion. The functionality of these devices on this first work has been simulated, while in a following paper (Lorenzelli et al., 2003) it has been tested with living cells (both cheratinocytes and Chinese Hamster Ovary (CHO) cells), also in presence of a toxicological agent. From this second published paper, it resulted that the device was able to measure the cell metabolism rate in a time scale of minutes.

1.4.3 Other FETs structures

Although ISFETs are the most commonly used FET structures for cellular applications, also other architectures have been proposed. One of the most known is the Extended Gate FET, in which the gate metallization is extended - as the noun itself suggests - outside the FET device and represents the point of contact between transistor and cells. In some cases, the electrode may not be an extension of the gate, but coupled through a capacitor with it: this variation is called Floating Gate FET. These devices have several advantages if compared with the ISFET-based devices (the so called *open-gate* since the electrolyte is placed between the oxide and the gate metallization):

- isolation and protection of the channel region - which is the most delicate part of transistor - from the cell culture medium. This also improves the durability of the devices;
- electrode and transistor can be designed and optimized (valid only for floating gate approach);

- as proposed by Cohen et al. (2004), there is the possibility to add a switch to the Floating Gate to use it also to stimulate cells (valid only for FG devices).

Both Extended Gate and Floating Gate FETs have been used to record extracellular signals of excitable cells(Cohen et al., 2004), (Meyburg et al., 2006), (Krause et al., 2000), (Ecken et al., 2003).

Very recently, Extended-Gate and Floating-Gate devices have been employed also to pH measurements, with encouraging results (Kang and Cho, 2019) but, as far as I know, at the moment devices for cells' metabolism monitoring have not been reported.

1.4.4 CMOS-MEAs

Another class of devices to consider is formed by the active MEAs, i.e. micro electrodes arrays in which each electrode is transistor-based, and between them a unique position is occupied by the so called CMOS (Complementary Metal-Oxide-Semiconductor) MEAs. Their name originates by the fact that their realization is made possible by the spread of CMOS technology and by the exploitation of concepts previously developed for light image sensors (for cameras, for example): with this technology it is possible to reach very elevated densities, i.e. several thousands of electrodes.

Indeed, it allows to reduce the area occupied by the wiring between electrodes and read-out electronics; in addition, with the CMOS technology it is possible to embed in the same substrate also other elements such as amplifiers, analog-to-digital converters and multiplexers, and this helps to improve the signal to noise ratio (SNR). With CMOS-MEAs, thousands of cells can be recorded and/or stimulated over time scales ranging from seconds to several weeks and, at the same time a single cell can be recorded by hundreds of electrodes, thus allowing the extraction of information at subcellular levels (for example, about the propagation of action potentials along axon of neuron). As a curiosity, figure 1.6 presents a graph showing a comparison between different kinds of MEAs (active or passive) reported in several works, with respect to electrode density and total sensing area. Between the CMOS-MEAs, the *APS-MEAs* (Active Pixel Sensors) are very interesting, in which all electrodes can be sampled at fast speed in a full-frame readout. Some examples of APS-MEAs are the device proposed by Johnson and coworkers in 2013 (Johnson et al., 2013) - that contains 1120 electrodes in a sensor area of 2.2 x 1.7 mm^2, with a spatial resolution of 50 μm to record biopotential from brain slices at a frequency of 20kHz - and, Tsai et al. (2017), that proposed a device with 65,536 electrodes. A huge quantity of works regarding the development of new CMOS-MEAs devices and their applications has been presented (for

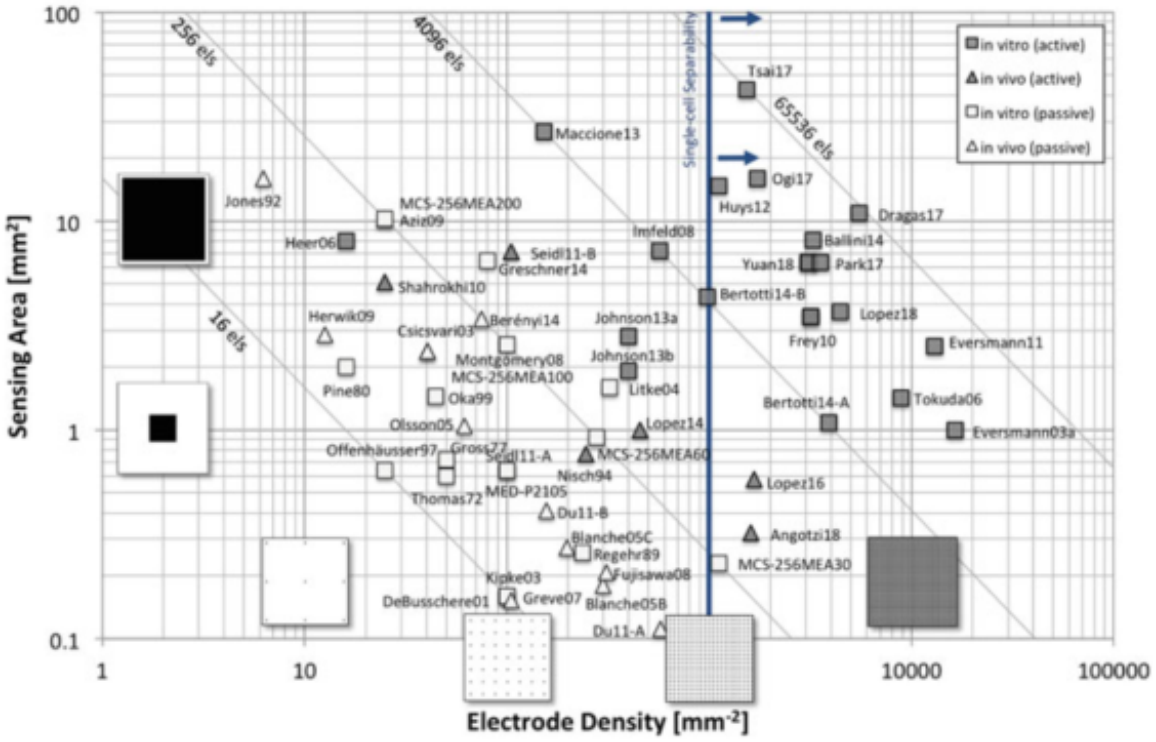

Figure 1.6 MEA (both active and passive, for *in vitro* and *in vivo* comparison with respect to electrode density and total sensing area. For devices with a regular sensor distance, such as most of *in vitro* MEAs, the total area is calculated as pixel area times number of electrodes. In all cases, the number of electrodes divided by the electrode density returns the total area. Figure taken from (Obien et al., 2019).

more information, please refer to (Obien et al., 2019) and (Obien et al., 2015)), and some of them are also commercially available, produced for example from Multi Channel System (www.cmos-mea.com) and 3Brain (www.3brain.com).

Chapter 2

Organic Field Effect Devices for *in vitro* cellular interfacing

Someone identifies the origin of organic electronics in the discovery of semiconducting properties of violanthrone, iso-violanthrone and pyranthrone by Akamatu and Inokuchi (Akamatu and Inokuchi, 1950), aided by the fact that Inokuchi is often regarded as "the father of organic electronics" (Forrest, 2020), while others recognize as the beginning of this field a following event, i.e. the discovery of the possibility to change the conductivity of polyacetylene of several orders of magnitude (over seven) by exposing it to halogens (chlorine, bromine and iodine) vapours by Shirakawa, MacDiarmid and Heeger (Shirakawa et al., 1977), that in 2000 received the Nobel Prize in Chemistry. Independently of which events made the field of organic electronics arise, it is undeniable that organic materials have received much attention as candidates for new electronic devices, and in a few years the first organic products have been presented: in 1986, at Kodak, the first efficient, all-organic bilayer rectifying solar cell was proposed by Tang (Tang, 1986); and in the same year also the first field effect transistor with a kind of conducting polymer, i.e. polythiophene, as semiconductor (Tsumura et al., 1986) has been proposed. The following year, was announced a 1% quantum efficiency, low voltage ($\approx$ 10V) bilayer organic light emitting diode, which will be later called OLED (Tang and VanSlyke, 1987). From then on, always a greater number of devices have been published, and several low cost fabrication techniques have been adapted to realize electronic devices. Indeed, organic electronic has various valuable advantages with respect to silicon; for example, the possibility to process organic semiconductors at low temperature reduces the production costs and permits to apply them over a vast range of materials such as plastic or paper, thus making possible to design flexible, transparent and lightweight devices with large areas methods. In this way, it is possible to overcome several problems

related to silicon technology. On the other hand, the organic semiconductors performances are not comparable with which of the inorganic competitors (mostly due to the intrinsically lower charge carrier mobility), and this limits their applications to relatively low frequencies, as an example. Despite this, organic electronics have furnished big improvements to the bioelectronics, since its advantages are substantial for biomedical applications: in fact, in the last decades, lots of works have been done, and several organic transistor structures have been studied to adapt to the generation of innovative sensors. In the following section, we will analyze the most commonly used architectures along with their principal results in the field of cellular interfaces and more precisely, in the field of electrophysiological and metabolic measurements.

2.1 Organic Field Effect Transistor

Organic Field Effect Transistors are thin film transistors (TFT), i.e. MOSFET in which the semiconductor is deposited in a thin layer, as well as the insulating layer and the metallic electrodes, over a supporting (non conductive) substrate. A big difference between MOSFET and TFT is the working principle: indeed, while the former works in inversion (i.e. the channel is formed by charges of opposite sign with respect to the doped bulk of material), the latter operates in accumulation, meaning that if the organic semiconductor is a p-type, the OTFT has a hole-constituted channel. In other worlds, when a voltage is applied between the gate and the source electrodes, an accumulation of opposite charges occurs at the insulator/semiconductor interface to balance the charges located in the gate electrode; thus generating the transistor channel. At this point, the application of a voltage between the source and drain electrodes allows a current to flow between them. Modifying the gate voltage leads to a change of the charge density at the insulator/semiconductor interface, and consequently to a variation also of the electrical conductivity of the channel; it follows that, also the drain current will change.

Another big difference is the fabrication process: while the production of a MOSFET involves several steps such as implantation, layered growth from the substrate and deposition; the TFT is fabricated using only deposition. This, from one hand affects the carrier mobility, that is higher for MOSFET because implantation preserves the crystallinity, while the deposition generates only amorphous layers. But on the other hand, it greatly simplifies the process of fabrication, and allows to use any kind of substrate (Tixier-Mita et al., 2016). The first TFT was described by Weimer in 1962 (Weimer, 1962), about two years after the fabrication of the first MOSFET, and was formed by a layer of semiconductor that in most

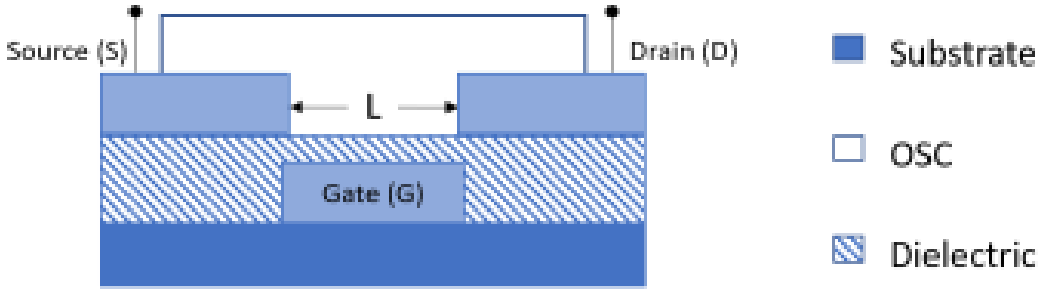

Figure 2.1 sketch of an OFET in the bottom gate-bottom contact configuration in which the various components are highlighted.

cases has been a micro-crystalline film of cadmium sulphide with a thickness lower than 1μm; the source and drain electrodes are made usually of gold (or other metals which make a low resistance contact to the semiconductor) and the space between them is $5-50\mu$m ; also the gate electrode could be made of gold, covered by a thin film of insulator, such as silicon monoxide. Nevertheless, the real spread of TFTs started with the arise of organic semiconductors, that allowed to create Organic Thin Film Transistors (OTFT). As previously mentioned, the first OFET, that was an OTFT, was proposed in 1986 by Tsumura and his coworkers (Tsumura et al., 1986). The transistor had a n-type silicon substrate covered with a thermally grown oxide film that acted also as Gate electrode; two Au-coated Cr electrodes installed on the same side of the SiO_2 layer and separated from each other by 10 μm (the channel length) operated as source and drain electrodes, and a polythiophene film was deposited between the gold electrodes. Authors noticed that the polythiophene layer they make grow between source and drain electrodes (that is highly ClO_4 -doped, resulting oxidized) does not show any field effect, i.e. the gate does not modulate the current flowing between source and drain; but the field effect becomes observable when the film is reduced, i.e. when it becomes to be electrochemically undoped by applying biases to the gate electrode. In particular, it showed the best properties when is undoped at 0V versus a Saturated Calomel Electrode, acting as an excellent p-type semiconductor. The source current can be modulated by a factor of 10^2-10^3 by varying the gate voltage between 0 and -50V while keeping the drain voltage between -10V and -50V. From then on, OTFT have been extensively used for several applications, and between them for bio-sensing. In 2002 Someya's group studied the interaction between a liquid solution and several conducting polymers, used as organic semiconductors of an OTFT and directly exposed to the liquid (Someya et al., 2002). They found not only that OFETs can operate in aqueous environments, but also that they may show interesting responses to analytes that can be exploited to create sensors and biosensors. In 2010 the same group proposed an array of Organic Transistors with an incredible low

bending radius, with which they produced a thin catheter that measures the spatial distribution of mechanical pressure (Sekitani et al., 2010). Some years later, an extended gate, OFET device has been proposed as a sensor to biotinylated immunoglobulin G (IgG) (Minamiki et al., 2014). The authors fabricated a gold thin film on PEN substrate as extended gate and functionalized it with strepatividin, thus exploited the interaction biotin-strepatividin to detect IgG. It resulted that the device is able to detect the antibody presence through a negative shift of its threshold voltage that depends on antibody concentrations, and its response is accurate also in the presence of a competing interference with two order of magnitude higher concentration. Several other OFET-based biosensors have been presented; since their detailed description is outside the scope of this thesis, please refer to reviews, as an example the one from Surya et al. (2019), recently published. Simultaneously, another OFET-based structure became common for biosensor application, i.e. the Ion Sensitive Organic FET or ISOFET, in which a layer of insulator separates the organic semiconductor from the electrolyte solution; its working principle is the same of ISFETs 1.4.2, and similarly to ISFETs, it is able to detect a wide range of biomolecules if its insulator layer is made sensitive to them. The first ISOFET was proposed by Bartic and coworkers in 2002 (Bartic et al., 2002), and thanks to the use of silicon nitride as insulator, it was sensitive to pH variations in aqueous solution. The following year, the same group described an enhanced version of their ISOFET which, thanks to the use of tantalum oxide (Ta_2O_5) as insulator, needs lower supply voltages (thus being more suitable for cellular applications). In addition to pH variations, this ISOFET had been used also as glucose sensor by immobilizing glucose oxidase (GOx) on the transistor insulator; indeed, the reaction between glucose and GOx provokes local changes in the pH value that are detected by the OFET (Bartic et al., 2003). Also in this case, a huge amount of ISOFET-based bio-sensors have been proposed; for more detailed information, see (Kergoat et al., 2012).

2.1.1 OFETs for electrophysiology

Albeit several of the characteristics of OFET raised the expectations about their employment in aqueous solution and in contact with cells, as far as I know, very few applications in the field of *in vitro* electrophysiology have been presented. The group of Benfenati in 2013 presented an OFET-based device, called *organic cell stimulating and sensing transistor* or O-CST, that were able to record and stimulate electrical activity of dorsal root ganglion neurons (DRG) [1] from post natal p14-p18 rats (Benfenati et al., 2013). In this work they

[1] DRG are mostly electrically silent neurons.

investigated the use of this device as a stimulator (while recording intracellular response with patch-clamp) and as a simultaneous stimulator and recorder; and their results showed that they are able to elicit responses to DRG that with other electrodes, such as standard MEAs, have failed to evoke also with similar protocols. However, further analyses were need to better understand the working process. In a second work published several years later by the same group (Borrachero-Conejo et al., 2019), the O-CST (which structure is shown in figure 2.2 A) was used to stimulate, in a sub-threshold operating mode, non excitable brain cells (specifically rat neocortical astrocytes) in order to study the variation of the concentration of Ca^{2+} ions. In order to do this, they exploited the transparency of the O-CST to perform on the cells cultured on it a calcium imaging while electrical stimulation was delivered to the astrocytes. It results that the device was able to elicit astrocytes' reaction also with protocols that failed with DRG in the previous work, demonstrating also that selective stimulations of targeted cell types can be obtained by varying the protocol.

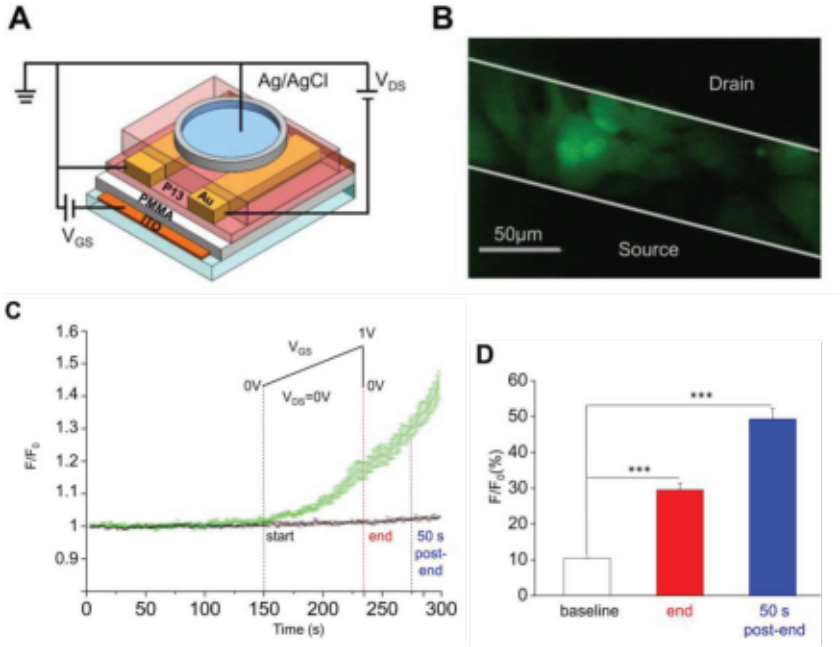

Figure 2.2 Inferring whether O-CST sub-threshold operation promoter the increase of calcium concentration in astrocytes. A) scheme of the O-CST device and B) fluorescent image of astrocytes (labelled with Fluo-4) plated on the O-CST device taken during a performed experiment. C) Representative averaged trace with standard error (SE) of calcium imaging experiment on O-CST device. The inset reports the stimulation protocol: 150s after the beginning of the experiment, a V_{GS} was spanned from 0 to 1 V in 85s while V_{DS} was kept at 0 V. black dashed bar indices the beginning of the stimulus, the red dashed bar its end; the blue dashed bar represents the time used for calculation, 50 s after the end of the stimulation. F is the fluorescence intensity while F_0 fluorescence intensity at time point = 0 s. (Borrachero-Conejo et al., 2019).

Figure 2.2 shows a protocol in which V_{GS} was spanned in a ramp between 0 and 1V while V_{DS} was kept at 0V, and the calcium imaging shows that the fluorescence rises slowly but constantly not only during the stimulus, but also in the 50 seconds following its end (figure 2.2 C and D). Repeating the same experiments with the addition of blockers of different ion channels, the authors deduced that the action of the ion channels' family called *transient receptor potential* or TRP, and in particular of TRPV4 and TRPA1, is critical for the increase of calcium. Since it is already demonstrated that TRPV4 is responsible for swelling-induced extracellular Ca^{2+} influx in astrocytes and it has been found that electric field induces cell swelling, they hypothesised that electric field generated by O-CST might induce cell swelling and, in turn, activate calcium signalling in astrocytes via TRPV4 and TRPA1. Finally, they found that are able to obtain this effect only when a transistor is used, thus demonstrating that the transistor architecture is causing the stimulation, probably due to the capacitive coupling enabled by close interaction and proximity between the organic layer and the cellular membrane. Nevertheless, in this device the transistor is used only to stimulate, and never to record signals from cells; in addition, it is always used in a sub-threshold operation mode.

2.1.2 OFETs for metabolic activity monitoring

As mentioned in previous chapter 1.4, there are several methods to monitor cellular metabolic activity, from oxygen uptake to glucose consumption, lactate production or extracellular pH variations. To the best of my knowledge, nobody has never performed experiments aimed at monitoring the metabolic activity of cells' culture *in vitro* using OFETs. Nevertheless, in the last years, some group started to work in this direction, and the first devices that may be used to this purpose have been presented, even if they have only been tested with preliminary protocols that don't include living cells. In 2010, an ISOFET with P3HT as organic semiconductor and in which the dielectric (PMMA) was covered by a Langmuir-Blodgett (LB) film (more precisely, an arachidic acid multilayer), have been proposed to monitor pH variations (Ritjareonwattu et al., 2010). The drain current I_{DS} of ISOFET decreased with the reduction of the pH of the solution (caused by the addition of acetic acid); indeed, a lower pH value leads to a higher density of H^+ ions in the electrolyte and at the electrolyte/insulator interface, leading to an electrostatic repulsion with the positive charges at the insulator/semiconductor interface that in turn induces a reduction in the density of holes in transistor channel. Authors also found that, by coating the PMMA layer with LB layer, the variation of I_{DS} with respect to pH increases of almost an order of magnitude, due

to the carboxylic groups in the LB film, that on one hand increase the negative charge at the solution/dielectric interface, thus increasing the conductivity of the channel and consequently the drain current; but on the other hand, carboxylic groups ionize in response to pH variations, thus allowing for the channel modulation. In 2016, another OFET device has been proposed to detect pH variations in aqueous solutions (Seo et al., 2016). The OFET has PMMA as gate insulator and a layer of P3HT as organic semiconductor; the latter is covered by a layer formed by a pH-sensitive copolymer (PAA-b-PCBOA) in which polymer-dispersed liquid crystals (LC) microdomains (i.e. with size minor than 5μm) are encapsulated. This cover layer does not affect the transistor behavior, but it is crucial for the device sensitivity. Indeed, results showed that the drain current decreases when pH was increased and vice-versa; while indicatively no current variations are exhibited when pH is neutral (i.e. 7). The working principle of the device is quite straightforward: the PAA is the pH-sensitive block of the polymer, and it undergo to deformation when pH changes (particularly, it stretches when pH is basic, and it is contracted when pH is acid: this implicate that, in acid environment, the liquid crystals are compressed and make close contact with the semiconductor, thus increasing the hole density in the channel. On the contrary, when pH is basic, the relaxed polymer configuration allow the LC domains to move away from the surface, leading to reduction in the output current. In 2020, Didier and his colleagues have presented an extended gate OFET to real-time glucose monitoring (Didier et al., 2020). The device is formed by an OFET which semiconductor is PBTTT, and by and extended gate of 15 mm^2 made of gold and functionalized with 4-MPBA (4-mercaptophenylboronic acid), that recognizes Glc also in the *in vivo* concentration range forming an anionic boronate ester, which affects the characteristics of the OFET, as shown in figure 2.3A. The devices comprised also a custom microfluidic to allow measurements at a constant flow rate. Using this device, the authors simulated glucose consumption and release by liver cells, by modifying the glucose concentration in phosphate buffer solution during a real-time recording; in particular, glucose concentrations ranged up to 20mM, covering both the normal and the abnormal glucose concentration in humans. It results that the output current I_{DS} gradually decreases with the increase of glucose concentration, and vice-versa, as it is possible to see in figure 2.3; in addition, it was found that the response time (80% of the response in ≈ 2 minutes) is adequate for detecting cells activities.

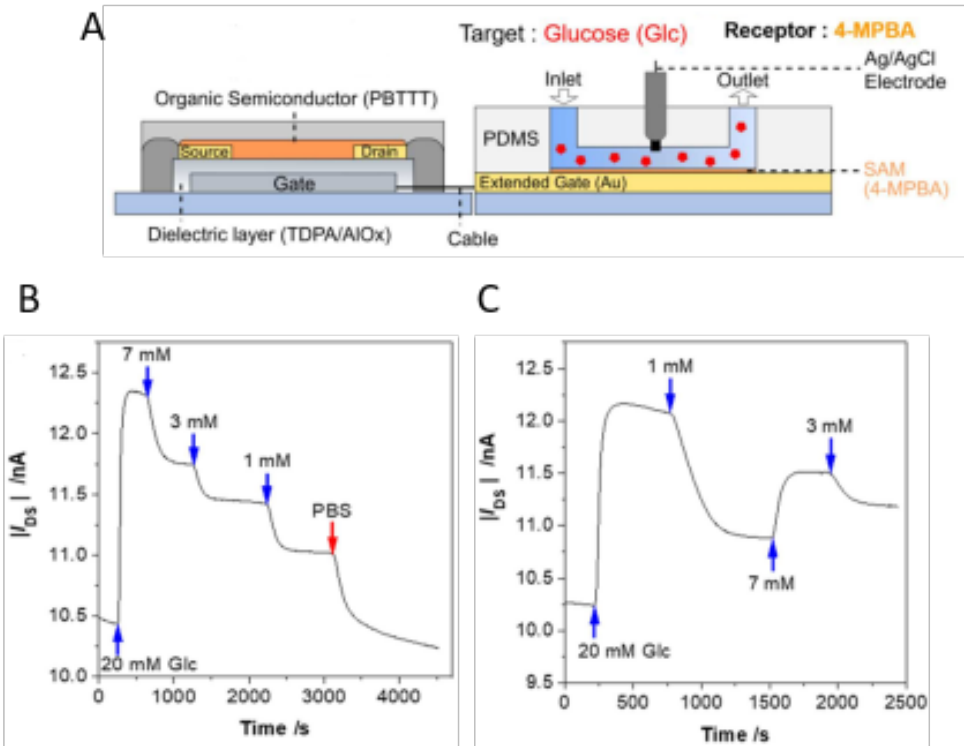

Figure 2.3 Extended-Gate OFET for real-time glucose monitoring. Sketch of the device architecture, in which also the most important material used are highlighted (A). Results of the simulation of glucose consumption and production by liver cells: graph B) shows how the output current varies in response to gradual reduction in glucose concentration, thus mimicking pseudo glucose consumption in cells, while C) represents the reaction of the transistor I_{DS} to random variations in glucose concentrations. Figure taken by (Didier et al., 2020).

2.2 Electrolyte-Gated Organic FET

The Electrolyte Gated Organic Field Effect Transistor, or *EGOFET*, is a three-terminal device in which two electrodes, i.e. the Source and Drain are connected through an organic semiconductor, while the Gate, i.e. the third electrode, is separated from the channel through an electrolyte (instead of the dielectric). The channel is modulated by capacitive effects at the interface between the semiconductor and the electrolyte, where an Electrical Double Layer (EDL) is formed (while a second EDL forms at the gate/electrolyte interface) following the application of a gate voltage. The presence of EDLs give to the EGOFET several advantages, such as a very high capacitance values (if compared to that of metal oxides usually employed in standard FET structures) consequently allowing for low voltage and water stable operation; and a high value of transconductance. In addition, thanks to the ability of EDLs to rapidly re-arrange itself after a perturbation, EGOFETs show relatively faster time responses. In

details, the EDLs that are created inside the electrolyte are composed by three ion layers; the first two are formed respectively by solvent molecules strictly packed and in direct contact with the semiconductor (or the Gate electrode) and by solvated ions, and together constitute the Helmholtz layer. The third is a diffusion layer and contains free ions, which drift for electrostatic interaction and thermal motion. Since the excess of ions decreases with the distance from the semiconductor (or gate electrode)/electrolyte interface, the potential drops only in the Helmholtz layers, which usually is very thin, leading to the very high capacitance value we have introduced in the previous lines (Schmoltner et al., 2013). In figure 2.4, a scheme of a p-type EGOFET structure and working principle in case of a negative applied gate potential is shown.

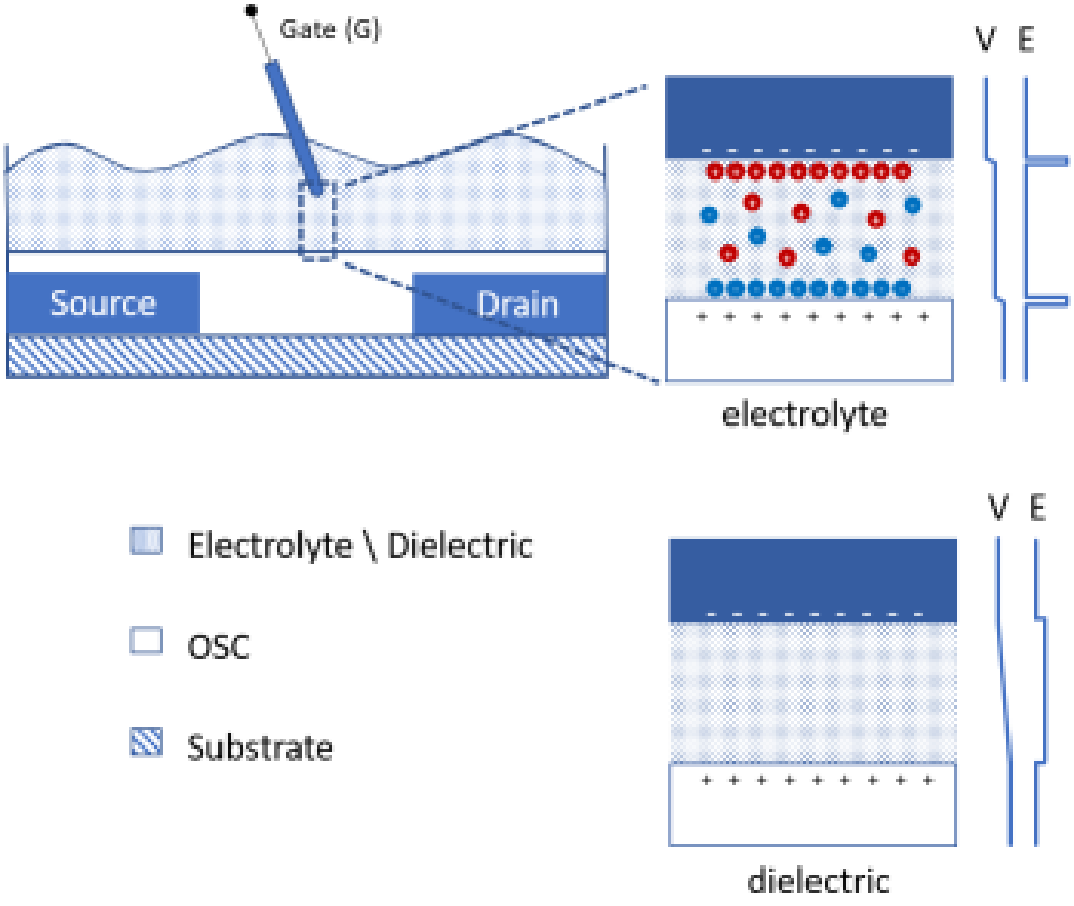

Figure 2.4 EGOFET sketch in which the various components are highlighted *left*, working principle of a p-type EGOFET in case of a negative applied gate potential, leading to the formation of an EDL at the gate/electrolyte and the semiconductor/electrolyte interface via migration of cations and anions to the respective interfaces, with the corresponding voltage and electric field distribution *center*. Voltage and electric field distribution in a classic dielectric material, as comparison *right*.

Despite the potentialities, EGOFETs have not been extensively used for these applications, even if some instances were reported: EGOFETs have been used to sense cell detachment (Zhang et al., 2017) or to detect analytes or biomarkers (Ricci et al., 2020), (Parkula et al., 2020) for example. In a recent review, Piro and colleagues (Piro et al., 2018) attribute this phenomenon to the fact that all the implementation currently reported in literature use a top-gate configuration while, in their opinion, a side-gated, fully printed EGOFET structure would be a more convenient approach. Unfortunately, a similar structure has not yet been proposed. In the next pages, the applications in the field of electrophysiology and metabolic activity monitoring will be described in more details, even though also in this case the number of works in this direction is limited. Its equations are the same used for conventional OFET, already described in section 1.4.

2.2.1 EGOFETs for electrophysiology

There are few examples of the application of EGOFETs for electrophysiology. In 2013, Cramer and his coworkers proposed an ultra thin pentacene-based device to record and stimulate neuronal networks (Cramer et al., 2013). In particular, they cultured murine neural stem cells directly on the semiconductor layer (without the addition of any molecules to promote cells adhesion) and measured the output current I_{DS} of the transistor for several days to monitor the evolution of the electrophysiological activity of the network during its formation. It resulted that a dense network developed onto the pentacene layer, with high interface capacitance also without the adhesion promoters, and that it was possible to stimulate and record extracellular activity only after the complete differentiation of stem cells. However, with this device it was possible to record only a population response i.e. *local field potentials* (LFPs), not a single neuron action potential, due also to the dimensions of the device, that is several order of magnitude bigger than usual electrodes. A curious application involving EGOFET is represented by the *Electrolyte Gated Organic Synapstor*, or EGOS, developed by the group of Desbief in 2016 (Desbief et al., 2016). This is a device that shows a plasticity-like behaviour due to the presence of gold nanoparticles at the interface organic semiconductor/gate dielectric interface, while the cells (i.e. human neuroblastoma cells) are not affected by the Nanoparticle.

Very recently, Kyndiah et al (Kyndiah et al., 2020) designed an EGOFET to record activity of human pluripotent stem cells-derived cardiomyocytes. This devise was produced on a flexible and biocompatible Kapton foil (75 μm thick), with channel width of 19680 μm and length of 30μm, using a polymer (polystyrene) as insulator and as active layer a blend

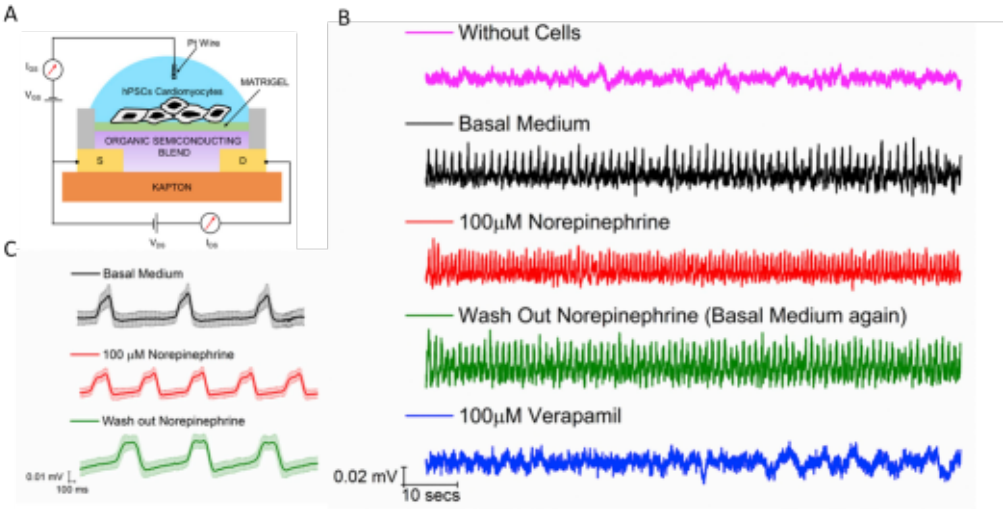

Figure 2.5 EGOFET for electrophysiological activity measurement of human pluripotent stem cells-derived cardiomyocytes. A) scheme of the EGOFET-based device used for the measurements; B) representative electrical recordings performed with the device in A) under different environmental conditions. The pink trace represents the recording in absence of cells, the black curves is recorded from cells immersed in basal medium, while red curve shown the cells activity after the addition of 100 μM of Norepinephrine is added to the basal medium. In the green curve the drug has been washed out and the culture is in basal medium again; finally, the blue curve is a recording after the addition of 100μM of verapamil. C) shape of extracellular AP obtained as average of 40 spikes under 3 different environmental condition. (Kyndiah et al., 2020).

of a small molecule (diF-TES-ADT) that was covered by matrigel to improve the adhesion of the cells to the OSC (figure 2.5 reports the EGOFET structure). To further prove that the recorded signals actually descend from cells' APs, the authors also modulate the cellular activity using drugs such as Norepinephrine [2] and verapamil [3]; they obtained action potential with a very reproducible shape, even if different from the one expected for extracellular potential of cardiac cells, as shown in figure 2.5, B and C. The causes of this difference are under investigation.

2.2.2 EGOFETs for metabolic activity monitoring

Also in this case, I did not find any application of EGOFET aimed at monitoring the metabolic activity of living cells, in none of the methodologies previously mentioned 2.1. The only indication that this structure could be used for similar purposes lies in the fact that some EGOFET have been used to detect pH variation in aqueous solutions, even though the authors

[2] Norepinephrine is a cardio-stimulant that acts on β-adrenergic receptors.
[3] Verapamil is a calcium blocker that acts as a cardio-relaxant

never declared the scope to move to cellular application. As an example, in 2011 an EGOFET which organic semiconductor is $\alpha 6T$ (i.e. α sexithiophene) has been presented as sensitive to pH variations in aqueous solution (Buth et al., 2011). In particular, the authors used 10mM PBS-buffered solution, and modified its pH by adding 0.2M if HCl or KOH solutions. It results a pH-dependence of the output current that causes a decrease of the current with decreasing pH, with a resulting pH sensitivity of 9mV/pH, that has been attributed to a the change of surface charge, in turn due to both the specific absorption of dissociated water ions or to protonation/deprotonation reactions. Unexpectedly, it was also found that the relation between I_{DS} and pH was linear for pH values up to 7, while for higher pH the devices appeared unstable; the reasons of this behavior were not fully understood.

2.3 Organic ElectroChemical Transistors

The last OFET-based device analyzed in this chapter is also the most commonly used in applications involving interfaces with living cells. It is the *Organic Electrochemical transistor*, or OECT, which is a three terminal device with a structure quite similar to the EGOFET, described in section 2.2. The idea of OECT was firstly developed by White and coworkers in 1984 (White et al., 1984). It consisted in three coplanar gold micro electrodes covered by polypyrrole, used as active material, while the substrate was a silicon wafer covered by a 0.45μm silicon oxide layer. By operating this device in an aqueous solution (precisely, in $CH_3CN/0.1M[n-Bu_4N]ClO_4$) with very low applied voltages (lower than 0.6V), they obtained transistor characteristics in which the turn on/off point is linked to the oxidation potential of polypyrrole. In particular, when V_G is lower than the oxidation potential, the polypyrrole behaves as an insulator and the device is off; on the other hand, when V_G became more positive than this potential, the device turns on. The authors also suggested that the properties of which, such as the threshold voltage V_{TH} and the switching times, can be adjusted by modifying the monomer used to prepare the polymer. After this first attempt, several other types of organic materials have been used as active layers, such as polyaniline, polythiophene and polycarbazole; but the real milestone in the evolution of OECT arrives with the adoption of the *poly(3,4-ethylenedioxythiophene) doped with poly(styrene sulfonate)*, commonly known as *PEDOT:PSS*. PEDOT:PSS is an heavily p-doped polymer that is easy to process (since it can be prepared in aqueous solution, it can be deposited by drop casting, spin coating or inkjet printing), and is highly conductive, biocompatible and chemically stable (Wen and Xu, 2017). Since the PEDOT:PSS polymer is conductive when gate voltage is not applied ($V_{GS} = 0$), it leads to the fabrication of normally-on OECTs. The main

difference between OECTs and EGOFETs lies in the working principle: while in EGOFETs the channel modulation is caused by the EDLs formed at the Gate electrode/electrolyte and electrolyte/semiconductor interfaces following the application of a Gate voltage (for further information please refer to section 2.2), in OECTs the application of V_G leads to the injection of ions from the electrolyte into the OSC or vice-versa, and these ions cause the doping/dedoping of the semiconductor itself, as shown in figure 2.6.

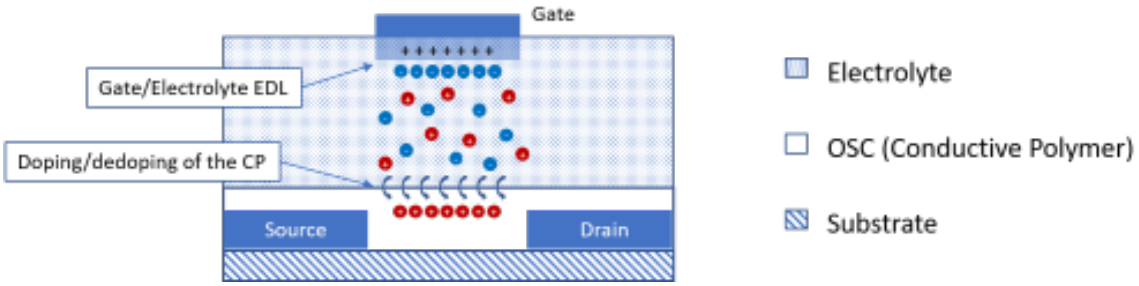

Figure 2.6 OECT sketch and working principle. The application of a gate voltage favours the doping/dedoping of the conducting polymer, thus modulating the output current I_{DS}. The doping/dedoping mechanism involves the whole volume of the semiconductor layer, and leads to higher transconductances, that in turn provokes better sensitivities and low supply voltages.

This is the practical consequence of the use of different organic materials; in fact, in OECTs usually the so called *conducting polymers*, CPs, are employed. These materials have both electronic and ionic conductivity, i.e. they can transport either electrical charge carrier (holes in case of PEDOT:PSS) or ions; property that makes the OECT an ideal converter of ionic current into electronic current, and consequently an ideal instrument for biological applications. As also highlighted by White, OECTs can be operated at ultra-low voltages (i.e. below 1V), thus avoiding the occurrence of electrochemical reactions; in addition they present very high transconductance (Kergoat et al., 2012). Indeed, for OECTs the transconductance g_m can be expressed as:

$$g_m = \frac{\partial I_D}{\partial V_G} = (\frac{W}{L})\mu\, d\, C^* (V_G - V_{th}) \tag{2.1}$$

where W and L are the channel width and length, respectively, μ is the charge carriers' mobility, d is the thickness of the CP layer, V_{th} the threshold voltage, and C^* is its volumetric capacitance, due to the fact that in this case doping/dedoping takes place also in the bulk of the CP layer, thus determining a linear scaling of the capacity (and consequently of the transconductance) with the volume. A higher transconductance value leads in turn to a bigger amplification of any little signal that perturbs the potential drops between the gate and the

channel, as for example could be the electrical activity of excitable cells plated on top of the channel, thus increasing the sensitivity of the device to this little signals. Thanks to all the just mentioned properties, OECTs have been vastly used in applications requiring interfacing with living cells. In particular, OECTs has been used in two different configurations, that differ for the position of the gate electrode; indeed, beside the so called *standard* or *vertical* configuration, in which the gate electrode is usually an Ag/AgCl electrode inserted in the electrolyte solution, there is also the *planar* configuration, in which the gate electrode is coplanar with the source and drain. The latter structure is compatible with low-cost and high-throughput production processes, and does not need the external Ag/AgCl gate electrode. Its applications in both the configurations, involved electrogenic and non-electrogenic cells, and as an example included the evaluation of tissue integrity, a field pioneered by Dr. Owens (Jimison et al., 2012) and extensively investigated in the last decade (Romeo et al., 2015). Between the other interesting applications, we found the distinction between healthy and tumor cells co-cultured on the same OECTs' array (Yeung et al., 2019), the wound healing monitoring of a cell culture (Curto et al., 2017), the impedance sensor for 3D structure such as spheroids (Curto et al., 2018) and cytotoxicity (Salyk et al., 2017) (Decataldo et al., 2020). In addition, the possibility of functionalize the surface of the gate electrode made it suitable as a sensor to specific compounds, such as N-glycans present on the surface of human breast cancer cells (MCF-7) (Chen et al., 2018). In the following sections, the applications of OECTs for electrophysiology and for metabolic activity monitoring will be thoroughly described.

2.3.1 OECTs for electrophysiology

In comparison with the numerous publications involving non-electrogenic cells, the effort made to investigate the applications concerning electrogenic cells is quite modest, but nevertheless it produced a good number of results. The first example in which an array of PEDOT:PSS based OECTs with *in vitro* excitable cells have been proposed in 2015 (Yao et al., 2015). The authors fabricated the OECTs on both rigid (glass) and flexible (plastic) substrates; in this case, the recorded signals origin from the ion exchange between the inside and the outside of HL-1 cells (seeded directly on OECTs' active layers) caused by the action potential, that modulates the I_{DS} of the transistors, while V_{GS} and V_{DS} are kept constant. Both rigid and flexible arrays recorded well defined spikes with good SNR. A year later, a 16-channels array of OECTs has been used to record the activity of primary neonatal Sprague-Dawley rat cardiomyocytes and demonstrated good stability and robustness (Gu

et al., 2016). Since several channels simultaneously detected the signal from the network with a good signal-to-noise ratio, the authors were able to study the propagation of the APs inside the array, and consequently inside the network, finding that the direction of the propagation changes after the addition of chronotropic drugs such as isoproterenol (ISO) to the medium. More recently, the same group (Gu et al., 2019) exploited 3D cultures, i.e. spheroid microtissue of primary cardiomyocytes, to validate their OECT array. They noticed that after being seeded, the spheroid adheres to the device, and the external parts expanded and thinned (see figure 2.7A); they were also capable to observe some feature of APs that primary cardiomyocytes monolayer usually do not show, such as different shapes of the signal generated by the different parts of the spheroid, that were identified by different OECT of the array. In particular, as can be seen in figure 2.7B the center of the spheroid generates a different signal than the sides, where it expanded after being plated; finally, the boundary of the two areas emits a third kind of AP. In the same paper, also a proof-of-concept of a 64-channel array has been introduced, in order to enhance the spatial resolution and match the one of the most commonly used micro electrode arrays (figure 2.7C).

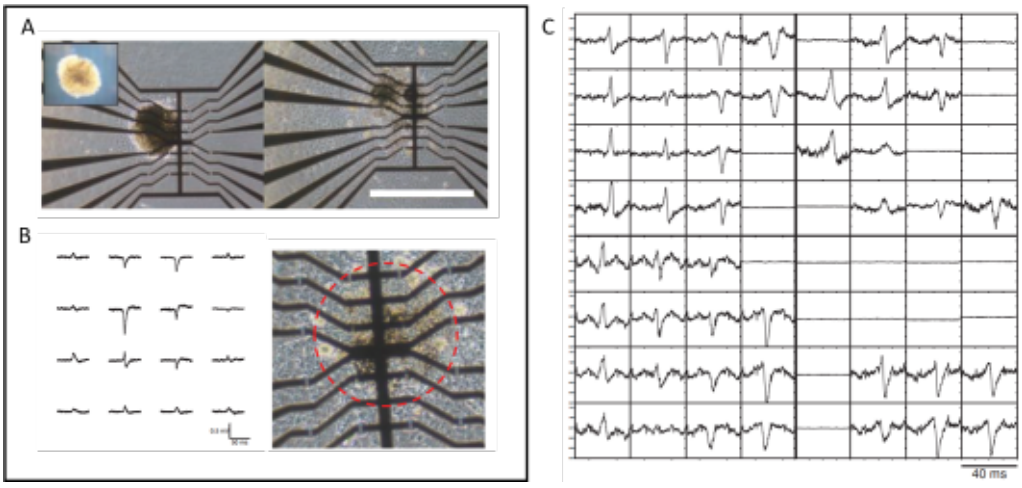

Figure 2.7 Images of the spheroid seeded on the array from 1 day *left* and 6 days *right*, while the inset shows the suspended microtissue. B) electrophysiological signals recorded from 16 OECTs array, displaying the 3 different shapes of APs: with a positive peak (external area), with a negative peak (central area) and with biphasic wave at the boundaries between the previous areas *left*, and an image of the spheroid at the recording time, while the red circle divides the expanded area from the core of the spheroid. Panel C represents a representative recording from a 64-channels array. (Gu et al., 2019).

Also OECTs with interdigitated source and drain electrodes have been proposed: in the 2017 a 16 interdigitated OECT array in a common source recorded APs generated from HL-1 cardiac cells (Hempel et al., 2017); the following year (Liang et al., 2018), HL-1 have

been plated also on a 27-channel, flexible array of interdigitated OECTs which properties have been later improved by the same group (Liang et al., 2019) by investigating the right set of design parameters such as number, width and length of electrodes' fingers (i.e. the extrusions of the interdigitated electrodes), as well as the channel length. In this way, they were able to record HL-1 electrophysiological signals with a SNR up to 18, and considerably higher than in the first work. Another appealing application of OECTs is the development of delaminating depth probes, designed for *in vivo* employment but firstly validated *in vitro* on a hippocampus preparation. This probe has three OECTs with a PEDOT:PSS channel and an adjacent PEDOT:PSS electrode embedded in the mechanically neutral plane of a flexible, conformal 4μm of Parylene C layer that works as flexible substrate and that - to give it sufficient strength to penetrate the brain - is weakly attached (by van der Waals forces) to a stiffer "shuttle" layer from which easily detaches after being in the targeted brain region. The electrode can be used as gate electrode but also to stimulate, when monophasic current pulses have sourced from the transistor's channel and the electrode acts as local sink in order to deliver a stimulation as local as possible. With this device, the authors delivered targeted stimulations to specific neuronal populations, such as CA3 region, and recorded the response on another region, such as CA1, in keeping with the projection zone from CA3 to CA1.

2.3.2 OECTs for metabolic activity monitoring

OECTs applications for metabolic activity monitoring are related principally to the control of cellular analytes and byproducts, such as glucose or lactate. Rarely this measures are carried out *in vitro*, i.e. with the cells in direct contact with the devices, but usually are performed *ex vivo*, i.e. the OECTs are put in contact with a solution (usually the culture medium) collected from the cell culture; albeit also in this case it is not present a cellular interface, these attempts represent a step forward the really online monitoring of metabolic parameters, and are also an advancement with respect to the works described in the previous sections of this thesis as in sections 2.2.2, 2.1.2 and 1.4.2 in which devices were only been tested with commercially available products. As an example, a PEDOT:PSS-PVA based OECT has been used to detect lactate and glucose by functionalizing the surface of the gate electrode with an enzyme trapped inside a photo-crosslinkable hydrogel and platinum nanoparticles (Strakosas et al., 2017). Briefly, the enzymatic reaction starting from glucose/lactate produces H_2O_2, that is then catalysed by nanoparticles producing an electron that can travel to the OECT's channel thus modulating the output current. The author tested this device with

complex media where cells had been cultured, and demonstrated that can coherently monitor metabolites concentrations even when cells are treated with cytotoxic drugs.

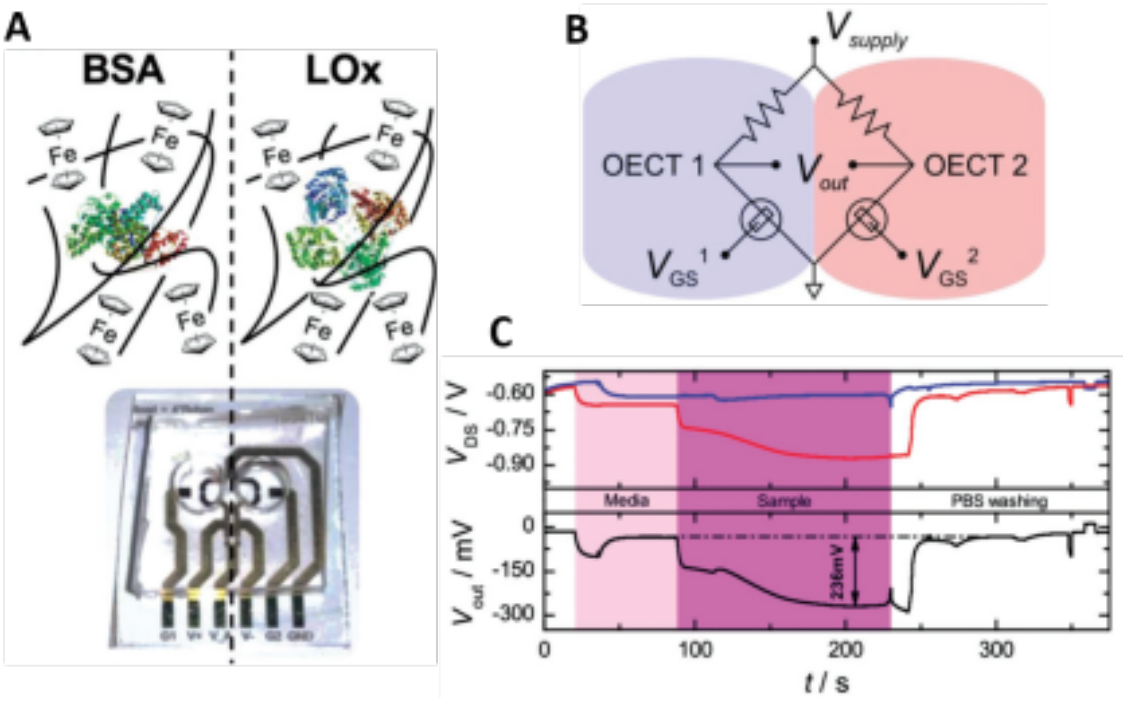

Figure 2.8 Reference-based sensor for lactate detection in tumor cells. A) picture of the device, and sketch of the procedure for functionalization: only one OECT is functionalize with Lactate Oxidase (LOx) to detect lactate, while the other is functionalized with Bovine Serum Albumine (BSA), a non specific protein. B) Scheme of the Wheatstone bridge sensor circuit: the load resistor are connected to the drain side of OECTs, and the two branches of the bridge (which transistors have separated electrolytes) are depicted in red and blue. C)Recording of a lactate analysis experiment: the upper graph shows the V_{DS} of the two transistor separately (the red trace represents the sensor signal, the blue one the reference) , while the lower graph displays the V_{out} signal. The first addition of fresh media (light pink area) is necessary to set the baseline, after which the real sample (dark pink area) is added; finally, the devices are washed with PBS solution. Figure taken by (Braendlein et al., 2017).

In the same year, a second example of metabolic sensor, designed to detect lactate concentration with an intrinsic subtraction of the background noise, has been proposed (Braendlein et al., 2017). This device is a reference-based sensor chip, developed by integrating 2 OECTs in a Wheatstone bridge configuration, in which only one transistor is functionalized with the Lactate Oxidase (LOx) enzyme to detect lactate, while the other is functionalized with non specific protein (in particular Bovine Serum Albumine, BSA) and acts as reference. The device has been validated using complex media hailed from healthy Peripheral Blood Mononuclear Cells (PBMCs) and from non-Hodgkin's lymphoma cells, and it results that

healthy cells produce less lactate than tumor, thus confirming the intrinsic enhanced metabolic activity of the latter.

Part II

Section Two

Chapter 3

Development of an OCMFET-based system for excitable cells studies

In the previous chapters, the most popular techniques and devices used for *in vitro* electrophysiology and biosensing have been briefly introduced. The evolution of the field of bioelectronics from the ancient times to now has been highlighted, together with the increasing interest gained by other parameters, in addition to electrical activity, to obtain more and more complete information about the state of cell cultures, making themselves fundamental in several analyses such as pharmacology and cytotoxicity, but also in order to better understand how cells interact with each other to form complex systems. It has been seen that a big effort has been put into developing always new and innovative devices, and that some of the presented architectures can be used to create sensors for different features, thanks to as an example the possibility of functionalizing their active area or their gate electrode. Nevertheless, it is impossible not noticing the big lack of systems embedding different types of sensors to perform simultaneous recording of various features of cell cultures. An example of such a system is found in section 1.4.2: the *Cell Monitoring System* cited by Baumann and coworkers in (Baumann et al., 1999), that allows parallel and non-invasive measurement of different parameters from cellular systems by the use of micro-sensors; but as far as I know there are very few cases in literature.

With the third chapter, we will get to the heart of this work of thesis, whose main goal was precisely to create an array of sensors capable to monitor simultaneously more parameters of a cell culture, such as electrophysiological and metabolic activities. To this end, a peculiar OFET-based structure called *Organic Charge Modulated Field Effect Transistor*, OCMFET, has been employed, because of its several crucial advantages. In the first part of the chapter, the OCMFET will be introduced: its OFET-structure will be illustrated, together

with its history and the previous applications to demonstrate its flexibility, that makes it suitable for designing different kinds of sensors. Between them, one essential application for our purposes will be highlighted, i.e. the design of an OCMFET-based detector for electrophysiological activity recording. After that, the results of this work of thesis will start to be described with the design of a metabolic sensor based on OCMFET have been depicted, that with its functionalization process definitively lays the foundation for the creation of the MOA for simultaneous sensing. Finally, we will show how the array of sensors has been developed for the simultaneous monitoring of two parameters of cell cultures. In particular, the major investigation's lines concern the choice of the floating gate materials, to find the best trade-off between ease of fabrication, transistor's performances and flexibility in terms of sensing areas functionalization. In parallel, the MOA's layout has been modified to match the improvements made on the side of the readout electronics; finally, the implemented procedure to functionalize both the kinds of sensors on the same substrate has been described, along with the observed issues and the proposed solutions.

3.1 The Organic Charge Modulated Field Effect Transistor

The first version of the Organic Charge Modulated Field Effect Transistor was actually a solid state device (called Charge Modulated Field Effect Transistor). It consisted in a double gated MOSFET in which one of the gates was floating, while the second one, called *control capacitor*, was coupled with the floating gate through a capacitor, as shown in figure 3.1A, thus allowing to set the transistor's working point. To convert this structure into a sensor, an active area was obtained by removing from a section of the floating gate the passivation layer until the underneath surface is reached. On the exposed active area, a thin layer of a second material, that is called *spacer* and must be carefully chosen to bound the charge to be sensed, was successively deposited. This device has been presented as a charge sensor for biological applications and its working principle has been extensively analyzed by their designers (Barbaro et al., 2005). Since the first application of the CMFET as a detector for DNA hybridization, the device showed promising properties: it was a label-free charge sensor, fully compatible with CMOS fabrication technique, that did not need of any external reference electrode. Thus, it could be used as a biosensor lowering the production costs and increasing the integration capabilities. Shortly after, the same group proposed the first organic version of the OCMFET, used as a pH sensor (Bonfiglio et al., 2007). It was a *free-standing*

device, in which the dielectric layer, i.e. a Mylar flexible film, acts also as substrate while the electrodes are placed on one side of the substrate and the floating gate on the other, as shown in figure 3.1B. It had the same structure of the silicon version, but its active area was functionalized with NH_2 groups to make it sensitive to pH variation; indeed, it actually displayed a dependence of the conductivity of the device from the pH of the aqueous solution in contact with the active area, as depicted in figure 3.1C. Nevertheless, this device needed to high supply voltages to be operated.

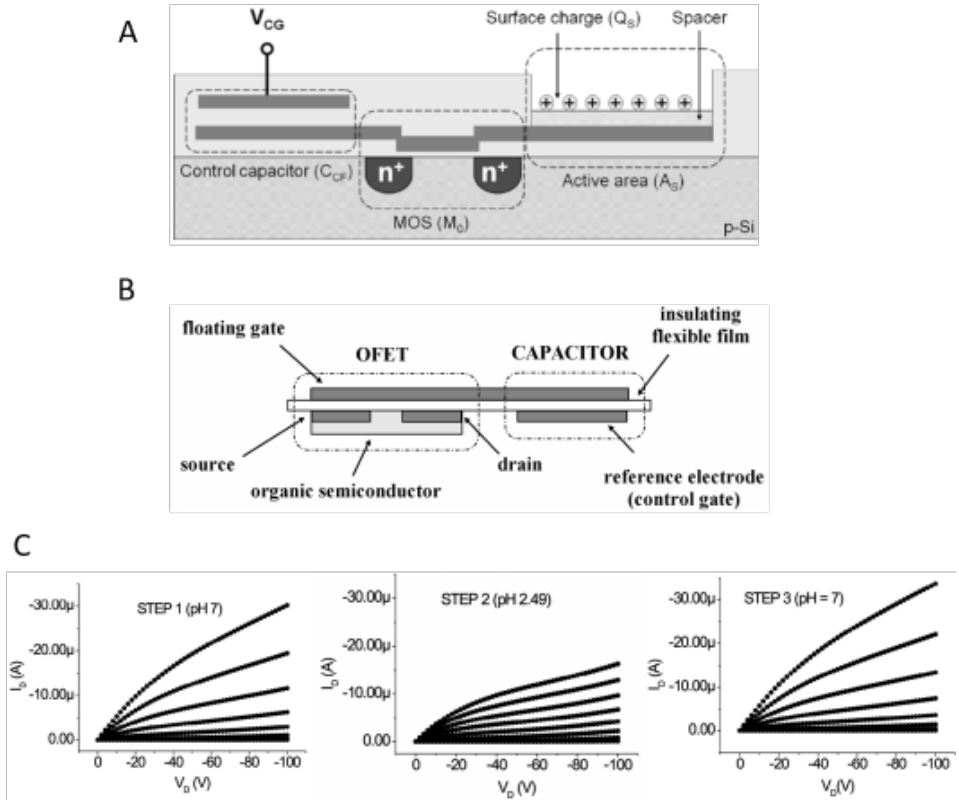

Figure 3.1 First CMFET and OCMFET structures. The first version of OCMFET was the solid state CMFET represented in panel A, in which it is possible to distinguish the control capacitor, the MOS and the active area (Barbaro et al., 2005). Shortly after, the first organic version has been presented, in the free-standing configuration shown in panel B. Also here it is possible to identify the different regions forming the structure. Panel C reports the first measurements performed using the free-standing OCMFET as a pH sensor: the maximum current value changes with the pH of the solution, and these changes are reversible (Bonfiglio et al., 2007)

.

In 2012, also this issue was overcome by Cosseddu and his colleagues (Cosseddu et al., 2012) that designed a low voltage version of OCMFET by using a gate dielectric made of a combination of an ultra-thin layer of metal oxide (usually 6nm of Al_6O_3, since aluminum is the most commonly material used as Floating Gate electrode) and a second 25nm layer of

Parylene C. With this structural change, the device can be operated at voltages lower than 1V. The last crucial step toward the realization of the current OCMFET corresponded to the introduction of the *self-aligned* structure (Lai et al., 2013). In this architecture, a new method has been employed to reduce the overlap between source/drain and gate electrodes, and consequently reduce the parasitic capacities: in particular, this result is obtained by a photolithographic process that can be performed using standard photoresists, without additional chemical treatments. The outcomes were very encouraging: by comparing the characteristics of self-aligned OCMFET with other fabricated with a standard technique, it was found that this process reduces the parasitic capacitances, as well as the leakage currents, of more than one order of magnitude. Moreover, several transistor characteristics as the I_{ON}/I_{OFF} ratio, current modulation and saturation were improved. But the most important effect of the reduction of overlap is the incredible increase of the cutoff frequency, from 100Hz in standard device to the 100kHz for the self-aligned, that allows to use this OTFT also for recording relatively high frequency signals.

3.1.1 OCMFET working principle

Rearranging the definition given in the previous lines for the CMFET, the OCMFET is a OFET with two gates, one of which is elongated, and in its distal end contains the sensing area. This gate is kept floating when the device is used as a sensor, even if it is possible to contact it to fully characterize the device in the previous phases. The second gate, through which the transistor working point is set, is called control gate and is coupled through a capacitor to the floating; the OCMFET architecture is depicted in figure 3.2A. While for the floating gate several materials can be used, the source, drain and control gate electrodes are usually made of gold, and the most commonly used organic semiconductor is the p-type TIPS-pentacene; to have a low voltage transistor, the dielectric is the combination of a thin metal oxide layer and a Parylene C film, as previously described.

The working principle of the OCMFET is based on a modulation of the transistor channel, caused by a charge variation occurring in the close proximity of the sensing area, as displayed in figure 3.2B and C, that in turn affects the threshold voltage. More in details, the working point of the transistor is set by imposing negative (in this case, since TIPS-pentacene is a p-type semiconductor) control gate and drain voltages V_C and V_D with respect to the source; in this situation, if a variation of charge density occurs near the sensing area, it causes a charge reorganization inside the floating gate that leads to a modulation of the conductivity of the transistor channel and results in a variation of the output current. In order to extract

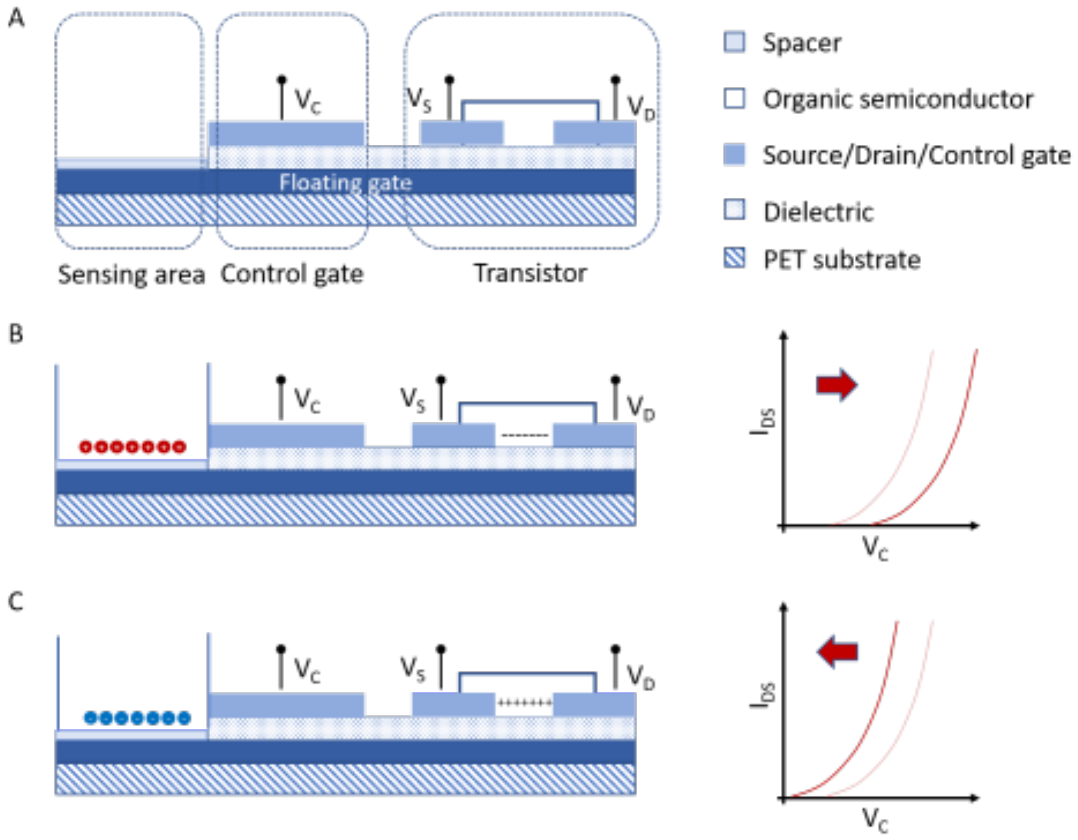

Figure 3.2 OCMFET structure and working principle. Panel A shows the architecture of the OCMFET, underlining the different parts, i.e. sensing area, control gate and OTFT. Panel B and C depicted its working principle: the presence of positive (panel B) or negative (panel C) charges in close proximity to the sensing area leads to a rearranging of the charges into the floating gate, thus provoking a variation of the threshold voltage.

the expressions of the most important parameters, it is possible to start writing the charge conservation principle applied to the floating gate:

$$Q_{TOT} = C_{CG}(V_F - V_C) + C_{SF}V_F + C_{DF}(V_F - V_D) \tag{3.1}$$

where $Q_{TOT} = Q_0 + Q_{SENSE}$, with Q_0 that represents the charge intrinsically entrapped inside the floating gate and Q_{SENSE} that is the charge capacitively coupled on the sensing area. C_{CG}, C_{SF} and C_{DF} are the capacitances between floating gate and control gate, source and drain respectively, while V_F, V_C and V_D are the floating gate, control gate and drain voltages. From this equation, it is possible to extract the expression of the floating gate voltage as follows:

$$V_F = \frac{C_{CG}}{C_{TOT}} V_C + \frac{C_{DF}}{C_{TOT}} V_D + \frac{1}{C_{TOT}} (Q_0 + Q_{SENSE}) \tag{3.2}$$

where $C_{TOT} = C_{CG} + C_{SF} + C_{DF}$

In the previous equation, most of the parameters depend on the device layout (such as the capacitances) or are externally set (as the drain and control gate voltages); the only term that can vary during the experiment, thus leading to a variation of the threshold voltage, is the last one:

$$\Delta V_{TH} = \Delta V_F = -\frac{\Delta Q_{SENSE}}{C_{TOT}} \tag{3.3}$$

3.1.2 OCMFET- based sensors

The device described here has several remarkable features that make it a very good candidate for many applications:

- thanks to its working principle, it is able to detect both positive and negative charges onto the sensing area, that will affect in opposite ways the output current;
- because of its structure, the OTFT is kept far from the analyte solution, thus preventing both the degradation of the transistor and also unwanted reactions between the semiconductor and the solution;
- it is in principle sensitive to every event that causes a charge variation nearby the sensing area.

Actually, it has already been employed to design several kinds of sensors. The first example of applications, also chronologically, is the sensor of DNA hybridization: as previously mentioned, it was the use with which the silicon version of OCMFET has been tested in 2006, but since then this sensor has been considerably improved. Indeed, in 2018 a new version of OCMFET in which hairpin-shaped oligonucleotides were immobilized on the sensing area as probes has been proposed (Napoli et al., 2018), and it showed the capability to detect DNA hybridization with a limit of detection (LOD) comprised between 10 and 100pM, distinguishing between complementary and not complementary target sequences.

A second application that started with the early versions of OCMFET and that has been improved in the next years is the OCMFET-based pH sensor: its presentation dates back to

the introduction of the Organic CMFET in its free-standing configuration (see figure 3.1B and C). Also in this case, from then on several studies have been performed and different functionalizations have been investigated: besides the anchoring of NH_2 groups onto the sensing area (Caboni et al., 2009) and (Demelas et al., 2013), has been considered also the possibility to exploit the metal oxide's (specifically, of Aluminum Oxide's) binding sites for the protonation and thus for the detection of H^+ ions (Spanu et al., 2013) and (Spanu et al., 2015b). More recently, a new OCMFET-based pH sensor has been proposed (Spanu et al., 2017), that is made sensitive to pH variations thanks to the deposition of a thin film of O_2 plasma activated Parylene C. Indeed, while in its pristine state Parylene C acts as an insulator and ion-blocker material, an oxygen plasma treatment causes the exposure of functional groups such as $C=O$, $C-O$, $O-C=O$ and CO_3 that can protonate and deprotonate in response to the H^+ ions concentration, thus making the Parylene sensitive to pH.

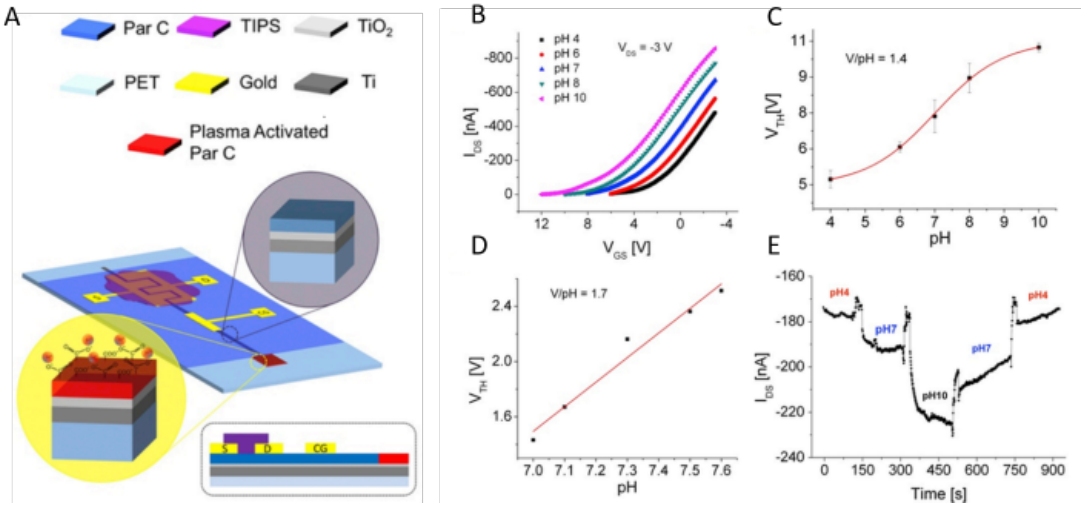

Figure 3.3 OCMFET for pH measurements. The structure of OCMFET-based pH sensor and the materials from which is composed are shown in panel A. Par C means Parylene C, TIPS stands for TIPS-pentacene, the organic semiconductor. Panel B shows how the transcharacteristic (and consequently the threshold voltage) shifts when the sensing area is put in contact with solutions at different pH, while in panel C is displayed the calibration curve of the sensor in B, in which the sigmoidal behaviour is clearly visible; the device is characterized more finely in the pH range between 7-7.6, as shown in panel D. Finally, panel E shows the dynamic characterization of the device, that distinguishes in a reliable and reproducible manner between 3 different pH values. (Spanu et al., 2017)

The obtained sensor has been tested using buffer solution at pH 4, 6, 7, 8 and 10 (figure 3.3B) and shows, as displayed in figure 3.3 C, a sigmoidal behaviour with a linear response

between pH 6 and 8. Its sensitivity is about 1.4V/pH, much higher than the Nernst limit [1] (probably due to the exploitation of the intrinsic amplification effect of the charge induced on the sensing area), while in the linear region it can discriminate a minimum pH interval of 0.1 (see figure 3.3C). The dynamic characterization of the device additionally demonstrated that the OCMFET response has a good reproducibility and repeatability, as shown in figure 3.3E. Furthermore, this type of functionalization has the advantage that, since Parylene C is used also for the insulating layer, no additional fabrication steps are required to produce it.

The OCMFET structure has been used also to generate tactile sensors. In 2016, an OCMFET which active area is connected to a PVDF [2] capacitor was found able to reliably transduce applied pressures with a limit of 300 Pa in a wide range of frequencies (Spanu et al., 2016). Two years later, a multimodal sensor for simultaneous temperature and force/pressure measurements has been proposed (Viola et al., 2018), in which the piezoelectric material was directly glued (or spin coated) on the OCMFET's sensing area and the overall thickness of the device was around 1.2 μm, allowing it to conform to any surface.

3.1.3 OCMFET for electrophysiology

Between the previously investigated applications, the one that has more importance for this project is the sensor for electrophysiology. Indeed, measuring electrophysiological signals is substantially different from recording biosignals such as pH variation or DNA hybridization, since they are at relatively high frequency and are produced by mature cell culture plated in direct contact with the electrode. Consequently, to effectively detect the electrical activity of living cells a sensor has to fulfill some additional requirements, such as being capable to record high frequency signals, using low supply voltages to avoid damaging the culture itself and being designed to have a long-term contact with aqueous solution. In addition, this devices have to be stored for several days into an incubator, i.e. a very harsh environment for organic semiconductors, in order to maintain the plated cells in physiological conditions and give them time to grow and form a mature network. Nevertheless, the OCMFET is a good candidate also for this application; in fact, as we previously introduced (please refer to section 3.1), thanks to the self-alignment technique, it has a cutoff frequency of 100kHz; moreover, using the two layers insulator it is possible to operate it with very low voltages. Finally, thanks to its peculiar structure, the sensing area where the aqueous solution is confined, is distant from the transistor; consequently, it is possible to protect the organic semiconductor from

[1] the Nernst limit is a sensitivity limitation to 59mV/pH at 25°C, that is typical of ISFETs in their classical configuration

[2] PVDF, or *polyvinylidene fluoride*, is a piezopolymer

moisture and also encapsulate it if necessary. Thanks to all these features, the OCMFET has been actually used to create a sensor for electrophysiology, that presents no functionalization of the sensing area: the spacer has been removed, and the portion of the floating gate metal is directly exposed to the liquid environment. Firstly, it was tested using cardiomyocytes-like HL-1 line cells (Spanu et al., 2013), later primary rat cardiomyocytes and neurons have been investigated (Spanu et al., 2015b) and (Spanu et al., 2015a). In particular, in the last two works the authors utilized an array of OCMFETs, in order to record the activity of the network in more points, thus matching what have been done with the other types of sensors. The firstly proposed Micro OCMFET Array, or MOA (shown in figure 3.4A and B), was an array of eight identical OCMFET fabricated onto a 175 μm thick polyethylene terephthalate (PET) substrate which dimensions are 50 x 50 mm (the same of classic MEAs produced by Multi Channels Systems, to guarantee the compatibility with the standard ground plates commercialized by that company). Each transistor had a metallic floating gate (made by aluminum or titanium) on which was grown a film of native oxide to form the first layer of the dielectric, while the second one was a 30-50 nm of Parylene C. Gold source, drain and control gate contacts are produced with a self-alignment process, while TIPS pentacene is drop-cast directly on the device channel as Organic Semiconductor. The so obtained transistor has a W / L ratio of about 650. A glass ring glued onto the substrate delimited the area in which cells are cultured. On the same PET substrate, also 8 micro-electrodes have been fabricated, to give a comparison of the recorded action potentials.

This array was tested firstly with primary cultures of cardiomyocytes from rat embryos, thus detecting the occurrence of the action potentials also when their frequency varied due to slow temperature changes of the culture's medium, or to positive or negative chronotropic agents such as 100 μM of Norepinephrine[3] and of Verapamil[4] (a positive and a negative chronotropic compounds, respectively) that were added to the solution to pharmacologically modulate cellular activity, as shown in figure 3.4C. The device was further investigated also with rat striatal cells (a type of neuronal cells), as depicted in the same figure 3.4D.

3.2 OCMFET for metabolic activity monitoring

Starting from the results concerning the detection of pH variations in aqueous solution with the device presented in (Spanu et al., 2017) (and briefly described in section 3.1.2), and considering the super-nernstian sensitivity of this OCMFET-based detector, was born the

[3]Norepinephrine is a cardio-stimulant that acts on β-adrenergic receptors.
[4]Verapamil is a calcium blocker that acts as a cardio-relaxant.

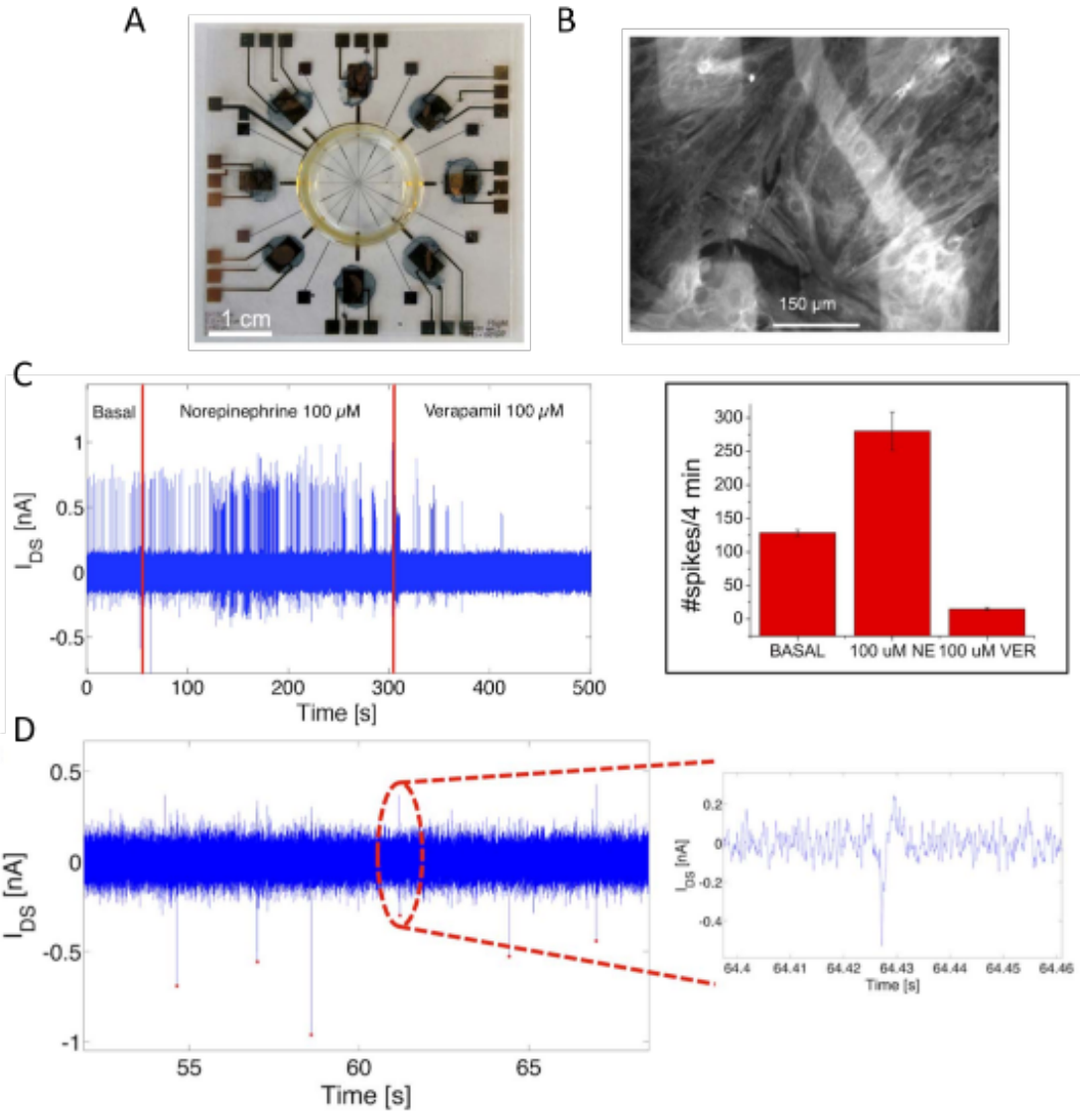

Figure 3.4 OCMFET for electrophysiological recordings. The electrophysiological recordings were performed using a MOA such as the one depicted in panel A (panel B shows an enlargement of the culture chamber with cultured cardiomyocytes. The cultures was fixed after a recording session). These devices were able to record the action potentials of cardiomyocytes during pharmacological experiments (panel C,left), in which their frequency greatly changed, as shown in the bar plot of the cumulative number of APs during the various phases (panel C,right). During preliminary experiments, they recorded also spikes of rat striatal cells (panel D,right) with good shapes, as demonstrated by the enlarged image of a neuronal spike recorded extracellularly by an OCMFET, represented in panel D,right (Spanu et al., 2015a).

idea of applying this type of sensor to monitor cell metabolism through the pH variations due to the accumulation of acidic byproducts that occur in the extracellular environment. Indeed, the materials interfacing with living cells are the same already used in the sensors

for electrophysiology, so they are proved to be biocompatible. In addition, the very high sensitivity increases the possibility to detect the very small variations caused by cells cultures. After having assessed that the functionalization of the O^2 plasma-activated Parylene C film of the sensing area allows for stable monitoring of the H^+ ions concentration for a fairly long period, the OCMFET-based pH sensor has been adapted to the new application.

In order to demonstrate the suitability of this approach to cells monitoring, the functionalization process described in (Spanu et al., 2017) is applied to a MOA specifically modified for this application; i.e. in which only two OCMFET-based sensors have been operated, since the employed readout electronics presented two channels specifically designed to filter low-frequency signals such as pH (for further information refer to Appendix B). Their architecture has been modified to obtain sensors of metabolic activity: the sensing areas have been enlarged up to $4.5x10^{-2}cm^2$ and, besides first Parylene C layer that acts as dielectric, a second thicker film (approximately of 600nm) has been deposited. Indeed, the high power O^2 plasma treatment employed to activate Parylene C (i.e. to make it expose the functional groups) also etches the film: thus the overall Parylene C layer of 750nm (150nm of dielectric and 600nm of additional film) is selectively thinned down to ≈300nm on the sensing areas following the plasma treatment. This further layer can be eventually used to encapsulate the OCMFETs, to protect them from moisture and oxygen, thus safeguarding the semiconductor's performances.

The experimental results obtained using these sensors will be described in details in section 4.1, while more details can be found in (Spanu et al., 2018).

3.3 MOAs for simultaneous sensing of electrophysiological and metabolic activity

As previously discussed (see section 1.4), cells react to external stimuli activating different signalling pathways in parallel, thus in order to better interpret their behaviour can be useful to measure simultaneously and in a non-invasive way several features. Among these, the pH value is one of the most interesting to monitor during electrophysiological applications, since cells are particularly sensitive to the variations in hydrogen ion's concentration occurring in the culture medium, and in turn local pH changes can be ascribed to their metabolic activity. On the other hand, OCMFET seems to have a particularly adapted architecture to this purpose, because of all the favorable properties previously listed (see section 3.1.2); among the others, we have:

- the possibility to sense both positive and negative charges near to the sensing area, that allows the OCMFET-based sensor to correctly reproduce also biphasic signals;
- the physical separation between the transistor and the sensing area that allow to limit the well-known stability loss of organic semiconductors when in contact with oxygen or moisture;
- the lack of the reference electrode in solution, that is particular interesting in applications involving living cells.

In particular, the most important characteristic that allows to design an array which embeds different sensors is the capability to sense each event that provokes a charge variation near to the sensing area, provided that it is correctly functionalized. In fact, this means that it is in principle possible to develop a matrix of OCMFETs that differ for geometrical parameters and for the sensing area functionalization, thus that can be produced without excessively increase the complexity of the fabrication process. Starting from these premises, we started to develop a MOA for simultaneous electrophysiological and metabolic activity monitoring. The main idea was to create a sort of lab-a-chip to gain more information on electrogenic cell cultures during *in vitro* experiments, suitable as an example for toxicological or pharmacological experiments. To this end, the fabricated MOA should be disposable, in order to allow for fast examinations without the need of sterilization procedures and instrumentation; for the same reasons, it should be low cost. Furthermore, it should be transparent to allow the researchers to inspect the state of the cultured cells through a microscope (a consolidated practice in the field of biology), and finally it should be flexible. The latter requirement it not fundamental for in vitro experiments, but became critical for *in vivo* applications, that can be a clear future perspective for this technology. Obviously, this means that the involving devices should measure very different signals, that have different frequencies, different range of variation and so on. We begin from the first layout of Micro OCMFET Arrays already introduced, that were similar to the one presented in figure 3.4A, and already described in section 3.1.3: they were fabricated on a substrate of 5x5cm, and their contacts were aligned with the outer borders of the substrate, while the sensing areas of all the sensors converge in a little area in the center, circumscribed by the ring that delimits the culture's chamber. In the following paragraphs, the investigated strategies for the design of the MOA for simultaneous measurements, along with the chosen solutions are reported.

3.3.1 Choice of the Floating Gate material

The choice of floating gate material is substantial since it influences the transistor operation but it constitutes also the sensing area of the sensor itself. For the investigated purposes, since as previously mentioned in OCMFET-based sensors for electrophysiology the sensing area is directly exposed to the culture medium, this material must be biocompatible. As earlier discussed, the floating gate of OCMFET-based sensors for electrophysiology was made of titanium, because of its biocompatibility and its capacity to form the native oxide layer required for the realization of the combined dielectric that guarantees low voltage devices. Unfortunately, titanium has also some important drawback, since it evaporates at very high temperatures (its melting point is 1668°C, while aluminum's melting point is 660°C and gold melts at 1064°C, as an example). This makes it tricky to deposit by thermal vacuum deposition also because reaching high temperatures leads the plastic substrates (used to obtain transparent and flexible devices, as already discussed) to easily deform and this has repercussions on the evaporation itself, that can result non homogeneous, and to the device performances in general. Consequently, the fabrication protocol can be continued only on a fraction of the evaporated substrates, thus provoking wastefulness of materials and time. In this research project, besides titanium also the possibility to use other materials for the fabrication of the floating gate has been investigated. In particular, Gold and a combination of Aluminium and Titanium have been tested.

OCMFET with Gold Floating Gate

The first material to be tested was gold, for several reasons: firstly, it is possible to functionalize gold with many different approaches, including the use of thiols that bind gold with a very good affinity and can be used to bind several different functional groups, and consequently to make the device sensitive to different compounds. This could be a precious advantage both to investigate the better solution to design a performing metabolic sensor, and also in the case of we should decide, as a future perspective, to add other OCMFET-based sensors to complete the lab-on-a-chip device. Secondly, the gold sensing area could be useful for other applications, such as the realization of 3D structures (that are usually made of gold and grow on gold surfaces) for the study of 3D cultures or brain slices. Finally, using a single metal for all the metal layers of the device simplifies the fabrication process. A previous OCMFET-based with a gold floating gate has already been proposed as a sensor for pH and DNA hybridization (Demelas et al., 2013); in this case, a very thick layer of Parylene C (1.5 μm) was used as dielectric, thus the transistor needed to be operated at high

voltages. The devices produced during this project have a dielectric layer of approximately 150 nm of Parylene C (supported also from the pinhole free nature of Parylene C layers above a thickness of 100nm (Trantidou et al., 2012)), thus one order of magnitude thinner than the previous one. This dielectric thickness leads to low-voltage transistors; indeed, the devices were characterized keeping both the gate and the drain voltages in the range between 5V and -5V (see figure 3.5). In addition, these devices demonstrated to be also stable in time, as can be seen in figure 3.5, in which the curves of characterization of a gold floating gate device taken during a time interval of 57 days are showed; this is a very important advantage for biological purposes, since it guarantees good devices performances for a long enough period to make cultures develop inside the incubator, even after that they have been stored at ambient conditions for several weeks. According to literature, in just a few of previous works was declared such a robustness of the devices: for example, in (Gu et al., 2016) the authors shown signals recorded after 42 days of incubation of OECT-based sensors for electrophysiology, while in (Kyndiah et al., 2020) the stability of an EGOFET-based sensor for electrophysiology was evaluated by periodically characterizing a device during 3 weeks (in which it had been maintained inside an incubator, with cell's culture medium as electrolyte) without observe electrical failures.

Despite the good performances exhibited by these devices, they showed also a huge drawback: they presented a particularly low fabrication yield, i.e. most of the OCMFET produced failed for short-circuits or for high leakage currents. We ascribed this phenomenon to the random presence of pinholes (despite the deposited layer of Parylene C was above the limit of 100nm proposed in literature), irregularities or other defects in the polymeric film that, when located nearby the transistor area, cause its breakdown. It is probable that this issue is observable in these devices because they lack of the metal oxide layer, that in the other cases contributes to the insulating efficiency, perhaps also by remedying the presence of defects. Since the optimization of a OCMFET with gold floating gate is not the main goal of this work, but our aim was to describe a system able to monitor simultaneously more parameters of cells' cultures, it will be decided to abandon the use of gold floating gate. Nevertheless, it might be possible to overcome the fabrication yield issue by finding, through a focused campaign of tests, a compromise between dielectric thickness and transistor's electrical properties.

OCMFET with Al/Ti combined floating gate

Aluminum was examined for this role before titanium, since it is the most commonly used floating gate material for OCMFET-based devices. It naturally oxides, and also the previously

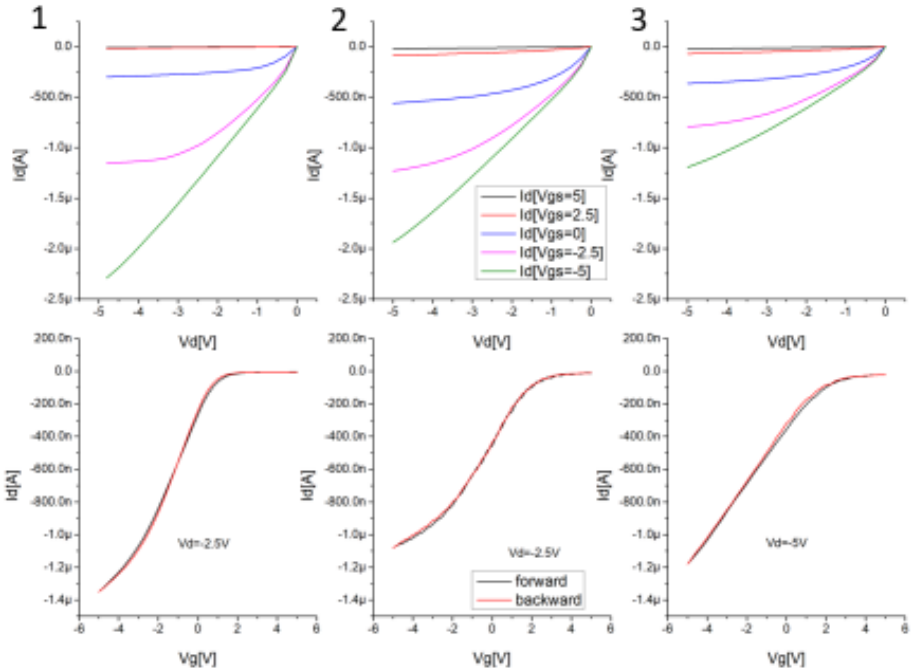

Figure 3.5 Ageing monitoring of an OCMFET with gold floating gate. Panel 1 (both up and down) shows the transistor's characteristic right after the end of the fabrication process, panel 2 displays the same characteristic after 24 days in which the device was stored at ambient conditions. Finally, panel 3 represents the same curves after other 33 days, 21 of which passed into an incubator. The device's ageing has been controlled for a total of 57 days.

mentioned self-alignment technique necessary to obtain low voltage transistors has been developed on OCMFET with aluminium floating gate. Unfortunately, for applications involving living cells it was rejected because it quickly degrades when in contact with culture medium, and it eventually vanishes after a few days of incubation, probably due to a defective aluminium oxide layer (Spanu, 2016). Despite this, we decided to try it again because it is easier to deposit than titanium through thermal evaporation; in addition, experimentally we found that is the floating gate material that ensures the best transistor performances. To overcome the problem of the degradation of the aluminum layer when it is directly exposed to the culture medium, a thin layer of titanium is deposited selectively onto the sensing area, thus protecting the aluminium from the attack of the solution. In order to do this, the fabrication process of the electrophysiological activity's sensors (exposed in detail in Appendix A), has been slightly modified as shown in figure 3.6.

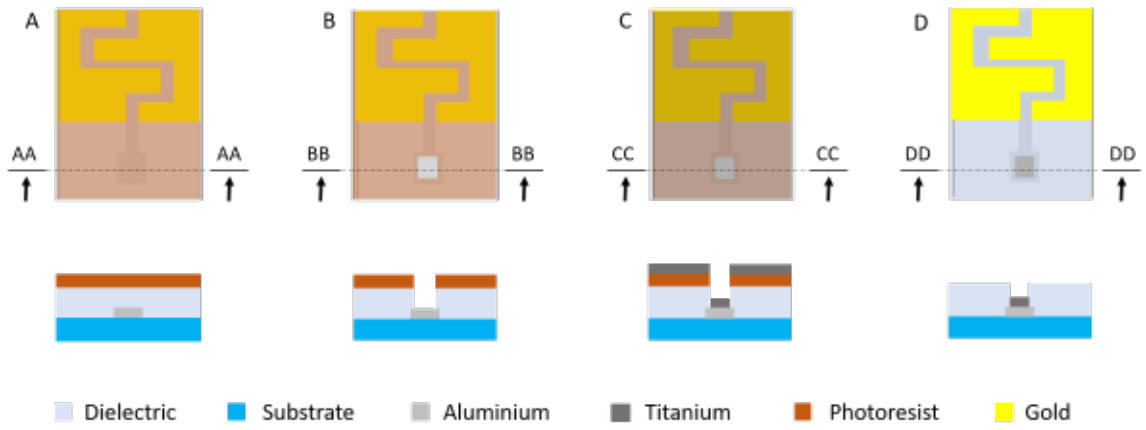

Figure 3.6 First attempt of protocol to fabricate OCMFET with Al/Ti. Each step is illustrated through a top image and a cross-section image (in the top and bottom part of the figure, respectively). After having spin-coated the photoresist (A), having performed the photolithography to expose the sensing area and removed Parylene C layer above it through plasma etching (B), a selective titanium deposition is performed to cover the exposed aluminum (C). Finally, the photoresist is cleaned away through an ultrasonic bath (lift-off process) as shown in panel D.

Briefly, the first step was the selective removal of Parylene C from the sensing areas through a photolithographic process followed by an oxygen plasma treatment (3.6A and B). Secondly, the photoresist layer used to protect the remaining part of the substrate from the plasma etching has been used as a mask to selectively deposit titanium on the sensing areas (3.6C). Finally, after the titanium deposition, photoresist has been removed using an ultrasonic bath, thus eliminating through a lift-off process also the metal deposited on it (3.6D): this fabrication process involves just one additional step, i.e. the titanium evaporation, if compared with the traditional one. Unfortunately, when the devices produced with this fabrication protocol have been tested, it resulted that the titanium was not able to prevent aluminium dissolution. Indeed as can be seen in figure 3.7, titanium protect the underlying aluminium, but it degraded near the edge of the sensing area, isolating it or interrupting the floating gate; in both cases, it results in sensors failure.

We hypothesized that this could be due to the fact that when the photoresist is removed using the ultrasonic bath, the titanium layer was irregularly ripped at the edges hence allowing the culture medium to seep under it and corrode the aluminium layer. To confirm the hypothesis and to overcome the issue, the production process was once more modified as shown in figure 3.8: during the oxygen plasma etching of the Parylene C deposited on the sensing area, it has been removed from an enlarged area centered in the sensing area; the following phase, as in the previous procedure, is the titanium evaporation on the substrate and after it the photoresist is removed using the ultrasonic bath (as in figure 3.6).

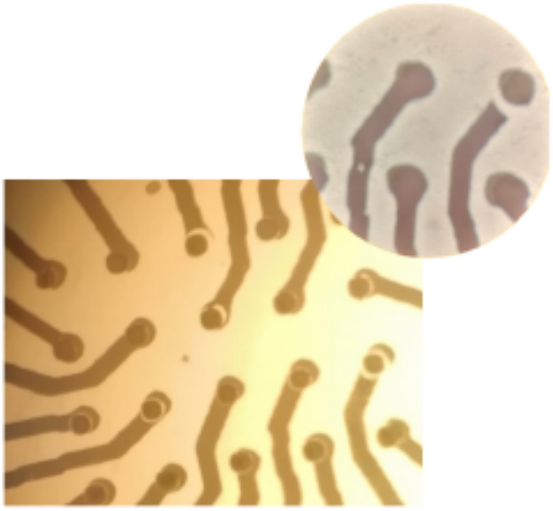

Figure 3.7 Images of the failed Ti/Al MOAs. The enlarged image shows a detail of a sensing area separated by its floating gate.

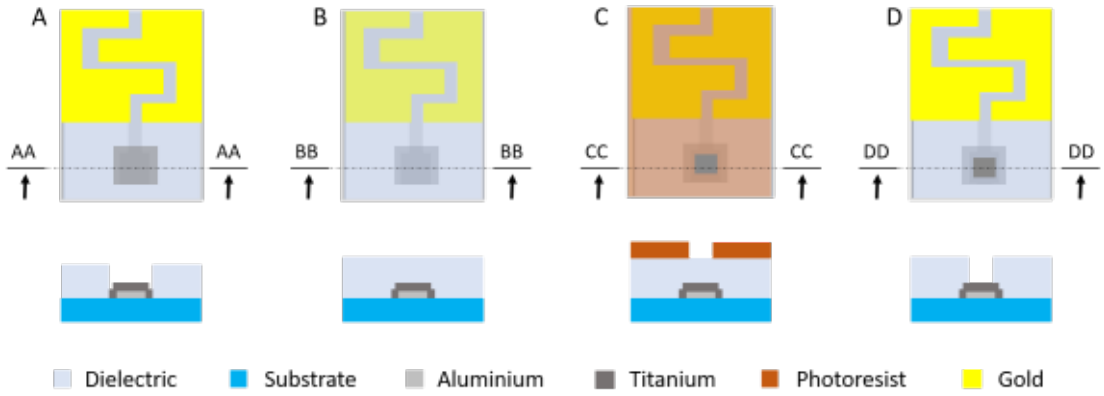

Figure 3.8 Modified protocol to create OCMFET with Al/Ti floating gate. Each step is illustrated through a top image and a cross-section image (in the top and bottom part of the figure, respectively). After the titanium deposition on an enlarged area (A), a second layer of Parylene C is deposited (B). With a photolithographic step, a smaller portion than the previous is exposed to the plasma oxygen, and the Parylene C is removed (C). Finally, photoresist is cleaned up (D).

In this case, a second Parylene C deposition is used to cover again the sensing area; followed by a second plasma treatment during which a smaller surface is cleaned away from the polymeric layer (3.8 C). In this way, under the Parylene C layer, the titanium film covers a bigger area than the aluminium and so can protect it even if the cell culture medium should leak (3.8 D). In addition, since the Parylene C layer acts also as passivation for the parts of the floating gate that are not employed as sensing area, the effective active area depends on the dimension of the second opening produced with the second etching phase, and so can

be arbitrarily chosen. The only needed change to the layout of the matrix of sensing areas is the inter-electrode distance, that has to be increased to avoid that the layer of titanium creates short-circuits between adjacent electrodes. This should not be an issue as, even by increasing the distances between the electrodes, the portion actually occupied by the active areas is much smaller than that enclosed by the plastic ring that delimits the culture chamber; therefore cell culture should be uniform on the electrodes. This second protocol actually solves the issue previously observed, and so resulting devices were used to perform the experiments with living cells. In this way, the titanium deposition must be excellent only in the small extent of the sensing areas, that is placed in the most convenient position to obtain a good metal layer with the instrument used in this work, i.e. center of the substrate (to mimic the layout of traditional MEAs, in which the culture chamber is in the center), while the performances of the transistors are ensured by the aluminium floating gate.

3.3.2 MOA evolution

All the MOAs used in this project have been designed and fabricated at the DEALAB (Laboratorio di Dispositivi Elettronici Avanzati) at the University of Cagliari, following the fabrication procedure illustrated in Appendix A. During the last three years, several versions of the MOA followed one another, differing each other for various reasons, the bigger of which is the compatibility with different readout electronics. Indeed, during this project, two custom electronics have been used (for further information refer to the Appendix B), that are different from many points of view. In particular, the number of OCMFET-based sensors that it is possible to operate simultaneously has been increased from a maximum of 16 channel in the first version, to a maximum of 56 in the second one, and the functioning configuration (i.e. the configuration used to apply the supply voltages to transistors) has been modified. In the following sections, the principal MOA layouts used, principally imposed by the readout electronics, will be described more in detail.

16-channels MOA

16-channels MOAs have been firstly employed during this project, and are compatible with the first readout electronic that, as just mentioned, can operate up to 16 OCMFETs simultaneously. In these arrays, MOAs are basically arranged in 4 rows aligned to the outer edges of the substrate and containing each 4 equidistant transistors. The number of active sensors embedded in each substrate depends on the presence in the same substrate of passive micro-electrodes (useful to record a reference electrophysiological signal to be compared

with the one recorded from the OCMFET-based sensors). Indeed, since the contact pads' positions are fixed by the layout of the contacts in the readout electronic and because, with the instrumentation available in the laboratory, it is not possible to further reduce the transistors' dimensions, the presence of passive micro-electrodes diminished the space available for transistors. For this reason, several layouts containing different quantities of active and passive sensors have been fabricated, i.e. with 8 OCMFETs and 8 passive electrodes, with 10 OCMFETs and 6 passive electrodes or with 16 OCMFETs and no passive electrodes. The most used combination is the second one.

The readout electronic operates the transistor in the so called *diode configuration*, i.e. by applying the same voltage to the drain and to the control gate; and this voltage is the same for all the FETs on the same substrate. This means that in this configuration it is possible to control only one voltage; consequently also the resulting MOA's layout is greatly simplified: as illustrated in figure 3.9, each OCMFET has independent Source, Drain Floating Gate contacts, while the Control Gate is common for all the transistors of the substrate, and a single wire deliver it to each control capacitor. In particular, the floating gate connection is guaranteed by removing the Parylene C layer from its pad before to evaporate the top contact (that is patterned from the gold layer together with source, drain and control gate), in order to put in direct contact the two metal layers. Obviously, this contact is floating during the recording (as discussed in Appendix B, the spring contact corresponding to the floating gate is not connected), but has been inserted to completely characterize the devices.

56-channels MOA

The second version of the readout electronics, called also *superOFET*, became available shortly after; it was conceived before the beginning of my PhD to be used with a new variant of MOA that was fabricated at the IBM laboratories in Almaden, California. In this IBM MOA, thanks to the different fabrication processes and instrumentation available in these laboratories, the transistor dimensions have been greatly reduced while maintaining a similar W/L ratio and thus similar transistor characteristics, hence allowing for a tighter packaging of the transistors that permits to insert 56 OCMFETs onto a substrate of the same dimensions of the previous. The main objective of this new electronics was to operate up to 56 OCMFET-based sensors at the same time but, in addition, several other improvements have been implemented, with the main purpose to increase its flexibility, so as to make it easily adaptable to perform different types of experiments. This electronics is extensively described in the Appendix B, but the bigger improvement that has been implemented is the possibility to set both the polarization voltages autonomously for each transistor; on one

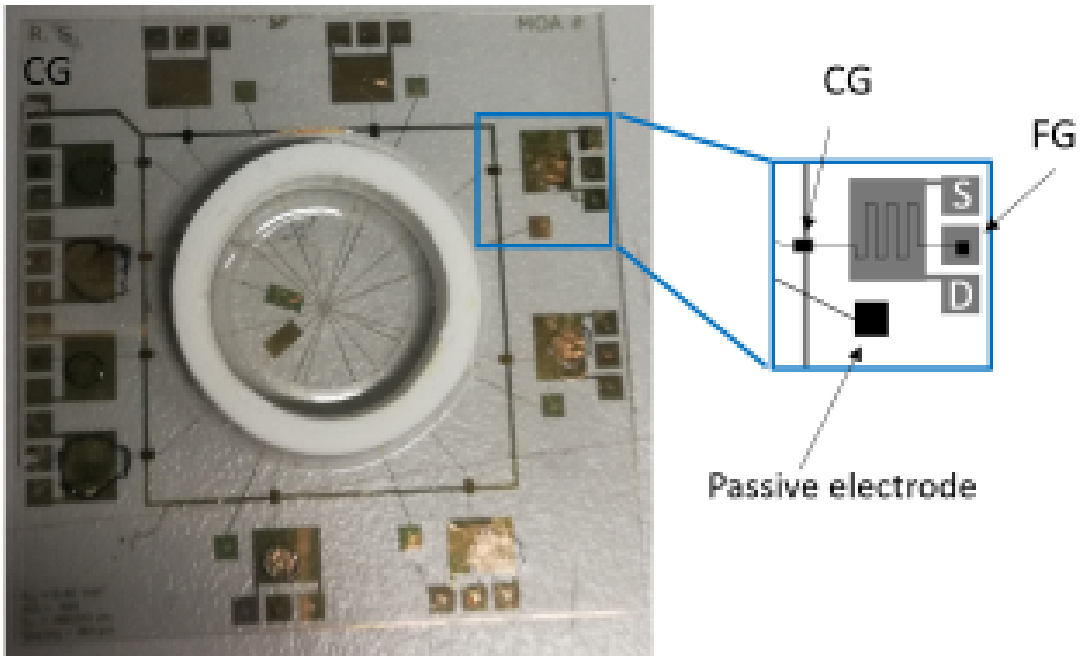

Figure 3.9 Layout of a 16-channels MOA, in which it is possible to notice the Control Gate wire that deliver the same Gate voltages to all the capacitors. The enlargement shows one OCMFET with its contact pads and a passive electrode.

hand, this means that each transistor can be set on its working point independently from the others, thus working in the best conditions. However, on the other hand it largely increases the quantity of connections to be established between the MOA and the electronics, inasmuch each transistor has four contacts, i.e. source, drain, floating and control gates, and this greatly increases the complexity of the electronics pin-out and of the corresponding MOA's layout. To solve this problem, on the electronics have been assembled eight modules (two for each side of the MOA), each containing two rows of 15 spring contacts with a diameter of 0.48mm that are distanced from each other of 1.27mm. Consequently, also the device must have a packed layout: each transistor has four square metal pads (which sides is 1.07mm and are separated by 0.2mm), that are organized in two lines, as shown in figure 3.10. Even if it is not possible to fabricate MOAs with 56 channels at the DEALAB since (with the available instrumentation) is not possible to further miniaturize the transistors, the new pin-out allows to save space and so to increase the number of sensors on each MOA to 16 OCMFET-based sensors and 8 passive electrodes. Furthermore, the pin-out of the new electronics leads to a change in the architecture of MOA and some of its design parameters, such as the position and the dimension of the control gate. Indeed in this new configuration the control gate is no more placed on the floating gate in the space between the sensing area and the transistor, as in the previous versions, but is placed under its pad. To avoid that the spring contact by

scratching the pad may eventually damage the gold and the Parylene C layer thus connecting directly the floating gate, this assumes the shape of a frame (i.e. an empty square near to the edge of the gold pad), as displayed in the inset of figure 3.10; consequently, also its total area has been reduced from 0.52 mm^2 in the previous versions to 0.17 mm^2 in the actual one.

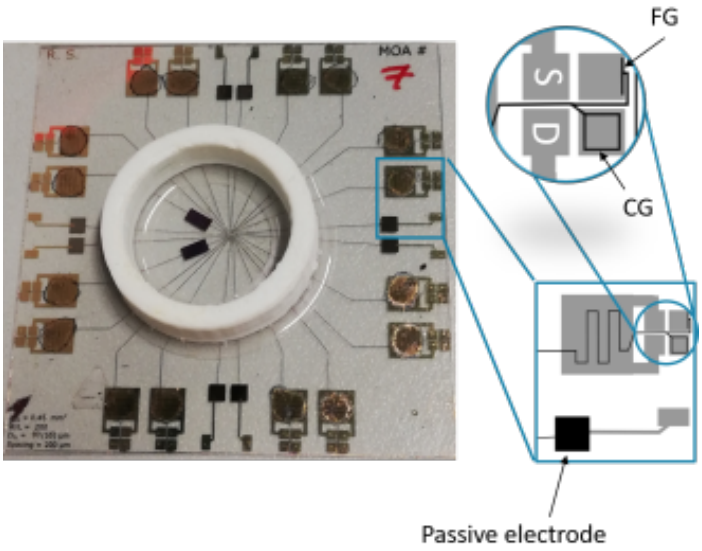

Figure 3.10 Layout of a 56-channels MOA, in which is possible to notice the separated contacts of Floating and Control gate, with its frame-like structure. With respect to the previous version, transistors are more densely packed onto the substrate.

When these devices have been characterized, an issue has been observed concerning the most of them, i.e. that when the transistors were operated through the control gate, their $I_{DS} - V_{DS}$ curves don't saturate for any voltage applicable to the control gate, while they saturate when operated by applying the same V_{GS} values directly on the floating gate, as can be seen in figure 3.11. We ascribed this behaviour to an excessive reduction of the control gate area, that impedes to the capacitor to induce enough charge to modulate the transistor channel; to prove this idea, a version of MOA slightly modified has been later introduced.

In this new version, the control gate area has been enlarged at the expense of the floating gate contact. Indeed, it was not possible to thicken the frame of the control gate to augment this area because it increases the risk of damaging the capacitor when the transistor is contacted to the readout electronic. Instead, we decide to renounce to the possibility to contact the floating gate and, exploiting the fact that the contact corresponding to the floating gate is not contacted inside the readout electronics, both the outer contact pads have been used as control gate. In this way, the pads associated to each transistor became only three, as depicted in figure 3.12A. With this approach, the control gate area became 0.65 mm^2, also

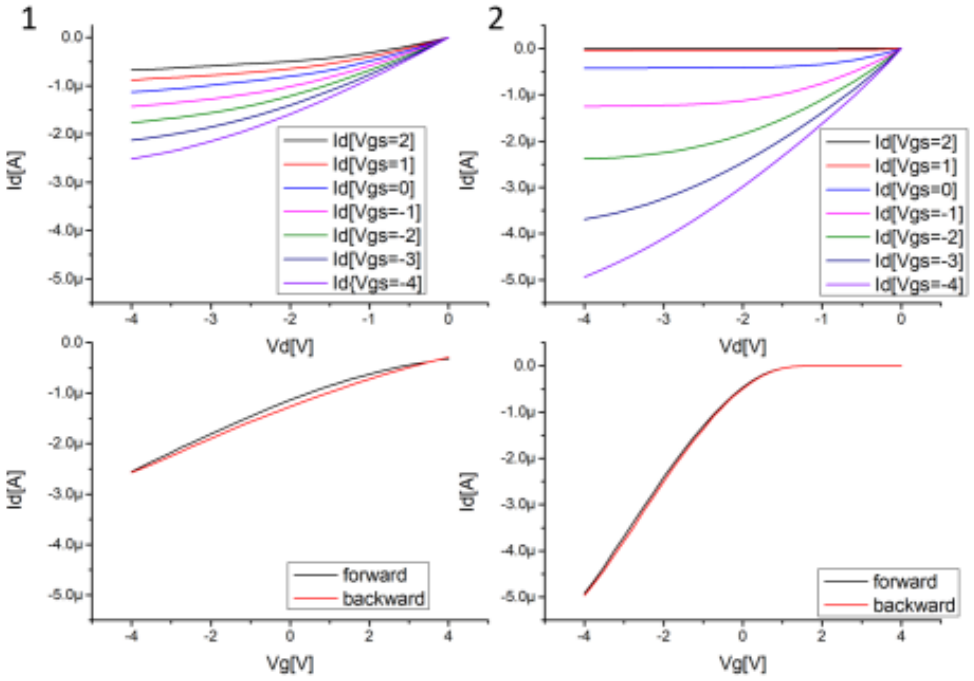

Figure 3.11 Characterization curves of a superOFET MOA that do not saturate when operated through the control gate (1, up and down) while they saturate when operated directly through the floating gate (2,up and down)

exceeding the initial value of 0.52 mm^2. From the characterization curves of these MOAs, it resulted that the previously spotted issue it is solved, as shown in figure 3.12B.

3.3.3 Sensing areas activation

The last issue to be solved was to find the best procedure to functionalize the two different sensors on the same substrate. The starting point was to exploit the results concerning the use of OCMFET sensors for electrophysiology described in section 3.1.3 and taking advantages of the success in monitoring the metabolic activity of cells' cultures with an OCMFET which sensing area is functionalized with oxygen plasma activated Parylene C (see section 3.2 for further details). The sensing area of sensors for electrophysiological activity is functionalized by removing the spacer and exposing the Floating gate electrode to the surrounding environment, while to sense pH variations, the sensing area must be covered by a thin film of oxygen plasma activated Parylene C, that is the same material used as dielectric, so the fabrication procedure needs to be modified only slightly. The critical

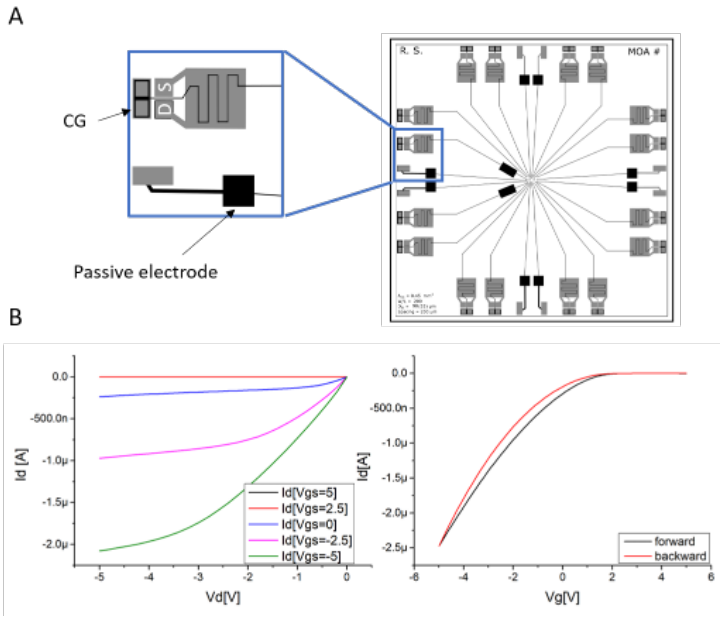

Figure 3.12 MOA 56-channels without Floating Gate contact. Panel A shows the scheme of a superOFET MOA with 16 OCMFET-based sensors and 8 passive electrodes. The enlargement displays the new arrangement of the contact pads, in which the control gate contact is doubled at the expense of the FG. Panel B shows the characterization curves of an OCMFET operated from the control gate.

points are substantially two. Firstly, as previously mentioned, the activation of Parylene C layer requires a high power ($\approx$ 200W) oxygen plasma treatment, powerful enough to etch the Parylene C layer; hence, the 150nm-thick layer deposited as dielectric is not sufficient because it risks to be excessively consumed by the oxygen plasma. To overcome this problem, a second selective deposition of this polymer become necessary. In fact, even if it could be used to encapsulate the transistor, it should be avoided that it covers the sensing areas of sensors for electrophysiology, otherwise additional cycles of oxygen plasma would be needed to etch a thicker layer. Briefly (to further information please refer to Appendix A, and in particular to section A.4), a multi-layer protection has been deposited onto the entire substrate, except for the areas in which the second layer of Parylene C must be deposited.

The second issue to be solved is linked to the fact that the plasma activation of metabolic activity's sensors decays with time, thus should be performed as late as possible, in order to assure the better sensitivity during the measurements; in addition, it could also decay if other fabrication processes were carried out after it, such as the gluing of the ring that forms the culture chamber, that implies a drying phase in the oven for 12 hours (see Appendix A for more information on the fabrication process). In other words, the oxygen plasma activation must be the last step, and must be performed as late as possible (experiments should be

performed 48 hours after the activation procedure to ensure a stable level of hydrophilicity, as stated in (Spanu et al., 2017) and in (Trantidou et al., 2012); but considering that by protocol the cells must be incubated for at least 5 days before carrying out the experiment this requirement is always respected). To this end, the fabrication procedure was modified once more, as described in detail in Appendix A, and in particular in section A.4. Briefly, we designed a protocol that allows to simultaneously activate the sensing areas of sensors for metabolic activity and to remove the Parylene C from the active parts of the detectors for electrophysiology as last step.

Interestingly, the same procedure can be implemented also on the OCMFETs with combined Al/Ti sensing areas; the only variation is that during the second Parylene C deposition, that has been performed after the selective titanium evaporation, the polymer will be deposited onto the whole area of the future culture chamber, and not only onto the sensing areas of OCMFET-based sensors for metabolic activity. In this way, it will cover the titanium and passivate the bigger electrodes and during the plasma activation of the Parylene C, also the real dimensions of the electrodes for electrophysiology can be chosen (i.e. the portion of the sensing area that will be exposed to the extracellular environment), that can be much smaller than the titanium covered area.

Chapter 4

Experimental Results

The first results described in this chapter refer to the application of the pH sensors to detect metabolic activity of *in vitro* neuronal cell cultures. As we will see in the next sections, they showed that it is possible to detect the local pH variations in the culture medium caused by the accumulation of acidic byproducts; indeed, when the culture is pharmacologically stimulated to increase its activity, and so its metabolic consumption increases, it also changes the transistor's output current.

Subsequently, the preliminary results obtained by using the MOAs for simultaneous recording of electrophysiological and metabolic activities are shown. As previously mentioned, this part of the project has been conducted at the University of Genova, since there are the facilities needed to seed and maintain the *in vitro* cells' cultures, and also the systems required to record their signals; in addition, the discussed results are based on recordings performed using the SuperOFET readout electronics. In order to execute these experiments, we chose to use cardiomyocytes because of their strong activity; indeed, their action potentials have a larger peak-to-peak amplitude and are highly synchronized, making their activity easier to recognize. Furthermore, they also require a shorter time to form a mature network and therefore allow us to shorten the overall duration of the experiment: a big advantage since the pandemic has reduced the time needed for this phase. These features make cardiomyocytes more suitable to be used to test SuperOFET electronics and the new MOA version. Beyond the experiments with cardiomyocytes, also those without cells (blank experiments) have been performed, in order to investigate the phenomena non correlated with cells' activity that can occur during the measurements and that can be caused by:

- the increase of the volume of solution inside the culture chamber following drug injections;

- the possible variation of charge inside the culture chamber that can happen during the compound addition (remembering that no reference electrode is immersed in the culture medium);
- the unexpected reactions between the sensors and the administered drugs.

These events can contribute to the recorded signal, summing their effects to that caused by cells. Although several blank experiments have been performed, in the following we will refer to only one experiment per type, in order to exhaustively describe and comment it. It was decided to proceed in this way also in virtue of the fact that all the blank experiments carried out showed consistent results.

In following sections, as previously stated, the first section is earmarked to the illustration of the use of the OCMFET-based pH sensor as metabolic activity detection. Thereafter, following the description of the protocols implemented in both kind of experiments, the recorded data will be depicted along with the main issues observed during the experimental phase. Subsequently, the analyses applied to the data will be illustrated, together with the resulting signals.

4.1 Metabolic activity OCMFET-based sensor

In this section, the results aimed to determine whether the OCMFET-based pH sensor is suitable for detecting the small variations in H^+ ions' concentration in the extracellular medium caused by the metabolic activity of cell cultures have been illustrated.

As stated in 3.2, this tests have been performed using hippocampal neurons from rat embryos, and the signal was recorded using the 16-channels readout electronics after 15 days from the seeding of cells in the culture chamber (i.e. when the neuronal network was mature and presented spontaneous electrophysiological activity). The designed experimental protocol lasts 10 minutes and it is constituted of two phases: the first one is the basal phase during which the activity of the cells is recorded for 3 minutes before bicuculline (BIC)[1] is added, while during the second one, the culture is monitored for 7 minutes after the administration of the compound in order to detect the eventual changes in the local pH value. This protocol is repeated twice for each experiment and between the two reiterations, the culture's medium is substituted with a medium containing tetrodotoxin (TTX)[2]. In addition,

[1] Bicuculline is a drug that acts as a inhibitor of GABA A receptor thus increasing the neuronal electrical activity, and consequently the metabolic activity of neurons.

[2] TTX compound that lead to a cessation of both the cells' electrical and metabolic activity, and eventually to cellular death.

only one of the two sensors optimized for pH monitoring included in the array has been activated through plasma treatment, while the second acted as a reference on which evaluate the response of the untreated Parylene C layer to the same conditions.

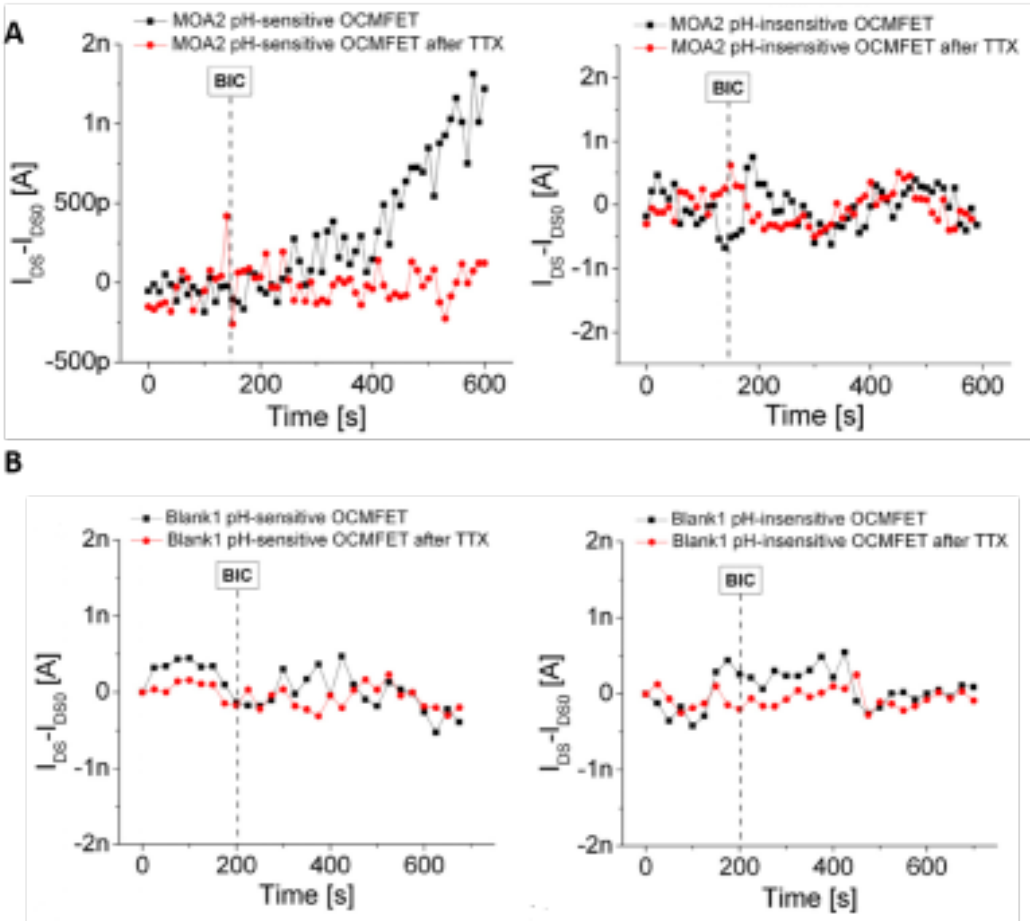

Figure 4.1 OCMFET for metabolic activity monitoring. Responses to the experimental protocol of the OCMFET-based sensor pH-sensitive (left) and pH-insensitive (right) of a MOA before (black curve) and after (red curve) the addition of TTX to the solution. Panel A shows the signal recorded from a device with cells' culture and B from a blank experiment. The dotted vertical line represents the administration of bicuculline. (Spanu et al., 2018)

To assess the repeatability of the results, the experiment has been replicated both on 2 MOAs onto which cells were seeded, and on two without cells (Blank experiments) to evaluate possible undesired phenomena that may influence the device's response, such as aspecific absorption of molecules on the Parylene C, and also spontaneous drifts of transistors' output current. In all cases, before to start with the recordings, the culture medium was

replaced with 100μl of a low buffered solution (Krebs-Ringer solution[3]), to avoid that the buffer balances even partially the pH variations.

The results (shown in figure 3.2) demonstrated that only the pH sensitive OCMFET of the substrates in which cells are plated displayed a clear current decrease following the addition of BIC (figure 4.1A *left*), indicating an increasing acidification of the extracellular medium due to the augmented cellular activity. On the other hand, no responses can be observed for pH-insensitive OCMFET (figure4.1A *right*), in the blank experiments (figure4.1 B *left* and *right*) or after the administration of TTX. Noteworthy, figure 3.2 shows the response of only one device of the two on which each type of experiment has been performed; nevertheless, the not-shown data are coherent with the one displayed in figure. Additional blank experiments stated that if the same protocol is applied without substituting the culture media with a low buffered one, no clear response can be noticed. This is due to the fact that the buffering effect of the standard medium balances the pH variations. All the results showed here are described in more details in (Spanu et al., 2018).

4.2 MOAs for simultaneous sensing

4.2.1 Experimental protocols

Protocol for simultaneous recordings

After the seeding of the cells onto the sensing areas (as briefly described in section A.6), the devices are stored inside an incubator for 5 days, at the end of which cells are grown and on the surface of the culture chamber it is possible to observe a mature and homogeneous network of cardiomyocytes as shown in figure 4.2, with a strong and repetitive contractile activity.

Approximately 15 minutes before starting the recordings, the culture medium is substituted with a 300μl of low buffered Tyrode solution[4] to better discriminate the local pH changes (that are of the order of tens of nanoampere) and then the device is stored once again into the incubator to give the culture time to recover from the shock caused by the change of the medium. Thereafter, the MOA is inserted into the readout electronics and all the OCMFETs are polarized (to further information see section B.2.3); after having assessed the

[3]The employed low buffered Krebs-Ringer solution contains 135mM NaCl, 2.8mM KCl, 1mM $MgSO_4$, 1.2mM $CaCl_2$, 10mM glucose, and 1mM HEPES. pH 7.4.

[4]Tyrode solution is used in physiological experiments and tissue culture since it is practically isotonic with extracellular fluid. It contains 136mM $NaCl$, 0.8mM $MgCl_2$, 1.2mM $CaCl_2$, 5.4mM KCl, 5.6mM glucose and 1mM hepes. pH 7.3

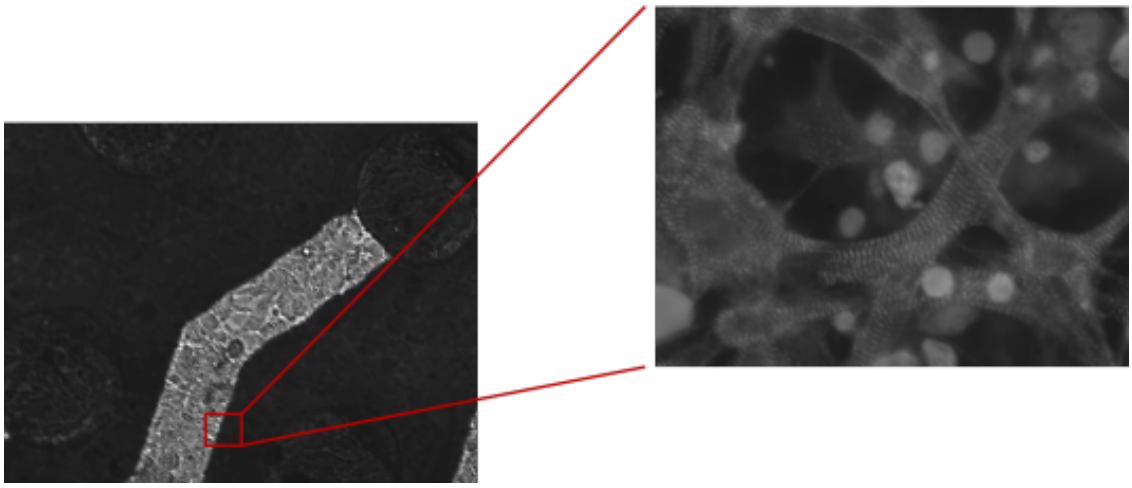

Figure 4.2 Photograph of a cardiomyocytes culture plated onto a MOA. A sensing area with its floating gate line, on top of which it is possible to notice the cells culture and, in the enlarged image, a fluorescence image in which is visible a blow-up of a few of cardiomyocytes.

culture's activity through electrophysiology sensors, we started to record. The experimental protocol consists of various recording phases that differ from each other because of the addition of a small amount of drugs that modify the dynamics of the network, while its activity is monitored through the two kinds of sensors. In particular, we recorded six different phases: the first is the basal one, during which it is recorded the activity of the network when no external stimuli are applied to it. After that, there are three phases during which we gradually added a solution of Tyrode containing isoprenaline[5], starting from a 3.3nM concentration, followed by a 6.6nM and finishing with a 13.2nM (it is worth noting that the given concentrations are the total ones, i.e. are the sum of both the newly added and of the previously administered doses). In the last two phases verapamil[6], a drug that have the opposite effect on the cardiomyocytes' culture, is added. It has been gradually added to the solution too: 20μM are added as first dose and other 30 μM (for a total of 50μM) in the second one. Noteworthy, the Tyrode solution have not been substituted during the experiment, so that also the different drugs remain in solution and it is likely that their effects can sum up. During each phase, both electrophysiological and metabolic activities are recorded.

Protocols for blank experiments

As previously mentioned, along with the experiments with MOAs in which were cultured cells' cultures, also experiments involving blank MOAs, i.e. devices that have been treated as

[5]Isoprenaline is a non-selective β adrenoreceptor agonist that has positive inotropic and chronotropic effects.
[6]Verapamil is a calcium blocker that acts as a cardio-relaxant.

the others but in which cells are not plated, have been performed. In particular, two different kinds of blank experiments have been designed: in a first series, we added to the Tyrode solution the same drugs used to induce changes in the cardiomyocytes' spiking frequency, i.e. isoprenaline and verapamil. In the second group of experiments, we added a solution of a strong acid (or a strong base) diluted in the same Tyrode, in order to investigate the reaction of the metabolic activity sensors to acidic and basic solutions.

Pharmacological blank experiments

The pharmacological experiments on blank MOAs are carried out using a similar protocol to that previously described for simultaneous recordings. In this case, since our interest was mainly linked to the possible undesired effects related to the addition of the solution containing the drugs, for each of them a single administration has been performed, containing an amount of compound comparable with the maximum dose used in experiments. In particular, we added a 10nM solution of isoprenaline and a 40 μM of verapamil, respectively. Before to add the first compound, 6 minutes of basal recording has been performed, while after each administration, we recorded for 6 minutes. Also in this case, to mimic the protocol for simultaneous recording, the Tyrode solution contained in the culture chamber has not been changed between the two drugs' administrations.

Blank experiments involving acidic and basic solutions

The experiments involving solutions at known pH value have been designed to investigate the response of metabolic activity's sensor to a known pH variation. In particular, a strong acid (hydrochloric acid) and a strong base (sodium hydroxide) have been diluted in Tyrode's solution to reach a concentration of 0.1M. Each solution has been administered to the devices after 5 minutes of basal recording, and between the two experiments the sensing areas are rinsed with clean Tyrode solutions.

4.2.2 Experimental data

In this section, the signals simultaneously recorded from an electrophysiological and a metabolic activity sensors on the same MOA have been illustrated (see figure 4.3). The aim of this section is only to give a qualitative idea of the recorded data and of how they appear; these have been therefore only pre-processed (i.e. converted from voltage to current) and the metabolic has been also down-sampled and filtered as described in section 4.2.3, but no additional analyses have been performed at this stage.

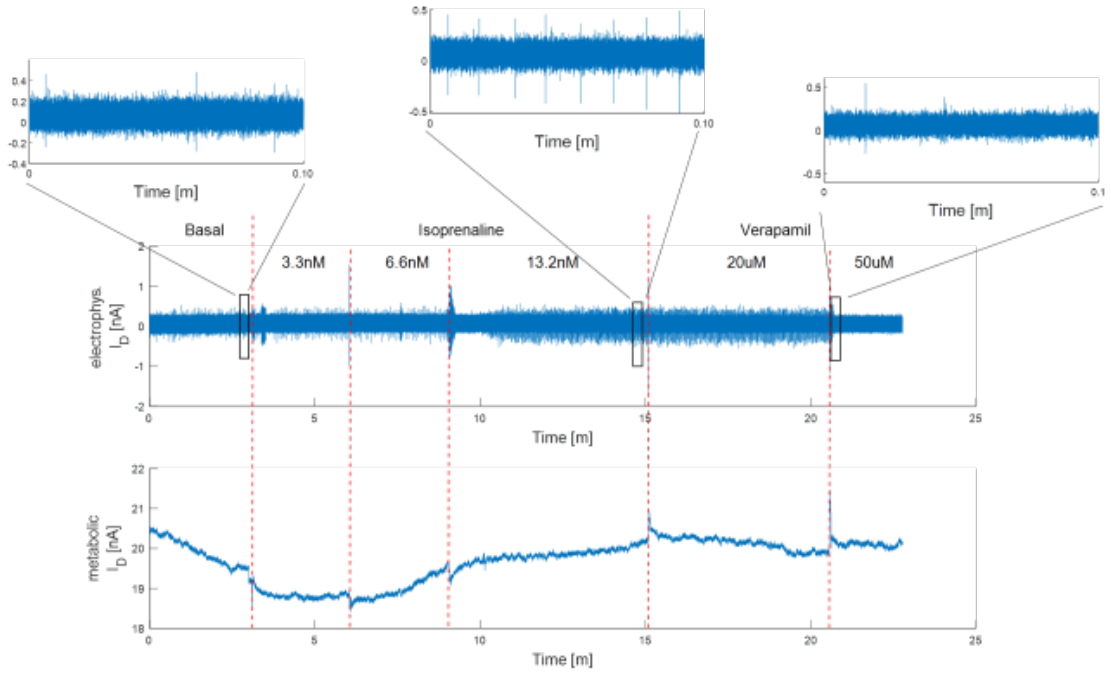

Figure 4.3 Signals recorded from an electrophysiological and a metabolic activity sensors. Both traces are converted from voltage to current, using the process described in the next section, and the metabolic activity signal has been filtered and down-sampled as described in 4.2.3. The enlargements in the upper part of the figure show better the cardiomyocytes' action potentials in three points of the recording.

In the graph, the red dashed lines represent the time instant in which a drug addition has been performed, while the total amount of drug administered is specified in the upper area of the image. The little observable discontinuities, situated near the red dashed lines, are the artefacts linked to the addition of the drugs.

Figure 4.3 makes clear the intrinsic dissimilarity between the two signals that, as we have already mentioned several times, are different by nature: the electrophysiological signal represents the fast charge variations induced in the extracellular environment by the cellular action potentials and so it has relatively high frequencies; on the other hand, the metabolic activity is a quasi-static signal that depicts the slow variation of H^+ ions nearby the sensing area. In addition, as it is possible to see, the two behave coherently with one another, i.e. when isoprenaline is added to the solution, at the increasing of the action potentials' frequency (as shown in the electrophysiological trace) corresponds an increase of the output current, while when verapamil is administered and a consequent reduction of the beating frequency is expected, we observe a decrease of the output current. Indeed, when the first dose of isoprenaline was added to the solution (i.e. in correspondence of the first red dashed line),

the shift that the current showed during the basal phase became less evident and after the second addition a clear trend inversion is noticeable. When the higher dose of isoprenaline is reached, the current is clearly increasing. After the administration of verapamil, a new inversion of the trend is visible, as the current started to decrease once again. It is important to underline that no reference electrodes are employed during these recordings.

A thing that draws attention is that, during the basal phase, the current shifts toward smaller values: this effect is likely to be caused by the phenomenon of the bias stress that, as better described in section C.2.2, causes a threshold voltage shift toward more negative values.

In addition, blank tests have been performed also using acid and basic solutions (i.e. solutions containing HCl or NaOH) to observe the system's (consisting of transistor and readout electronic) response to a clear H^+ ions increment or reduction.

These issues will be investigated in more details in the following sections, also with the help of the data analysis methods implemented during this PhD project.

4.2.3 Data Analysis Methodologies

Signal pre-processing

The readout electronics, as detailed in Appendix B, firstly convert the transistors' output current to voltage, and the employed software displays and records voltage signals. On the other hand, in order to evaluate the real output variations of the sensors and also to apply the proposed model (to further information please refer to Appendix C) we need to come back to the output current I_D. This is true both for electrophysiological and metabolic sensors recordings. To this scope, for the electrophysiological signal it is sufficient to take into consideration the overall amplification gain of the filtering circuit (as described in Appendix B.2.1), since the pre-processing stage for electrophysiological signal includes only the conversion from voltage to current.

Regarding instead the metabolic activity sensors, the algorithm employs a single coefficient - extracted from the ratio between output and input values of the LTSpice simulation of the low-pass filter - to convert the recorded voltage to the output current of the transistor (see section B.2.1 for more information about filters' simulations). After the conversion, this signal is down-sampled through a moving average filter in order to reduce both the noise and the effect of quantization error in the slowly varying signal.

Parameter's extraction from measured data

Parameters' extraction from the characterization curves

In order to apply the equivalent electrical model proposed in this thesis (and described in Appendix C) to the data measured from a specific OCMFET-based sensor, the first step is to extract the values of the parameters a and b for the specific transistor (see section C.2.1 to the description of the parameters' extrapolation) as follows:

$$a = \frac{\sqrt{K/2}}{CR} \tag{4.1}$$

$$b = V_{TH}\sqrt{K/2} \tag{4.2}$$

where $CR = 1 + C_{Ch}/C_{CG}$ is the ratio between the two considered capacitances, i.e. the channel and the control gate, and therefore it is constant once defined the FET's layout. To this end, it is necessary to remember that the ΔV_{CF} represents the variation of the voltage drop across the control gate capacitor, i.e. between the control and the floating gates, due to the charge rearrangement occurring in the floating gate following a charge variation in the sensing area. Thus, assuming that $\Delta V_{CF} = 0$ (i.e. that no charge variation is detected nearby the sensing area and $Q_S = 0$) the equation

$$I_D \approx \frac{K}{2}\left(\frac{V_C - V_S}{CR} + \frac{\Delta V_{CF}}{CR} - V_{TH}\right)^2 \tag{4.3}$$

can be linearized as $y = ax - b$ where

$$y = -\sqrt{I_D} \tag{4.4}$$

$$x = V_{CS} \tag{4.5}$$

and consequently the two parameters can be obtained through linear regression starting from a series of couples of values (I_D, V_{CS}) - where I_D is the transistor's output current and V_{CS} the voltage applied between the control gate and the source contacts - extracted from the characterization curves of the device, to favor the optimization of the extracted parameters. In particular, since the a parameter contains the K value of the FET, in which the only factor that can vary (reflecting the transistor's loss of performances due to the ageing or the storing

in an harsh environment such as the cell culture incubator) is the charge carriers mobility μ that is however considered constant during the experiment, the so obtained value is valid in each condition. On the other hand, the b/a value represents the threshold voltage in the dry condition (i.e. when no stimuli are applied to the sensing area).

Parameters' extraction from $I_D(t)$

Indeed, it has been already shown in section C.2.1 as the charge variation induced in the sensing area changes the output current just as a variation of V_C or of V_{TH} would modify it. Consequently, the effects of a ΔQ_S can be assimilated to the ones provoked by a variation in the threshold voltage, ΔV_{TH}. From the values of I_D over time, it is possible to obtain the variations of the threshold voltage in time; in order to do this, the evolution of the threshold voltage over time can be calculated as

$$\frac{b_m(t)}{a} = V_{TH}CR = V_C + \frac{\sqrt{I_D(t)}}{a} \tag{4.6}$$

where a is the one derived from the characterization curves, and remembering that CR is a parameter that depends only on the transistor's layout, and so can be considered as a constant.

From the equation 4.6 it is possible to obtain also an expression for ΔV_{CF} as

$$\Delta V_{CF}(t) = -\frac{\sqrt{I_D(t)}}{a} - V_C + \frac{b_m(t)}{a} \tag{4.7}$$

Bias stress removal on measured data

As previously mentioned in section 4.2.2, one of the issues observed in the experimental data is the shift of the output current toward lower values during the basal phase, when instead the system should be at the equilibrium; this effect can be ascribed to the bias stress phenomenon, described in more detail in section C.2.2. Since the proposed model allows to separate the effects derived from the "sensor", i.e. from a charge variation on the sensing area, from those determined in the active zone of the transistor itself (as for example the bias stress), and considering that the latter are assumed to be constant during the experiment, in principle it should be possible also to remove them. In order to do this, the threshold voltage shift induced by the bias stress is described as a stretched exponential function, as previously

proposed by Zschieschang and its coworkers in (Zschieschang et al., 2009), and as mentioned in section C.2.2:

$$\Delta V_{TH}(t) = [V_{TH}(\infty) - V_{TH}(0)][1 - \exp(-(t/\tau)\beta)] \tag{4.8}$$

where $V_{TH}(0)$ is the threshold voltage in the initial state, $V_{TH}(\infty)$ is the threshold voltage when the equilibrium has been reached; τ is the time constant and β is the stretching parameter that indicates the degree of diversion from the exponential function (see section C.2.2 to further information).

In addition, since during the experiments' basal phase no charge variations should occur near to the sensing area, because no external stimuli (such as drugs) are delivered to the culture in this stage; we have assumed that the observed variation in the output current must be mainly ascribed to the bias stress effect. Consequently, we fit the $b_m(t)/a$ curve of the basal phase, corresponding to the threshold voltage changes, with a stretched exponential function using the linear regression algorithm. In this way, we obtain the trend of the variation induced by the bias stress phenomenon that subsequently has been subtracted to the ΔV_{CF} curve, as a matter of fact removing the effect of this undesired phenomenon from the recorded data. The signals resulted from the application of this reasoning will be showed in the next sections.

Extrapolation of pH variations from ΔV_{CF}

An attempt to extract the pH variations induced by the metabolic activity of cardiomyocytes cultures starting from the V_{CF} variations has been performed. No calibration curve can be experimentally obtained from the pH blank experiments since only three pH values has been investigated, i.e. a neutral (7.3), an acidic (2.8) and a basic (11.4) values, as better described in next sections; therefore, it has been decided to start from that presented in (Spanu et al., 2017), that has been calculated from data acquired with similar devices to those used in this work. Subsequently, this curve (that showed to be a sigmoid) has been fitted on the pH values measured during this project in terms of initial and final values, maintaining the same time constant, that stands for the detection principle of the peculiar sensor. The so fitted calibration curve represents the relationship between the pH value and the variation of V_{CF}, and can be employed to extract the pH value from the ΔV_{CF}.

4.2.4 Processed experimental data

As described in previous section 4.2.2, observing the recorded data it is possible to note some issues to be solved, such as the existence of a drift of the output current, that has been imputed to the bias stress effect, to be removed. To try to solve these issues, an equivalent electrical model has been proposed: in this section the results obtained applying it have been presented.

Bias stress correction on experimental data

The blue curve in figure 4.4 shows the signal recorded from the metabolic activity sensor's (in terms of b_m/a that is equivalent to the variation of the threshold voltage multiplied by the constant term CR). On the basal phase of this curve, whose decreasing trend is evident, has been fitted the stretched exponential described by equation 4.8 (that is the black dashed line in figure), and finally the orange curve is the signal resulting from the bias stress removal, extracted by substituting the fitted stretched exponential equation to the previous value of b_m/a in the expression 4.7, thus obtaining ΔV_{CF}

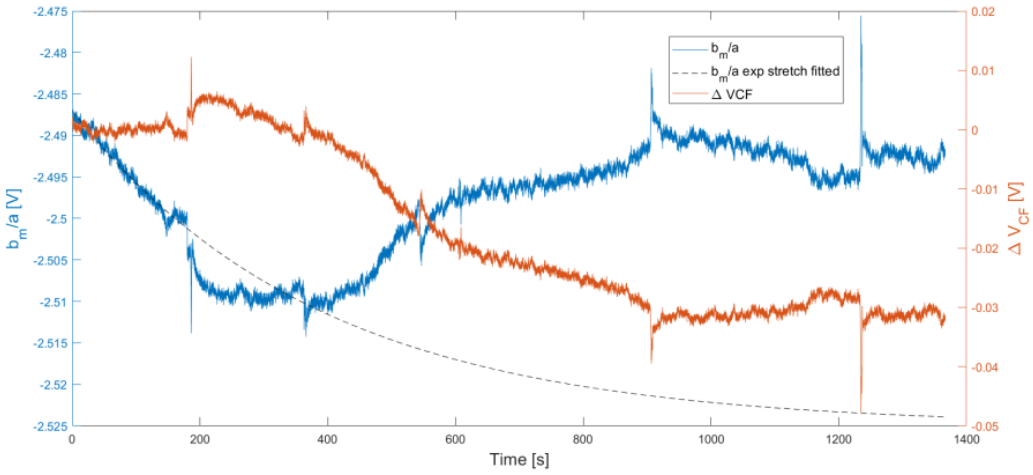

Figure 4.4 Bias stress correction through a stretched exponential. The blue curve represents the threshold voltage variation (b_m/a) before the bias stress removal; the black dotted function is the stretched exponential fitted on the basal phase of the previous one. Finally, the orange curve represents the ΔV_{CF} signal in which the bias stress has been corrected by subtracting the stretched exponential. Isoprenaline's additions occur after 186, 366 and 545 seconds after the recording's beginning, while verapamil's after 907 and 1235 seconds, respectively.

As it is possible to see from the figure 4.4, after the correction, the signal corresponding to the basal phase is horizontal and at $\Delta V_{CF} = 0$, since it has been taken as a reference;

nevertheless, the phases in which isoprenaline has been added show a decrease of voltage values, while the verapamil administration makes the curve become horizontal again, even if a slight trend to a voltage increase can be grasped in these last stages. It is noticeable that the two curves have mirror-like symmetry due to a sign variation between formulas C.23 and C.22. The ΔV_{CF} decreasing is equivalent to an increase of the transistor's output current since, referring to the model constituting of a series of two capacities (i.e. the control gate and the transistor's channel) shown in figure C.3, if the voltage drop between the control gate voltage V_C and the floating gate V_F (i.e. across the control gate capacitor) decreases, it has to increase the voltage drop between the floating gate and the source, i.e. across the transistor's channel; consequently more current will flow in the channel. Therefore, the I_D current will increase, when it should decrease following the OCMFET operational principle; the issue regarding the discrepancy previously mentioned come back once again.

Comparing the processed signal to the electrophysiological one as in figure 4.5, it is possible to observe that ΔV_{CF} starts to decrease when isoprenaline is added to the solution, and its slope slightly changes after each of the two initial administrations (at the same time, also the heartbeat increases a little), while after the third a boost in the spiking frequency, that doubles its value, matches with a decreasing V_{CF} that has a point of flex. On the other hand, after the addition of verapamil, the curve became more or less planar again, with a faint trend to increase while the electrophysiological activity slows down only a little bit, while after the second injection the spiking frequency rapidly zeroes (while only slightly variations occur on the metabolic activity sensors, maybe ascribed to the short recording time after the second addition of verapamil).

The same data analysis has been applied to the pharmacological blank experiments (i.e. devices on which no cells were plated and on which the protocol described in 4.2.1 has been performed), to investigate the direct reaction of the employed compounds on the metabolic sensors. The results are depicted in figure 4.6, in which is showed a representative pharmacological blank experiment (chosen because of the similarity between this transistor's performances and those of the OCMFET sensor for metabolic activity in the experiment with cardiomyocytes).

As it is possible to see, artifacts are formed in correspondence of the drugs administration; in particular the first one - identified by the first vertical, red dashed line and linked to the addition of isoprenaline in the solution - is bigger than the second one (addressed by the second vertical, red dashed line), that in turn is barely detectable (to recall the experimental protocol of the pharmacological blank experiments please refer to section 4.2.1). This is observable also in the corrected data (the orange curve) but, once applied the bias stress

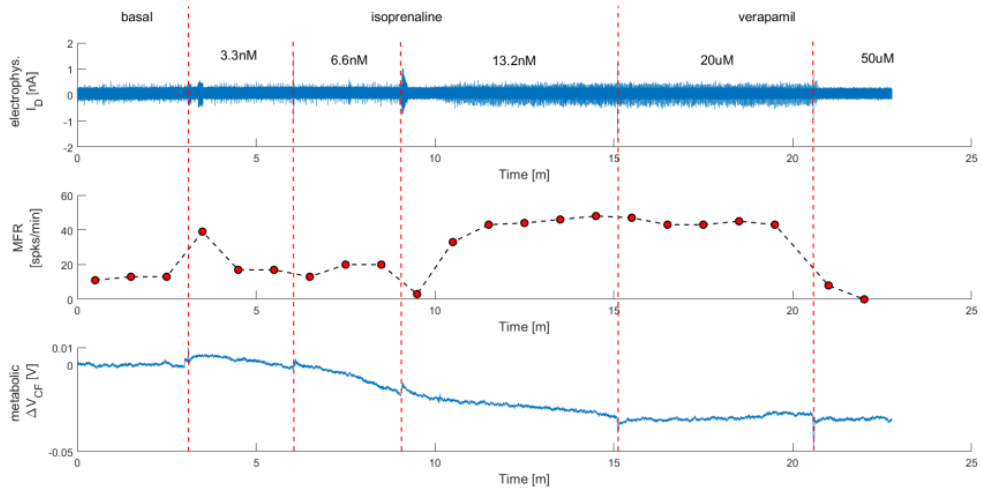

Figure 4.5 Processed signals recorded from electrophysiological and metabolic activity. The first trace is converted from voltage to current, using the process described in 4.2.3, the *mean firing rate*, MFR is calculated for each minute of the electrophysiology signal; while the metabolic activity signal has been filtered and down-sampled and converted in ΔV_{CF}. Finally, the bias stress has been removed using the proposed model.

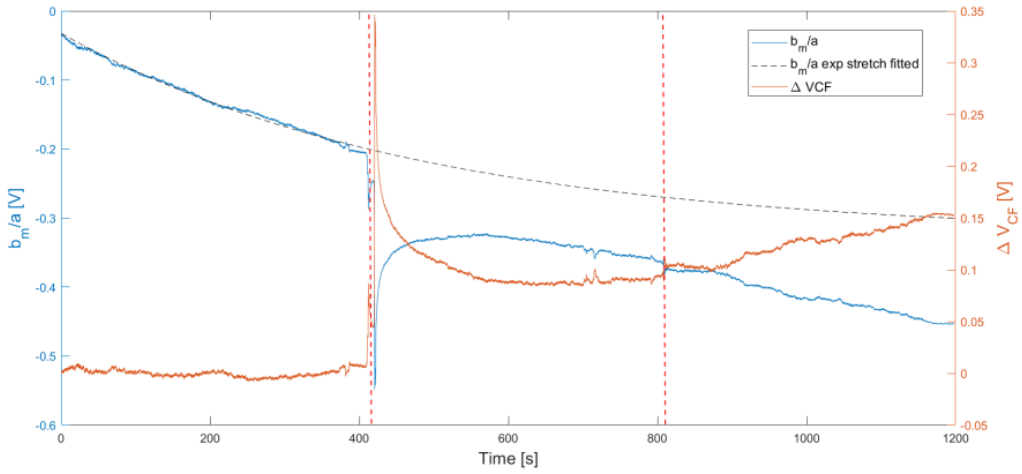

Figure 4.6 Bias stress correction through a stretched exponential of the blank pharmacological experiment. The blue curve represents the threshold voltage variation (b_m/a) before the bias stress removal; the black dotted function is the stretched exponential fitted on the basal phase of the previous one. Finally, the orange curve represents the ΔV_{CF} signal in which the bias stress has been corrected by subtracting the stretched exponential.

correction on the signal, seems that after the verapamil addition the curve changes slope. Indeed, the non-modified curve (blue in figure) decreases constantly after the first addition of drug and its slope appears to remain unchanged after the second one; but after the bias stress

removal the (orange) curve shows a change of slope also in correspondence of the second drug injection. These results can be caused by several effects, as for example the changes of volume due to the compound's addition: as a matter of fact, the first drug administration that provokes a bigger effect also provokes the bigger volume changes (approximately 10%, while the volume variation induced by the verapamil addition is around 3%); a second reason can be a charge variation induced by the approaching of the researcher with the pipette to insert the drug (if the pipette or the operator are charged, they can modify the total amount of charge in solution, that is not grounded since no reference electrode is used during experiments). Further investigation are needed to certainly state which is the cause of this behaviour, but for sure it is necessary to keep in consideration this effect on the trend of the curve.

Evaluation of pH variations

As previously mentioned (see section 4.2.2), measures with acid and basic solutions have been performed in order to investigate the response of the sensor to pH changes occurring in the solution. To this end, those signals have been converted into voltage variations through the equivalent model, as previously described for the experimental data and for the pharmacological blank experiment. The results are shown in figure 4.7 and, as it is possible to see, they are coherent with the one showed previously: also in this case, when the acidic solution is put in contact with the sensing area the ΔV_{CF} decreases, while it increases when the basic solution is employed.

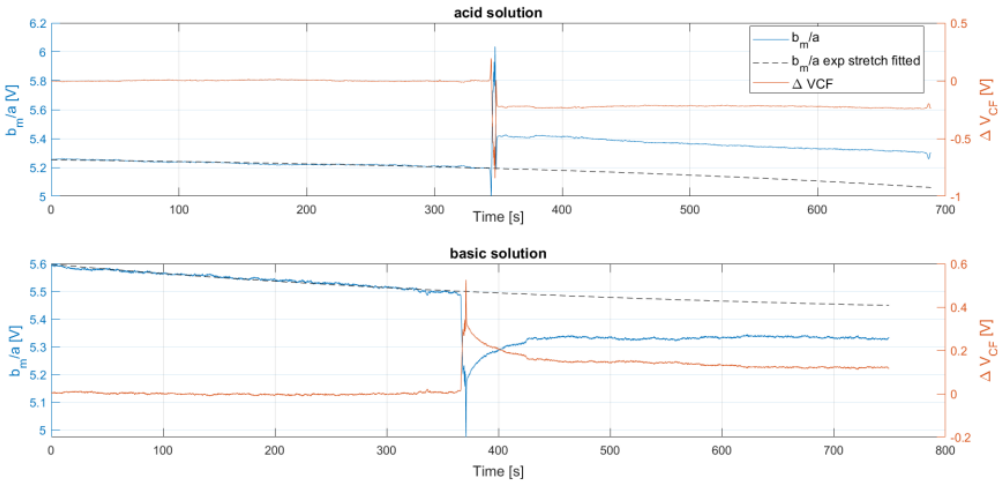

Figure 4.7 Processed signals recorded employing acid (up) and basic (down) solutions. In both cases, the blue curve represents the signal converted in terms of b_m/a, i.e. the threshold voltage multiplied by a constant; while the black, dashed curve is the stretched exponential fitted on the basal phase of the previous one. Finally, the orange curve is the bias stress corrected.

This is an important result, since it means that the behaviour of the transistor is consistent with the supposed behaviour of the cells culture stimulated by the drugs. In addition, these signals involving acid and basic solutions have been used to extrapolate the relationship between ΔV_{CF} and pH variations used to fit the previously presented calibration curve to the currently used devices. The ΔV_{CF} signal has been converted into pH variations, through the fitted sigmoid, is shown in figure 4.8.

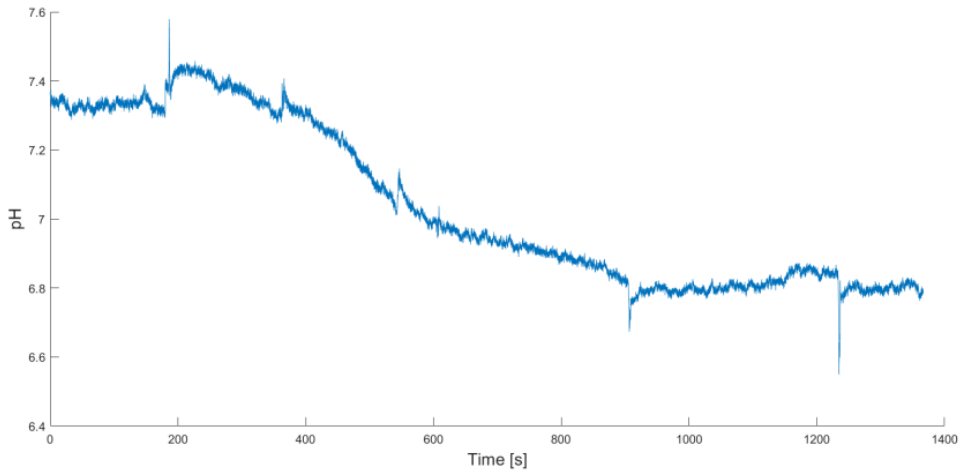

Figure 4.8 pH variations extracted from the experimental data.

From this graph it is possible to obtain an estimate of the acidification rate of the medium, that resulted

$$\Delta pH_{isoprenaline} \approx -0.04/min \quad and \quad \Delta pH_{verapamil} \approx -0.008/min \tag{4.9}$$

where $\Delta pH_{isoprenaline}$ is considered between the basal phase and the maximum dose (13.2nM) of isoprenaline, and $\Delta pH_{verapamil}$ between the maximum dose (50μM) of verapamil and the 13.2nM of isoprenaline. According to literature, a generic cell (this value is not specific for cardiomyocytes) produces approximately $10^8 H^+$ ions per second (Owicki, 1992), (Poghossian et al., 2009), and the expected value of $\Delta pH/minute$ is around 0.001 (Lorenzelli et al., 2003). It can be noted that the $\Delta pH_{isoprenaline}$ is an order of magnitude greater than those found in literature, but this can be partially due to other factors: first, in literature it is reported that following the stimulation the amount of produced protons can raise from 10 to 100 % depending on the cell type, the receptor and the coupling pathway (Poghossian et al., 2009); in addition, it must be taken into account that these data derived from a fitting

of the calibration curve, and this can affect the result's precision. On the other hand, the $\Delta pH_{verapamil}$ is in line with the results present in literature, but it is always decreasing the pH value, even if slower than before. This can be due to the fact that the records have been stopped too early after the administration of the second dose of verapamil, so even if the electrophysiological activity has been interrupted by the drug (as it is possible to see in figure 4.5), the pH variation has not inverted its slopes yet.

Conclusions

This work of thesis is aimed at designing a device that allows the simultaneous recording of both electrophysiological and metabolic activity of excitable cells. To this end, we exploited a peculiar OFET structure called OCMFET, that was already employed as a sensor for electrophysiological activity, and whose capacity of being used as a pH sensor had been demonstrated yet. In particular, first we evaluated the capability of the OCMFET-based pH sensor to detect the small changes in the concentration of H^+ ions due to the cell culture's metabolism and successively we designed an array that embeds both kinds of sensors to simultaneously monitor the two features. Several versions of the device for the simultaneous monitoring have been fabricated and modified to improve its performances and to adapt it to different readout electronics; subsequently, the validation experiments both involving living cells, and in particular primary cardiomyocytes from neonatal rats, and without cells (called blank experiments) have been performed. In particular, the blank experiments included some pharmacological tests, to evaluate the response of the device to the administered compounds, and pH tests performed with acidic or basic solutions to investigate the device reaction to known pH. With these experiments, we demonstrated the feasibility of the simultaneous recording of such different signals, even if some issues have not been resolved yet. Indeed, due to the Covid-19 pandemic that hit the whole world during the last year, stopping for several months the research activities and slowing down them until now in order to respect the anti-contagion regulations, this project underwent to an abrupt slowing down. The main effect of this was that a reduced amount of experiments with living cells have been performed during last year, that should have been the crucial points of this last stage. Nevertheless, an equivalent electrical model representing the OCMFET-based sensor has been designed, that helps to separate the effects attributed to the sensor itself (i.e. caused by charge variations onto the sensing area) from those linked to the transistor itself, such as the bias stress caused by the prolonged application of the gate voltage, in the recorded signals. The latter effects are expected to be bigger in amplitude than those provoked by the sensor and so can hide them. Consequently, the possibility to remove the effects belonging to this category should

allows to better observe the variations induced by the cells. However, after having removed the bias stress contribution to the signal, it became clear that also some other phenomenon affects the recorded traces and, even if it is not possible to certainly associate these effects to a pH variation since other events can provoke it (such as the volume change that follow the solution with the drug), we have to keep in consideration this outcome. The electrical model has been used also to "convert" the signals, expressed in terms of multiple of the threshold voltage in pH variations: also in this case, the obtained results showed a value that is an order of magnitude bigger than those presented in literature; nevertheless, analysing them we have to consider both that the calculated values refer to a stimulated culture, and that the presented pH values are extracted from a fitting and this can influence their precision.

This project demonstrated the feasibility of the simultaneous recording of the electrophysiological and metabolic activities using organic field effect transistors. In addition, through the equivalent model, a deeper knowledge of the OCMFET-based sensor has been acquired, and a way to improve the analysis methodologies of the recorded data, supporting the experimental results with an analytical validation, has been found.

In the near future, further investigations are needed to understand the causes of the sensor's response to the drugs; in addition, also the calibration curve for the metabolic sensor in this configuration must be extracted. As future perspectives, the idea of adding other sensors to the device (such as a sensor for detecting the contraction of cardiomyocytes) to further enhance the range of information that it is possible to acquire can be intriguing. On the other hand, also the using of these devices for *in vivo* applications is a charming outlook to exploit all the properties of these sensors at their best.

Appendix A

Sensors fabrication

This appendix contains a detailed description of the general fabrication process used to produce each MOA. During this PhD project, some changes have been brought to this procedure in order to optimize the devices' performances: these are explained and partly described in the sections relative to the design of the MOA for simultaneous recordings (please refer to section 3.3), but the technical details are reported in the following sections.

A.1 Floating gate deposition and patterning

The MOA fabrication starts with the substrate preparation: a piece of 250 μm-thick PET sheet (Goodfellow, Huntingdon, UK) is cut, carefully washed with acetone, ethanol and deionized water and dried with nitrogen. This is the standard cleaning procedure that is applied before each step of the fabrication protocol.

The second step is the metal deposition, that is performed through thermal evaporation: the clean substrate is immobilized onto a substrate holder and inserted into vacuum chamber of the thermal evaporator, that deposits a thin ($\approx$ 50-100nm, corresponding to $\approx$ 60mg of titanium or gold, or $\approx$ 10mg of aluminum, that are the material tested, as described in section 3.3.1) metal layer all over it.

A photolithographic process is then applied to pattern the floating gates starting from the uniform metal layer. To this end, after a second cleaning procedure, a thick layer of a positive photoresist (AZ1518, from Microposit) is deposited on the metal through spin coating, and dried for 3 minutes at approximately 85°C on an hot plate. Successively, a mask is aligned on the substrate and it is exposed to UV light for about one minute and a half. The following step is the development, during which the photoresist in excess is removed by immersing the substrate in bath containing sodium hydroxide (NaOH) solution and rinsing it with deionized

water. Since the employed photoresist is positive, after this phase it reproduces exactly the superimposed mask, i.e. the floating gates layout. To obtain the same layout on the underneath layer, all the excess of metal is etched using hydrofluoric acid (HF) solution if the deposited metal is titanium or aluminum, or potassium iodide (KI) solution if it is gold. Lastly, another cleaning procedure helps to remove the residual photoresist, leaving the device ready for the following fabrication stages.

Together with the floating gates, during this phase are patterned also the passive microelectrodes, that are thus made of the same material used for the floating gates.

A.2 Dielectric deposition

If floating gate material is titanium or aluminum, we exploit the optimal capacitive performances of the combined native oxide (≈5nm) and Parylene C (≈150nm) bilayer dielectric. Consequently, to promote the native oxide film formation, the device undergoes to a thermal process (65 °C for 12 hours); alternatively, a quick oxygen plasma treatment at medium power (at 100W for 60 seconds) is used. If the chosen material is gold, the dielectric layer is formed only by the 150nm-thick layer of Parylene C, thus the previous process it is not performed.

The Parylene C is deposited through a chemical vapour deposition (CVD) process, using a *PDS2010 LabCoater* from Special Coating Systems; to reach a layer thickness around 150nm, approximately 300mgr of Parylene C are deposit. In addition, a small amount (≈ 1ml) of silane are added in the deposition chamber in order to improve the Parylene C adhesion to the substrate.

A.3 Self-alignment procedure and source, drain and control gate pattering

As previously discussed in section 3.1, the self-alignment procedure allows to increase the transistor's performances (between which the most important is the cutoff frequency) by decreasing the parasitic capacitances between the gate and the source and drain contacts. It consists basically in a photolithographic process (thus performed as described in section A.1 in which the floating gate itself is used as mask. In this way, final result of the photolithography is that the thick photoresist layer remains only onto the transistors' channel. The process is showed in figure A.1.

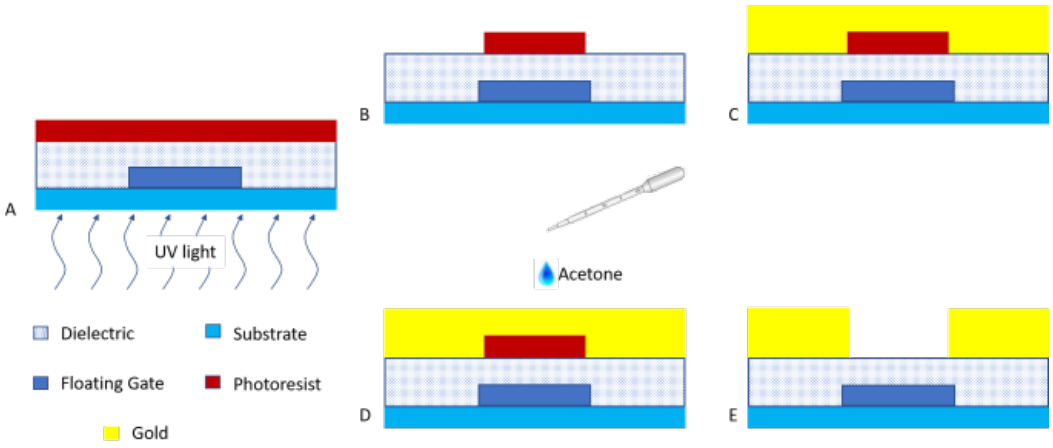

Figure A.1 Self-alignment procedure. After the deposition of a thick layer of photoresist, the floating gate is used as a mask for a photolithographic process (A); following the development of the resist, it remains only on the transistor's channel (B). A gold thermal deposition is then performed (C) after which the remaining photoresist is removed by a washing with acetone (D), thus provoking the lift-off of the gold deposited on top of it (E).

The following step is the thermal evaporation of a layer of gold, that covers the whole substrate.

Subsequently, the remaining photoresist is removed from the channel areas of the transistors by washing it with abundant acetone thus causing the lift off of the overlying gold layer. After that, source, drain and control gate contacts are patterned through a further photolithographic procedure; to align the masks with a good precision (with a tolerance of 10 μm), concentric rectangular frames circumscribing the MOA are used as references. Finally, the substrate is newly cleaned and it is ready for the next stage.

A.4 Sensing areas' functionalization

To activate both the type of sensors (for electrophysiological and metabolic activities) on the same substrate, as previously explained in section 3.3.3, an additional Parylene C layer must be selectively deposited onto the metabolic activity sensors' sensing areas. To this end, since the Parylene C is deposited through chemical vapour deposition (CVD), a technique that deposits it uniformly onto the whole surface to create a high conformable layer, the parts on which polymer deposition must be avoided have been protected by a thick layer of photoresist that in turn is covered by adhesive tape. The latter can be easily removed after deposition (while the photoresist alone would be incorporated into the Parylene C, thus making it very difficult for the solvent to reach and clear it away), while the former prevents

the tape glue from damaging the device. After that, a photoresist layer is deposited to protect all the substrate except for the OCMFETs' sensing areas (independently of their final use), that are exposed through a photolithographic step. Subsequently, a 3D-printed plastic ring (which internal radium is 8.5mm and height is 9mm) is glued using polydimethylsiloxane (PDMS, which biocompatibility is well-known) onto the device's surface to delimit the culture chamber. The next step is an oxygen plasma exposure that remove the dielectric from the sensing areas of the electrophysiological sensors simultaneously activating the Parylene C on the sensing areas of the sensors for metabolism. The O^2 plasma exposure time has been carefully computed in order to remove all the Parylene C from the electrophysiology sensors' sensing areas without excessively etch the layer on top of the sensing areas of metabolic activity sensors. Consequently, it is necessary to precisely know the thickness of the first Parylene C layer: to this end, during the CVD, Parylene C is deposited also on a microscope glass slide which extremities are covered by adhesive tape. Subsequently, after having removed the tape (under which Parylene C doesn't deposit) the thickness of the polymer deposited onto the glass slide is measured through a profilometer (from Bruker), and the plasma time is calculated considering that the plasma etching rate is approximately 90nm/min. Finally, the photoresist is removed only outside the culture chamber (while inside it, the photoresist acts as an additional passivation layer since it has already been demonstrated that it is biocompatible and adapt for this role (Spanu, 2016)). The final procedure employed to activate the sensors is shown in figure A.2.

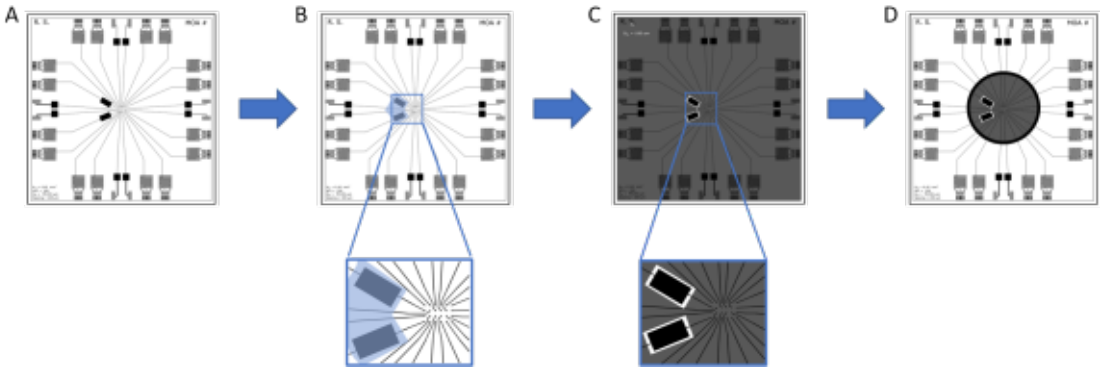

Figure A.2 OCMFET-based sensors' activation procedure. Before to remove the Parylene C from the OCMFET-based sensors for electrophysiological activity (A), a second selective deposition of Parylene C onto the sensing areas of sensors for metabolic activity has been performed (panel B). The next step is a photolithographic process to cover the whole substrate except for the sensing areas (panel C). Finally, after the gluing of the plastic ring, the photoresist has been removed only in the surface external to the ring, while inside the culture chamber it serves as additional passivation layer (D).

A.5 Organic Semiconductor deposition

To complete the fabrication process, the last two steps are missing. The first is the cut of the device from the larger portion initially collected from PET sheet, in order to make it fit with the standard Multi Channels Systems ground plate used as base for the readout electronics, and also to maintain the culture at the right temperature (37 °C) during the experiments. To do this, the inner rectangular concentric frame is used as reference, since cutting above this line guarantees to get a device of the right dimensions.

Finally, the organic semiconductor is deposited on the channel of each transistors of the MOA. In particular, a small amount (approximately 0.8-1μL) of a solution of 6,13-Bis(triisopropylsilylethynyl)-pentacene (TIPS Pentacene, Sigma Aldrich) in anisole (1 w/v%) is drop-cast on each OCMFET and let dry under a chemical hood until solvent is completely evaporated.

The devices are then completely characterized and the fabrication process is completed. The main steps of the protocol are showed in figure A.3

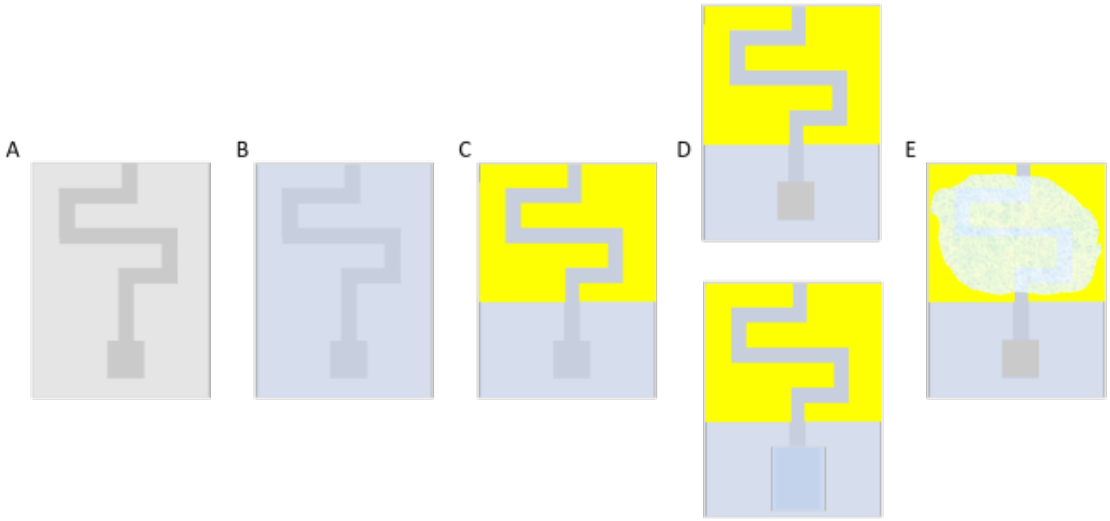

Figure A.3 Scheme of a general fabrication process. Firstly, the floating gate material is evaporated and patterned (A); after that the Parylene C layer acting as dielectric is deposited (B) and the gold source, drain and control gate are generated by thermal evaporation and photolithography (C). The following step is the sensing area's activation, that depends on the kind of sensor: for the electrophysiological activity's detector, Parylene C is removed from the sensing area by an oxygen plasma etching (D, up), while for metabolic activity's one a second layer of Parylene C is deposited and subsequently activated through plasma exposure (D, down). The last phase is the organic semiconductor deposition by drop casting (E).

A.6 Experiments with living cells

A.6.1 MOA sterilization and preparation

The day before cell plating, the culture chamber is sterilized through a mild oxygen plasma treatment (40 Watt for 40 seconds) and by a wash of approximately 25 minutes with 70% ethanol solution (if Parylene C is used as passivation layer) or, alternatively, by an UV light exposure (if the photoresist covers part of the chamber, since ethanol modifies this layer). This procedure at the same time sterilizes, increases the degree of hydrophilicity of the culture chamber surface (onto which cardiomyocytes should adhere) and removes residues of organic molecules, improving cell health and development. If ethanol is used to sterilize, the chamber is then rinsed with sterile water. Subsequently, the culture chamber is covered with adhesion factor (laminin, 50/80 μg/ml), and the devices are stored into the incubator for 12 hours. Finally, the day of the cells collection, the solution containing the adhesion factor is removed and the chamber newly rinsed with 300 μl of sterile water to clear away the non-bounded molecules of laminin.

A.6.2 Cardiomyocytes cell cultures

To obtain cardiomyocytes to be plated and grown onto the MOA devices, post-natal hearts are micro-dissected within 5 days after the rat pup's birth. Briefly, the atria and vascular tissues are removed while the ventricles are minced into small pieces (1-3 mm^3); these pieces are then enzymatically digested using a solution of Collagenase type I and Pancreatin diluted in a buffer solution containing 100mM $NaCl$, 10mM KCl, 1.2mM KH_2PO_4, 4mM $MgSO_4$, 50mM Taurine, 20mM Glucose and 10mM Hepes, with pH 7. The so dissociated cells are centrifuged and re-suspended in culture medium consisting in DMEM-M199 (8:1), 4% FBS (Fetal Bovine Serum),6% horse serum, glutammine and 10 μg/ml Gentamycin. Subsequently, they are pre-plated in no-precoated Petri dishes to decrease the percentage of non-cardiac cells by separating the two main populations composing this tissue, i.e. cardiac fibroblasts and cardiomyocytes, since the cardiomyocytes adhere slower than the fibroblast population to the dish. The pre-plating process takes about two hours, at the end of which the medium with the cardiac cell fraction still in suspension is recovered from the Petri dishes and collected in a conical centrifuge tube in order to concentrate the cardiomyocytes and subsequently dilute them at the desired final concentration. Cardiomyocytes are then plated onto the sensing area of the devices in about 200 μl of solution to reach a final density of 500/800 cells/mm^2; after few hours, when cells began to settle and adhere to the detection areas, total volume of

culture medium is increased to 400μl. After 48/72 hours from cells plating the medium is substituted with a new one composed by Neurobasal, β27, 1% Glutamax100 and 30μg/ml Genamicyn, with the addition of 1% horse serum. The subsequent day the horse serum is completely removed by changing the culture medium with one with the same concentration of the previous. From then on, the culture's medium is changed every 3 days. The recordings of spontaneous heartbeat activity generally begin around the 4th Day in Vitro (DIV) and continue until the 7th-8th DIV. After, the presence of fraction of cardiac fibroblasts alters the balance of the heart syncytium.

A.6.3 Neuronal cell cultures

The employed neuronal cells derived from hippocampus of rat embryos at day 18. After having removed the brain from the skull, the hippocampuses were isolated from the single hemispheres; the tissue was then dissociated in 0.125% of Trypsin/Hank's solution containing 0.05% of DNAse for 15-18 minutes at 37°C. After having removed the supernatant solution, the enzymatic digestion was stopped by adding 10% fetal bovine serum (FBS) in Neurobasal medium. After 5 minutes, the medium with FBS is substituted with Neurobasal supplemented with β27, 1% Glutamax, and 10 $\mu g/ml$ Gentamicyn. After that, cells are plated onto the MOA culture chamber at a total density of 10^5 cells per device and incubated at 37°C in a humidified 5% CO_2 incubator. After plating, half of the medium was exchanged every 3-4 days.

Appendix B

Readout electronics

Any new matrix of sensors for living cells monitoring needs a compatible readout electronics to pre-process the signals and deliver them to a device in which a software will display and save the recorded data. The sensors arrays available on the market have their own electronics and software (see sections 1.3 and 1.4), while for the MOAs, readout electronics have been implemented *ad hoc*. In particular, these circuitry have been designed to be used with the standard base of the Multi Channel Systems, to exploit its integrated cells culture heater, and are compatible with the proprietary software of the same company, that allows to monitor in real time up to 64 channels (corresponding to the number of microelectrode fabricated onto a standard Multi Channel Systems MEA). Unfortunately, with this software is far more difficult to evaluate in real time the slower variations due to the pH changes in solution, since it was designed for higher frequency signals such as electrophysiological ones. The principal characteristics of these electronics are obviously imposed by the typical features of the signals to be recorded: in this case, the two signals are quite different from each other since the electrophysiological activity is a small ($\approx$ 100pA-10nA), relatively high frequency signal ($\approx$ 10Hz-1KHz); while the pH variation is a very low frequency signal. MOAs contain also a variable number of passive electrodes (please refer to sections 3.3.2 and 3.3.2) that can be used both to record the culture's activity (to have reference signal with which compare the shape/frequency of the signal recorded from transistors) but also - in principle - to stimulate cultures. However, it is not possible to record simultaneously from OCMFETs and passive electrodes, since the latter are compatible with the original readout electronics made by Multi Channel Systems for its devices.

As previously mentioned, during this PhD project two different versions of readout electronics have been employed, that differ for several reasons. In the present appendix, the two systems have been illustrated, with a description of the blocks composing each channel

(from the point of view of both transistor's polarization and filtering of the output signal). In particular, more attention has been put on the second version, that in the next sections is called *SuperOFET*, also highlighting the improvements implemented on the second version with respect with the first one, since it has been described here for the first time and it has been used in the last part of the PhD project, when the experiments involving the simultaneous recordings (described in section 4.2) have been performed.

B.1 16 channels readout electronics

As previously shown (see section 3.3.2), the first electronics used can operate simultaneously up to 16 OCMFETs, and it is connected through a traditional SCSI port to a computer in which the proprietary software of the Multi Channel System is installed. Between its principal characteristics, it includes:

- It can be powered using both an USB (to improve its portability), a single not stabilized or a double stabilized external power supply;
- It polarizes transistors in *diode* configuration, i.e. with the same voltage applied both to the (control) gate and to the drain, with respect to the source. The available voltage range is -1/-4V;
- It is possible to contact the passive micro-electrodes to exploit them for electrical stimulation (as we said previously, it is not possible to record simultaneously from both active and passive sensors).

A photograph of the 16-channels readout electronics is shown in figure B.1

B.1.1 Filtering stages

The filtering stages are composed by a first current-to-voltage converter, that is necessary since the transistor's output is a current that must be converted in a voltage; in particular, a *transimpedance amplifier* (TIA) has been used, since it is a broadly recognized way to amplify sensors' low current outputs. It is however crucial to carefully chose the operational amplifier's feedback resistance in relation to the expected input currents, in order to avoid its saturation; in this case, it has been chosen a feedback resistance of 1MΩ.

Following the TIA stage, there is the filtering one; in which it is selected the interval of signal frequencies we are interested in, that obviously will be different for electrophysiologi-

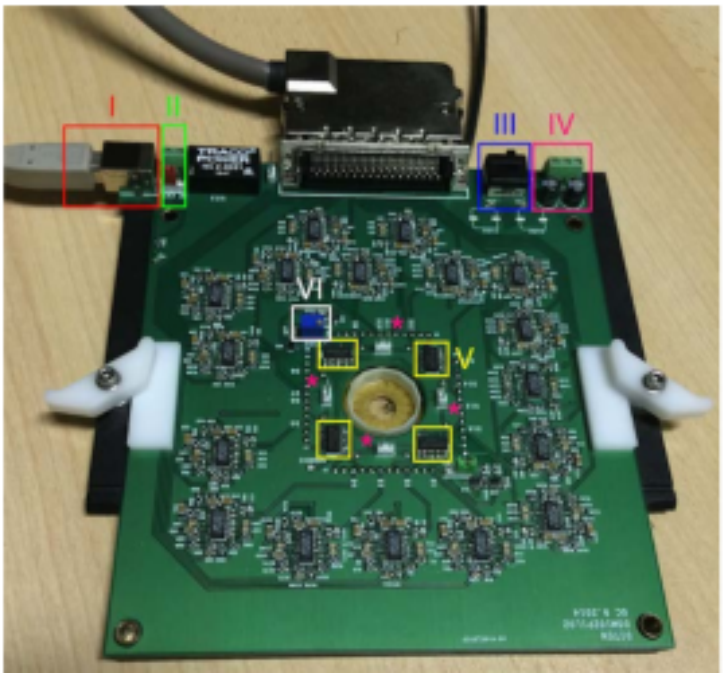

Figure B.1 Photograph of the 16-channels readout electronics. Some features of the electronics have been highlighted, such as different power supplies: USB (I), single not stabilized external power supply (II), power supply switch(III) and dual stabilized external power supply (IV). In addition, there are the 16 buffer to assure independent source polarizations, and bias circuits (VI). From (Spanu, 2016).

cal and metabolic activity. In the following lines, a brief description of the solution adopted to filter both kinds of signals is provided.

Filtering stages for electrophysiology sensors

Filters for electrophysiology sensors are band-pass, in order to remove (thus avoiding to amplify) all the noise that is outside the frequency range of the signal itself. In particular, these filters have been designed employing the so called *Sallen-Key configuration*, that is an electronic filter topology introduced by R.P. Sallen and E.L. Key in 1955, from MIT Lincoln Laboratory (Sallen and Key, 1955). It is commonly applied because of its flexibility; indeed, starting from the general configuration, it allows to implement second-order active high-pass, low-pass, band-pass or band-stop filters merely modifying the impedances types and values. In addition, it also permits to easily chose the filter gain and to generate high-order filters by cascading more filtering stages, since this topology is characterized by a huge (practically infinite) input impedance and a very tiny (almost zero) output impedance which ensures that stages can be set independently and without affecting each other.

In particular, in this version of readout electronics, the filtering stage implemented for the sensors for electrophysiology signals is a band-pass filter constituted by a cascade of two Butterworth filters: a IV order high-pass filter (formed by a cascade of two II order filters), and a II order low-pass filter, that has an overall bandwidth of 150Hz-4.8kHz, and a total gain of 140.

Filtering stages for metabolic activity sensors

Since pH variations occur at very low frequencies, the filters for these channels are usually low-pass with a cutoff frequency of approximately 10Hz, thus allowing the reading of the direct current and rejecting all the higher frequencies.

B.2 SuperOFET readout electronics

This second version of the readout electronics became available after I started my project. As previously mentioned in section 3.3.2, it was designed before the beginning of my PhD to be compatible with a new variant of MOA (fabricated at the IBM laboratories in Almaden, California) that contains 56 OCMFET-based sensors. During the design of the SuperOFET electronics also several other improvements have been implemented, with the main purpose to increase its versatility, so as to make it easily adaptable to perform different types of experiments. Principally, with this version it is possible to:

- independently operate each OCMFET, also by applying different voltages to drain and control gate. On one hand, this means that each transistor can be set on its own working point, thus working in the best conditions. But on the other hand, this largely increases the quantity of connections to be established between the MOA and the electronics, inasmuch each transistor has three (source, drain and control gate) or four contacts (adding the floating gate, even if it is not connected) and this greatly increases the complexity of the electronics pin-out and of the corresponding MOA's layout;
- improve flexibility, since the overall system is composed by two different types of Printed Circuits Boards (PCBs): the main PCB is the one in which the spring contacts that connect the MOAs to the electronics are placed; moreover it contains the current to voltage converters (TIA) and the channels' multiplexers. All the other analog and digital circuits necessary to the polarization of the transistors and the filtering of the output signal are situated in the secondary PCBs, that are one for each channel. The secondary PCBs are connected to the main one through DF3 connectors so that

they can be assembled and disassembled each time it is needed. In this way, it is possible to modify the filtering stages of each channel every time is required by the experiment conditions without modify the main PCB. Interestingly, the digital part of the circuit, that is needed only during the set-up phase of the electronics, is powered by an Arduino device (more details will be furnished in the next sections), that is disconnected before the experiments starting, to avoid that digital clocks introduce noise during the recording phase;

- be powered both using an USB power supply (to improve its portability), or through single not stabilized or double stabilized external power supply, as the previous version. In this case, since the electronics is more complex and thus absorbs more current, it is usually power through the external stabilized power supply.

As in the previous case, also this electronics is connected to a computer through a traditional SCSI port.

A photograph of the SuperOFET electronics is depicted in figure B.2

B.2.1 Filtering stages

As in the previous case, the first stage of the electronic filtering system is the current-to-voltage converter, necessary for the same reasons previously mentioned: the transistor's output is a current. The transimpedance amplifier has been confirmed as the chosen solution for this step, again with a feedback resistor of 1MΩ thus allowing for input currents up to approximately 5μA to guarantee that the TIA is out of its saturation region; this circuit is placed on the main PCB.

The following steps, i.e. the filters themselves, are instead situated on the secondary, interchangeable PCBs. Indeed, the main idea was to create different sets of secondary PCBs implementing different filters in terms of bandwidth, gain and so on, in order to easily adapt the readout electronics to the various possible measurements. In addition, this allows to modify the number of sensors dedicated to the different measurements to meet specific experimental requirements. To this end, a batch of secondary PCBs have been purchased in which the skeleton of a four-stages Sallen-Key topology filter has been implemented, in order to exploit also the intrinsic flexibility of this filter's architecture. Indeed, modifying the values and types of inductances it is possible to design different filters, as has been described in section B.1.1. Indeed, starting from these same secondary PCBs, filters for both electrophysiological and metabolic activities have been designed.

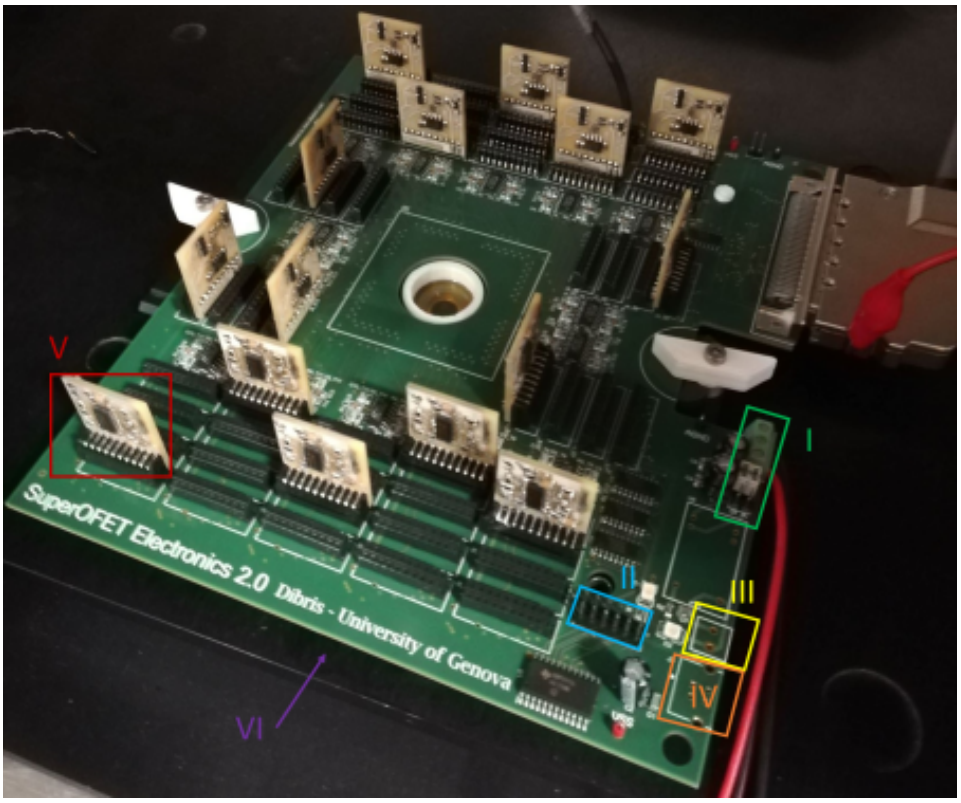

Figure B.2 Photograph of SuperOFET readout electronics. Some features of the electronics have been highlighted, such as different power supplies circuits: the dual stabilized external power supply (I) is the one current used, USB (III), single not stabilized external power supply (IV). In addition, the connector between Arduino and the electronics (II), the main (VI) and a secondary (V) PCBs are pointed out.

Filtering stages for electrophysiological sensors

In this version, the filter's bandwidth has been narrowed, going to 150Hz-4.8kHz to 150Hz-3kHz; and also the overall gain has been reduced from 140 to 20. The band-pass filter is again composed by a cascade of two Butterworth filters but, in order to make the filter more selective (i.e. to increase the steepness of its transfer characteristic), in particular to reject frequencies such as the power line interference (50Hz) and its principal harmonics, the high-pass filter order has been increased from IV to VI, while the low-pass filter remains of II order. Figure B.3 represents the schematics of the complete filter for electrophysiological sensor, along with its frequency response, calculated through a simulation performed with the open-source program LTSpice.

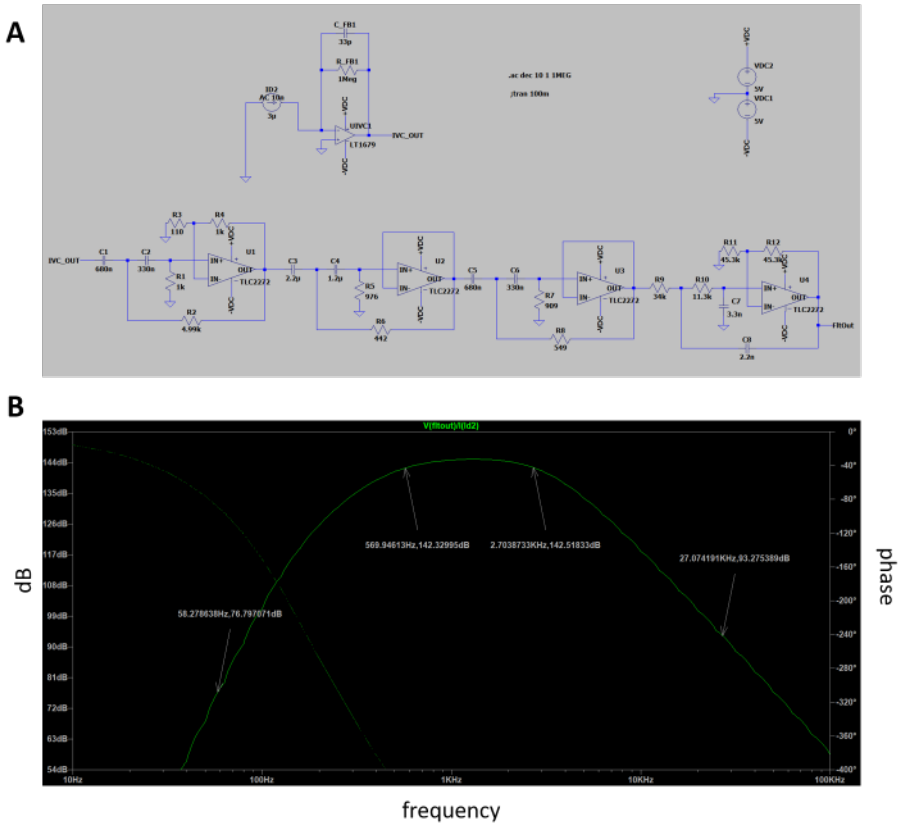

Figure B.3 Electrophysiology filter, schematic (A) and frequency response (B). The filter is composed by a current/voltage converter, a VI order high-pass and a II order low-pass Butterworth filters. The band-width is 150Hz-3kHz.

Filtering stages for metabolic activity sensors

The signal recorded by pH sensors due to the cells culture's metabolic activity is a slow varying signal, so a band-pass filter like the one described for the electrophysiological signal is not suitable. In this case, a simple low-pass filter is needed, which bandwidth allows to amplify all the signals between the direct current and the 10Hz, while rejecting all the higher frequencies. By exploiting the same Sallen-Key filter's topology used for the previous filters, composed by a cascade of four single blocks, a Butterworth low-pass filter of the VIII order with a unitary gain (no amplification) has been designed. Schematics of the complete filter for metabolic activity sensor, along with its frequency response, calculated through a simulation performed with the open-source program LTSpice are shown in figure B.4. From this simulation, also the conversion factor between the recorded signal (i.e. voltage variations) and the actual transistor's output (i.e. current variations) has been obtained, as better described in section 4.2.3.

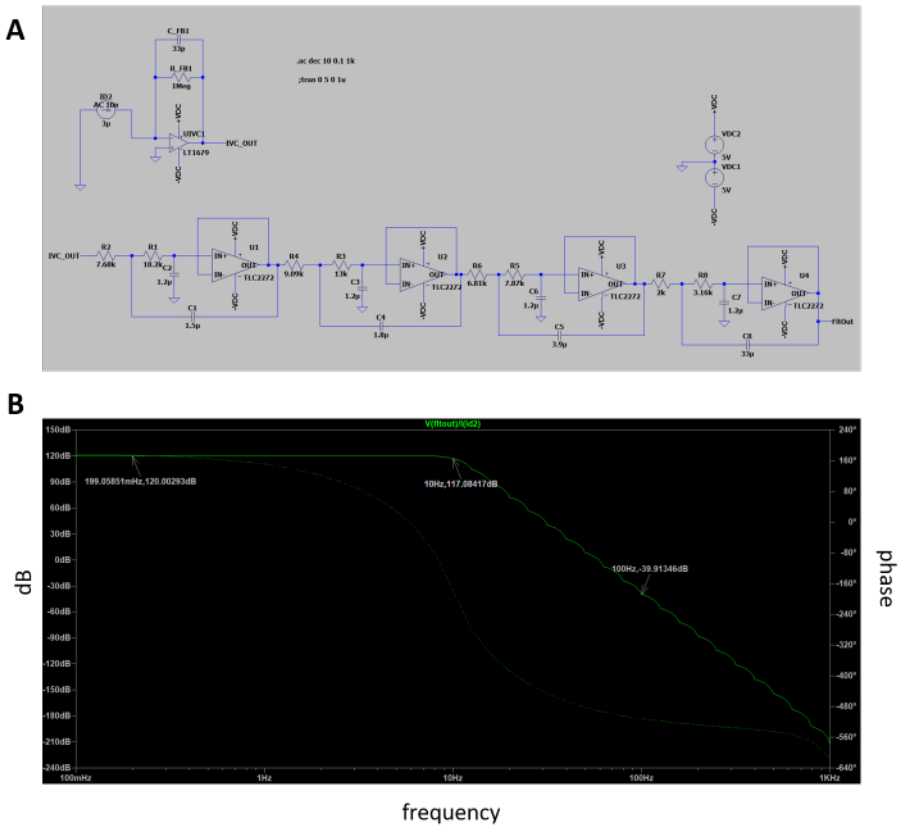

Figure B.4 Metabolism filter, schematic (A) and frequency response (B). The filter is composed by a current/voltage converter, a VIII order low-pass Butterworth filter with cutoff frequency at 10Hz.

B.2.2 Polarization stage

The polarization stage, as can be deduced from the name itself, is the circuit designed to supply the operating voltages to each transistor, to set its working point. In this case a particular polarization configuration has been used, in which the independent voltages are applied to the Source and Control Gate contacts, while the output current is read on the Drain by connecting it to the transimpedance circuit. Since at the input of the TIA circuit there is the (virtual) short circuit with the ground, it can be assumed that the drain contact is connected to ground itself, as shown in figure B.5.

It follows that the voltages are imposed between source/control gate and the drain that in this case acts as a reference. Consequently, to extrapolate the supply voltages in the standard configuration it is necessary to apply the mesh equation to obtain:

$$V_{GS} = V_{GD} - V_{SD} \tag{B.1}$$

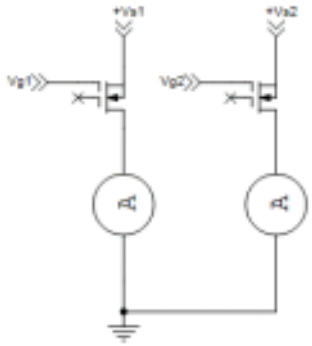

Figure B.5 SuperOFET polarization stage. Supply voltages are applied to the Control Gate and the Source contacts, while the Drain, on which the output current I_{DS} is collected, is connected to the ground through the transimpedance amplifier (TIA), indicated with the amperometer A in figure.

and

$$V_{DS} = -V_{SD} \tag{B.2}$$

From these equations it is possible to see that not all the combinations of voltage values can be implemented, and in particular that the gate voltage can't be greater that the source, since in this case V_{GS} should be positive (and the organic semiconductor used is p-type, so it is not conducting for positive voltages). Nevertheless, the main attempt is to use transistors in saturation regime, and it is guaranteed only when $V_D > V_G$.

Polarization circuit

As previously mentioned, this readout electronics allows to set independently the two polarization voltages, applied to the gate and the source, from which it is possible to came back to the V_{GS} and V_{DS} as indicated in the previous section. To this end, on each secondary PCB is placed also the digital circuit to polarize the OCMFET: in particular, two twin circuits are designed to set the V_C and V_S, each of which is formed by a potentiometer followed by an operational amplifier and allows to set each voltage in a range between 0 and 4V with steps of 62.5mV. The regulation of each potentiometer is made through a digital circuit that is powered only during the research of the polarization condition (during which all the transistors are polarized), while it is disconnected during the experiment's recording phase; indeed, potentiometers have memory, thus are able to maintain the received setting also when they are not powered. To address and regulate each potentiometer, it is needed a microcontroller

board; in particular, Arduino Uno is chosen because of its low cost, robustness and because it supports the easy and broadly known languages C and C^{++}, that makes it easy to write its scripts. In addition, it is the most used and documented board of the whole family.

B.2.3 Polarization's digital control

The possibility to set independently each transistors' supply voltages through the use of digitally controlled potentiometers offers the opportunity to test various polarization's configurations that differ for the relationship between the voltages, simply by writing different Arduino Uno scripts. During my project, two different polarization's modes have been tested, i.e. a diode polarization and a so called *current-driven configuration*. In the following rows, both of them are described in further details.

Diode configuration

The diode configuration has been implemented to maintain continuity with the previous version, i.e. to investigate the devices in the same conditions. It is the simplest way to operate the device, since a single voltage has been chosen and applied as V_{GS} and V_{DS} for all the available transistors. Referring to the previous equations B.1 and B.2, to set both of them to the same negative voltage value, V_{GD} must be set to zero, in order to obtain $V_{GS} = V_{DS} = -V_{SD}$. The software sets the potentiometers of the secondary PCBs related to the employed transistors, the list of which is given by the operator, simply addressing each of them in series and modifying its output voltage.

Current-driven configuration

The current-driven configuration is a more complex algorithm, based on the idea of setting all the OCMFETs in order to have similar output current to assure similar performances. The value of the output current is set by the operator as an adequate trade-off between the goodness of the transistor's performances and the guarantee to avoid the saturation of the transimpedance amplifier; since it is unlikely to exactly reach the targeted value, a confidence interval of accepted values was calculated (during this work of thesis, I chose 1μA, and the confidence interval include all current values that vary for less than 5%, i.e. 50nA). In this case, for each transistor an iterative algorithm has been applied, that schematically described by the flowchart in figure B.6.

Going more in details, it starts by setting an average value of voltages, then reads the direct output current and consequently modifies the supply voltages to make the current

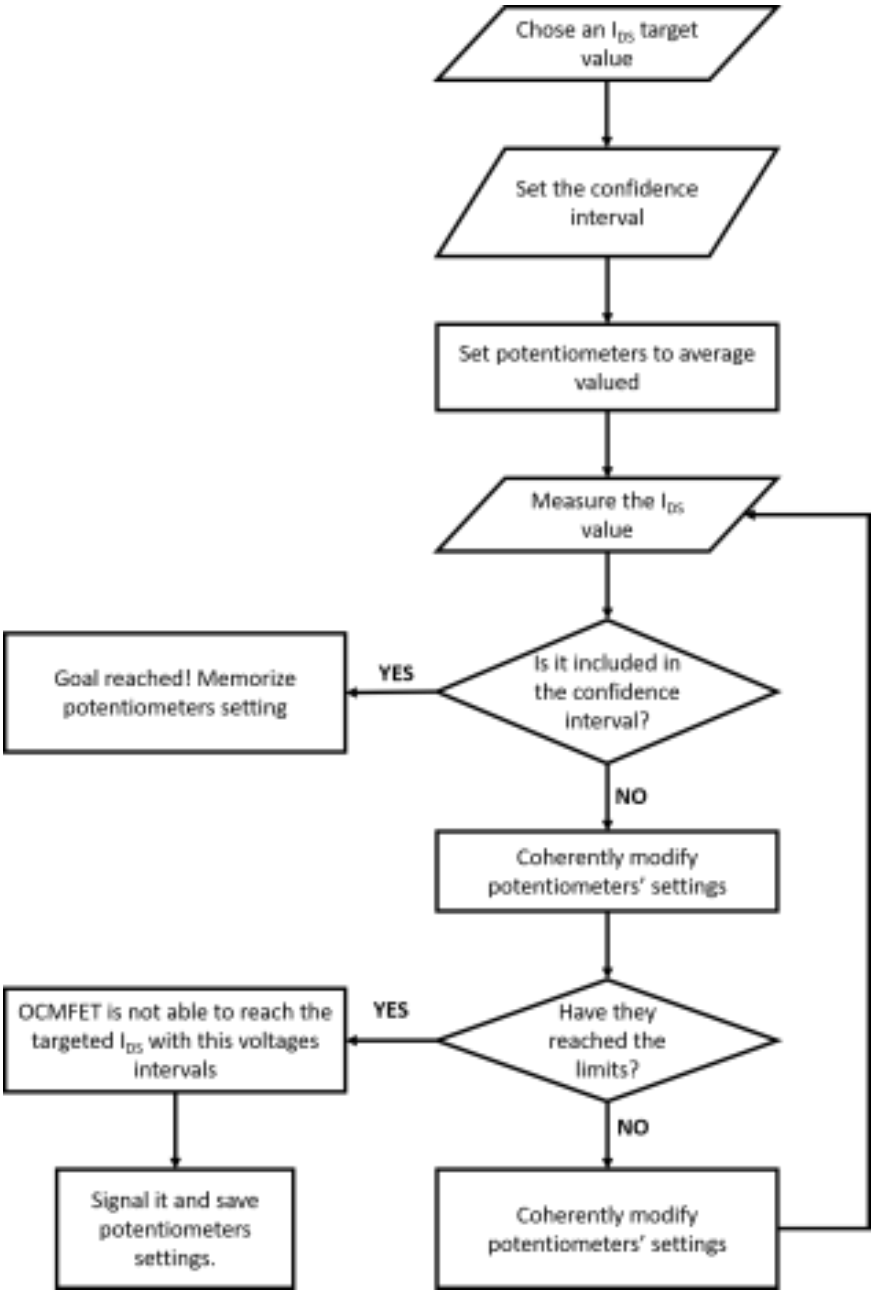

Figure B.6 Flowchart describing the current-driven algorithm.

match the desired output value: i.e. it increases the voltages if the measured current is lower than the targeted one and vice versa. In order to read the direct current, that is not directly suitable from the electronics, on the secondary PCBs has been added a contact that collect the pristine OCMFET's output current, without any pre-processing; this contact is connected to the Arduino board through a wire, thus allowing it to perform the iterative process. In addition, since the output current is negative and the Arduino's analog input pins are not able

to read negative current, a shift of the current through positive values has been implemented. After that, the mean of 10 output current's measurements is calculated, to avoid that the noise superimposed on the signal affects the measurement, and the voltages are changed relating to the mean value. When the requested current value is reached, the code plots the voltages' values and they are saved in a file using another software in a way that, if the same MOA has to been used newly in a time interval short enough to reasonably assure that the semiconductor performances have not changed, all the transistors can be polarized without repeat the process. If, on the other hand, the targeted value has not be reached, the operator is warned and the transistor is operated with the maximum voltages, to reach the highest current possible.

Appendix C

Equivalent electrical model for OCMFET-based metabolic sensor

The equivalent electrical model of the OCMFET-based sensor described in this appendix is based on a previous version, depicted in (Spanu et al., 2017). It has been developed to better understand the functioning of the sensors used during this PhD project, and in particular to try to solve the issues noticed observing the experimental data recorded from the sensor for metabolic activity; these issues (described in chapter 4), consist mainly on an output current shift toward more negative values during the basal phases and are ascribed to the bias stress effect; and on a divergence between the expected trend of the output current variation of the sensor and the measured one. The proposed model allows to separate the effects deriving from the sensing activity, i.e. caused by a charge variation occurring in the nearby of the sensing area, and the phenomenon ascribed to the transistor itself, like the bias stress, thus allowing in principle to remove the undesired effects. In this appendix, after a brief summary of the previous model, the proposed one will be described.

C.1 Previous model

A model for OCMFET-based metabolic sensor was previously published (Spanu et al., 2017) that started from the charge conservation principle applied to the floating gate (already reported in equation 3.1), and considered that $Q = \sigma A$, where σ is the superficial charge density and A the area. Going in more detail, referring to figure C.1 for the identification of the different areas constituting the device, it is possible to obtain:

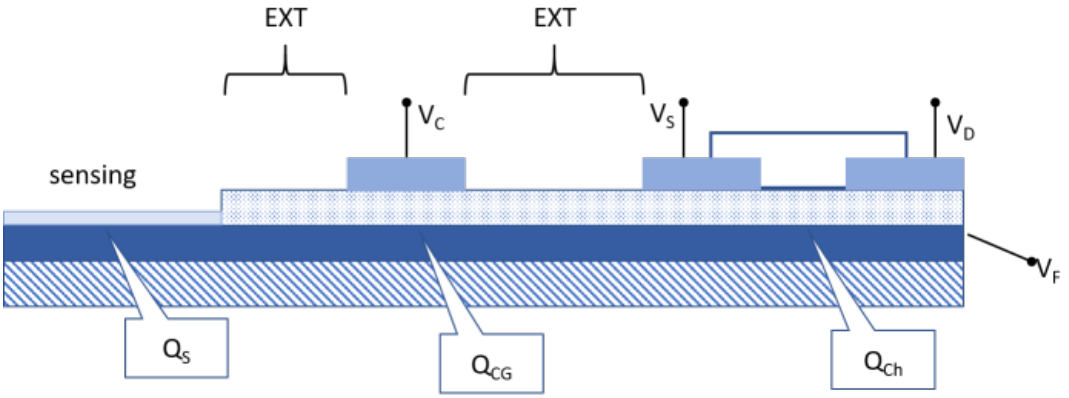

Figure C.1 Sketch of the OCMFET structure; the different areas constituting the device have been highlighted, along with the points where charges are accumulated.

$$\Delta Q_S = \Delta\sigma_S A_S = -(\Delta\sigma_{CG}A_{CG} + \Delta\sigma_{Ch}A_{Ch} + \Delta\sigma_{EXT}A_{EXT}) \tag{C.1}$$

where $\sigma_{CG}A_{CG}$, $\sigma_{Ch}A_{Ch}$, $\sigma_S A_S$ and $\sigma_{EXT}A_{EXT}$ are the amount of charges collected under the control gate, the transistor's channel, the sensing area and the external areas (i.e. the portions of the floating gate that act as interconnections between the considered areas) respectively. From equation C.1 are excluded both the charge variations in the control capacitor and in the elements that do not influence the charge balance such as the external areas, where there is not charge accumulation since no electric field is applied. In addition, are neglected the charges accumulated in the parasitic capacitances, much smaller than the other capacities in the system. This model concludes that the charge variations onto the sensing area cause a change of the charges' amount only under the transistor's area, thus modulating its threshold voltage, as shown in the equation C.2.

$$\Delta Q_S = -\Delta Q_{Ch} \quad \Leftrightarrow \quad \Delta\sigma_S A_S = -\Delta\sigma_{Ch}A_{Ch} \tag{C.2}$$

By applying equation C.2 and considering the OCMFET's working principle, described in section 3.1.1 and summarized in equation 3.3, it is possible to obtain the following equation:

$$\Delta V_{TH} = \Delta V_F = -\frac{\Delta Q_{Ch}}{C_{SUM}} = -\frac{\Delta\sigma_S}{C_{SUM}}A_S \tag{C.3}$$

Where $C_{SUM} = C_{CG} + C_{PARASITIC}$. This equation represents also an equivalent capacitance in which a charge variation ΔQ_S causes a change of the voltage ΔV_F across the capacitor, as shown in figure C.2A.

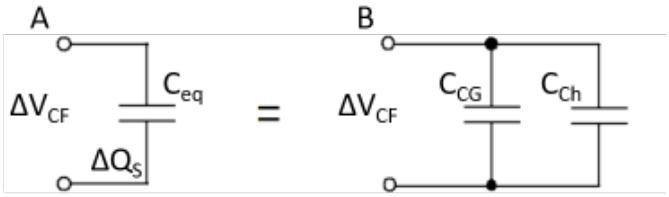

Figure C.2 Floating gate voltage variations for both the previous and the proposed model. The previous model considered only the effect of Q_S on the channel capacitance, so it is described by a single capacitor, like in panel A. The proposed model considered also the contribution of the control gate capacitor, and so it is represented by a parallel of two capacitors, as shows panel B.

During this project, this model has been improved by considering also the contribution of the control capacitor to the system, i.e. the charge variation that occurs in the control capacitor when charges approach the sensing area. In this case, the equivalent circuit became a parallel of two capacitors representing the control gate and the channel, depicted in figure C.2B. Consequently, the equation C.3 became:

$$\Delta V_F = \frac{\sigma_S A_S}{C_{CG} + C_{Ch}} \tag{C.4}$$

In which the parasitic capacitances are considered in the equivalent capacity of the transistor's channel, since it is not numerically calculated.

C.2 Proposed model - mathematical description

In order to mathematically obtain this equation, it is necessary to first model the OCMFET-based metabolic sensor when no stimuli are applied on the sensing area, i.e. to imagine the device in a situation in which no charge variations can occur nearby that space; in this case, the hypothesis is that $Q_S = 0$. Since the OCMFET device can be represented by a series of two capacitors (symbolizing the control gate and the transistor itself) with a plate in common, i.e. the floating gate, as depicted in figure C.3, when $Q_S = 0$ the equations that solve this circuit are:

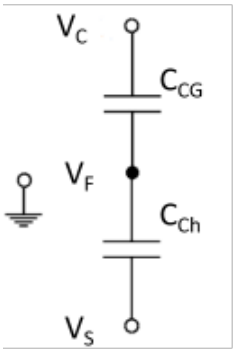

Figure C.3 Electrical model of the OCMFET. The two capacitors representing the control gate and the transistor's channel have a common plate, that is the floating gate.

$$V_C - V_F = \frac{\sigma_{CG} A_{CG}}{C_{CG}} \quad and \quad V_S - V_F = \frac{\sigma_{Ch} A_{Ch}}{C_{Ch}} \tag{C.5}$$

$$(V_C - V_F) - (V_S - V_F) = V_C - V_S \tag{C.6}$$

with the constraint that $\sigma_{CG} A_{CG} = -\sigma_{Ch} A_{Ch}$. From these equations originated those representing the potential difference between the control gate or the source voltages and the floating gate one:

$$V_C - V_{F0} = \frac{V_C - V_S}{1 + C_{CG}/C_{Ch}} \tag{C.7}$$

$$V_{F0} - V_S = \frac{V_C - V_S}{1 + C_{Ch}/C_{CG}} \tag{C.8}$$

Where V_{F0} is the floating gate voltage when no stimuli are applied. Using this model, we obtained the relationships between the applied voltages V_C and V_S and the voltage V_F that varies with the charge in the floating gate surface.

At this point, it is possible to abandon the hypothesis of no external stimuli applied and to start again from the charge conservation principle (equation C.1) in which the term linked to the charge variation in the control capacitor is maintained. This leads to the fact that the equation C.2 in this improved model acquires an additional term linked to the newly considered contribution thus becoming:

$$\Delta Q_S = -(\Delta Q_{Ch} + \Delta Q_{CG}) \quad \Leftrightarrow \quad \Delta\sigma_S A_S = -(\Delta\sigma_{Ch} A_{Ch} + \Delta\sigma_{CG} A_{CG}) \tag{C.9}$$

Assuming that - due to the floating gate hypothesis - the charge variation occurring onto the sensing area in addition to the variations in the amount of charge accumulated beside the control gate and transistor's channel, causes also a variation in the floating gate voltage, we can express these physical quantities as:

$$Q_{CG} = Q_{CG0} + \Delta Q_{CG} \tag{C.10}$$

$$Q_{Ch} = Q_{Ch0} + \Delta Q_{Ch} \tag{C.11}$$

$$V_F = V_{F0} + \Delta V_F \tag{C.12}$$

At this point, remembering equations C.5, C.6, C.8 and C.7 it is possible to obtain the equation from which we started, i.e. equation C.4.

C.2.1 Parameters of the model $I_D(Q_S)$

The present model is based on the hypothesis that the OCMFET is operated in saturation regime during the experiment; so, if V_{DS} is kept constant, the transistor's output current can be described as followed:

$$I_D \approx \frac{K}{2}(V_F - V_S - V_{TH})^2 = \frac{K}{2}(V_{F0} + \Delta V_F - V_S - V_{TH})^2 \tag{C.13}$$

By substituting $(V_{F0} - V_S)$ with the equation C.8 and ΔV_F with the C.4 and by considering that $C_{CG} + C_{Ch} = C_{CG}(1 + C_{Ch}/C_{CG})$, the previous becomes:

$$I_D \approx \frac{K}{2}\left(\frac{V_C - V_S}{1 + (C_{Ch}/C_{CG})} + \frac{Q_S/C_{CG}}{1 + (C_{Ch}/C_{CG})} - V_{TH}\right)^2 \tag{C.14}$$

This expression contains:

- two variables, i.e. the operating voltage $V_{CS} = (V_C - V_S)$ and the charge variation occurred below the sensing area, Q_S;

- two parameters linked to the FET's working principle, i.e. $K = \mu C_{ins}(W/L)$ and the threshold voltage V_{TH};
- two parameters concerning the OCMFET's layout, i.e. the capacitance of the control gate, C_{CG}, and the term containing the ration between the channel and the control gate capacitances, that we called *Capacitors Ratio*, CR and that values $CR = 1 + (C_{Ch}/C_{CG})$.

Where, by definition must be $CR > 1$ and $K > 0$. In addition, it is worth noting that the numerator of the second addend in equation C.14 dimensionally corresponds to a voltage, and therefore can be interpreted as the voltage across the control gate capacitance. It means that a charge variation below the control capacitor induces an output current variation in the same way in which a change in V_{CS} would induce it; indeed, indicating that

$$\Delta V_{CF} = Q_S/C_{CG} \tag{C.15}$$

it is possible to rewrite the I_D expression also by highlighting the indicated parameters:

$$I_D \approx \frac{K}{2}\left(\frac{V_C - V_S}{CR} + \frac{\Delta V_{CF}}{CR} - V_{TH}\right)^2 \tag{C.16}$$

To easily extract these parameters, the previous equation can be linearized as follows:

$$\pm\sqrt{2/K}\sqrt{I_D} = \frac{V_{CS}}{CR} + \frac{\Delta V_{CF}}{CR} - V_{TH} \tag{C.17}$$

where the square root of I_D has, for p-type transistors like our OCMFETs, the negative sign. From this expression we can extrapolate:

$$y = -\sqrt{I_D} \tag{C.18}$$
$$x = V_{CS} \tag{C.19}$$
$$a = \frac{\sqrt{K/2}}{CR} \tag{C.20}$$
$$b = V_{TH}\sqrt{K/2} \tag{C.21}$$

Where the numerical values of a and b can be easily obtained from the measurements of I_D - V_C (such as the output characteristics) when V_D is kept constant and when no stimuli are applied. From the expression C.17 it is possible to extract the expression of ΔV_{CF},

$$\Delta V_{CF} = -\frac{\sqrt{I_D}}{a} - V_{CS} + \frac{b}{a} \tag{C.22}$$

C.2.2 Bias stress

The bias stress is a phenomenon that occurs in field effect transistors when a gate-source voltage is applied to create the channel and its effect is to change the transistor's threshold voltage in a specific direction. In particular, a p-type transistor polarized with a negative V_{CS} shows a threshold voltage shift towards more negative values, while a positive V_{CS} applied to a n-type FET provokes a positive threshold voltage shift. The bias stress is ascribed to the trapping of charges into localized electronic states, and it increases with time (the longer the gate voltage is applied, the more carriers are trapped and hence the larger is the threshold voltage shift) (Zschieschang et al., 2009). Since this effect of threshold voltage shift concerns only the transistor operating principle and thus it is independent from the sensor's activity, but in turn it can hide the output current changes caused by the charge variation near the sensing area, it can be appropriate to remove it from the recorded signal.

To this end, it has been made the assumption that during the basal phase of each recording the system is at equilibrium (no charge variation takes place on the sensing area) as its conditions have remained unchanged for a sufficiently long time, so that the threshold voltage variations occurring at this stage can be principally attributed to the bias stress. Exploiting the presented model, it is possible to obtain the time dependence of V_{TH} considering the equation C.22 when $\Delta V_{CF} = 0$, and remembering that (from the C.20 and C.21) it is $b/a = V_{TH}CR$, where CR is a constant value

$$\frac{b_m(t)}{a} = V_{CS} + \frac{\sqrt{I_D(t)}}{a} \tag{C.23}$$

this equation allows to extract the measured value of b/a, called b_m/a, in each instant of time from the recorded output current. According to (Zschieschang et al., 2009), the threshold voltage shift for an organic thin film transistor over time under constant gate-source and drain-source voltages is typically described by a stretched exponential function:

$$\Delta V_{TH}(t) = [V_{TH}(\infty) - V_{TH}(0)][1 - \exp(-(t/\tau)\beta)] \tag{C.24}$$

where $V_{TH}(0)$ is the threshold voltage in the initial state, $V_{TH}(\infty)$ is the threshold voltage when equilibrium has been reached; τ is the time constant and β is the stretching parameter $(0 < \beta \leq 1)$ that indicates the degree of diversion from the exponential function: if $\beta \approx 1$, the expression is similar to exponential, if it is near zero implies a broader distribution of time constants. This equation can be linearized through a log-lin transformation and then (exploiting a linear regression) it is possible to extrapolate the best parameters' values to fit the stretched exponential to the basal phase of the measured threshold voltage trend of metabolic activity signals, thus modelling the bias stress of the device. The so derived curve of the threshold voltage (since CR is a constant value determined by the OCMFET layout) can be then applied to the expression C.22 to correct the trend of ΔV_{CF}, thus removing the effect of the bias stress.

References

Akamatu, H. and Inokuchi, H. (1950). On the electrical conductivity of violanthrone, iso-violanthrone, and pyranthrone. *The Journal of Chemical Physics*, 18(6):810–811.

Barbaro, M., Bonfiglio, A., and Raffo, L. (2005). A charge-modulated fet for detection of biomolecular processes: conception, modeling, and simulation. *IEEE Transactions on Electron Devices*, 53(1):158–166.

Bardeen, J. and Brattain, W. H. (1948). The transistor, a semi-conductor triode. *Physical Review*, 74(2):230.

Bartic, C., Campitelli, A., and Borghs, S. (2003). Field-effect detection of chemical species with hybrid organic/inorganic transistors. *Applied Physics Letters*, 82(3):475–477.

Bartic, C., Palan, B., Campitelli, A., and Borghs, G. (2002). Monitoring ph with organic-based field-effect transistors. *Sensors and Actuators B: Chemical*, 83(1-3):115–122.

Baumann, W. H., Lehmann, M., Schwinde, A., Ehret, R., Brischwein, M., and Wolf, B. (1999). Microelectronic sensor system for microphysiological application on living cells. *Sensors and Actuators B: Chemical*, 55(1):77–89.

Benfenati, V., Toffanin, S., Bonetti, S., Turatti, G., Pistone, A., Chiappalone, M., ..., and Muccini, M. (2013). Benfenati, valentina, et al. "a transparent organic transistor structure for bidirectional stimulation and recording of primary neurons. *Nature materials*, 12(7):672–680.

Bergveld, P. (1970). Development of an ion-sensitive solid-state device for neurophysiological measurements. *IEEE Transactions on Biomedical Engineering.*, 1:70–71.

Bergveld, P. (1972). Development, operation, and application of the ion-sensitive field-effect transistor as a tool for electrophysiology. *IEEE Transactions on Biomedical Engineering.*, 5:342–351.

Bergveld, P., Wiersma, J., and Meertens, H. (1976). Extracellular potential recordings by means of a field effect transistor without gate metal, called osfet. *IEEE Transactions on Biomedical Engineering*, 2:136–144.

Bernstein, J. (1868). Ueber den zeitlichen verlauf der negativen schwankung des nervenstroms. *Archiv für die gesamte Physiologie des Menschen und der Tiere*, 1(1):173–207.

Bernstein, J. (1912). *Bernstein, Julius. "Die Lehre von den elektrischen Vorgängen im Organismus auf moderner Grundlage dargestellt.* Braunschweig: Vieweg & Sohn, Berlin.

Bonfiglio, A., Manunza, I. C., A. Cambarau, W., and Barbaro, M. (International Society for Optics and Photonics, 2007). Organic field effect based sensors for body parameters monitoring. *Organic-based Chemical and Biological Sensors.*, 6659:665904.

Borrachero-Conejo, A. I., Saracino, E., Natali, M., Prescimone, F., Karges, S., Bonetti, S., ..., and Benfenati, V. (2019). Electrical stimulation by an organic transistor architecture induces calcium signaling in nonexcitable brain cells. *Advanced healthcare materials*, 8(3):1801139.

Bove, M., Grattarola, M., Martinoia, S., and Verreschi, G. (1995). Interfacing cultured neurons to planar substrate microelectrodes: characterization of the neuron-to-microelectrode junction. *Bioelectrochemistry and bioenergetics*, 38(2):255–265.

Braendlein, M., Pappa, A. M., Ferro, M., Lopresti, A., Acquaviva, C., Mamessier, E., ..., and Owens, R. M. (2017). Lactate detection in tumor cell cultures using organic transistor circuits. *Advanced Materials*, 29(13):1605744.

Buth, F., Kumar, D., Stutzmann, M., and Garrido, J. A. (2011). Electrolyte-gated organic field-effect transistors for sensing applications. *Applied Physics Letters*, 98(15):76.

Caboni, A., Orgiu, E., Barbaro, M., and Bonfiglio, A. (2009). Flexible organic thin-film transistors for ph monitoring. *IEEE Sensors Journal*, 9(12):1963–1970.

Cajavilca, C., Varon, J., and Sternbach, G. L. (2009). Luigi galvani and the foundations of electrophysiology. *Resuscitation*, 80(2):159–162.

Chen, L., Fu, Y., Wang, N., Yang, A., Li, Y., Wu, J., ..., and Yan, F. (2018). Organic electrochemical transistors for the detection of cell surface glycans. *ACS applied materials & interfaces*, 10(22):18470–18477.

Cohen, A., Spira, M. E., Yitshaik, S., Borghs, G., Shwartzglass, O., and Shappir, J. (2004). Depletion type floating gate p-channel mos transistor for recording action potentials generated by cultured neurons. *Biosensors and Bioelectronics*, 19(12):1703–1709.

Cole, K. (1949). Dynamic electrical characteristics of the squid axon membrane. *Arch Sci Physiol*, 3:253–258.

Cosseddu, P., Lai, S., Barbaro, M., and Bonfiglio, A. (2012). Ultra-low voltage, organic thin film transistors fabricated on plastic substrates by a highly reproducible process. *Applied Physics Letters*, 100(9):61.

Cramer, T., Chelli, B., Murgia, M., Barbalinardo, M., Bystrenova, E., de Leeuw, D. M., and Biscarini, F. (2013). Organic ultra-thin film transistors with a liquid gate for extracellular stimulation and recording of electric activity of stem cell-derived neuronal networks. *Physical Chemistry Chemical Physics*, 15(11):3897–3905.

Curto, V. F., Ferro, M. P., Mariani, F., Scavetta, E., and Owens, R. M. (2018). A planar impedance sensor for 3d spheroids. *Lab on a Chip*, 18(6):933–943.

Curto, V. F., Marchiori, B., Hama, A., Pappa, A. M., Ferro, M. P., Braendlein, M., ..., and Owens, R. M. (2017). Organic transistor platform with integrated microfluidics for in-line multi-parametric in vitro cell monitoring. *Microsystems & nanoengineering*, 3(1):1–12.

Danielli, J. F. and Davson, H. (1935). A contribution to the theory of permeability of thin films. *Journal of cellular and comparative physiology*, 5(4):495–508.

Decataldo, F., Barbalinardo, M., Gentili, D., Tessarolo, M., Calienni, M., Cavallini, M., and Fraboni, B. (2020). Organic electrochemical transistors for real-time monitoring of in vitro silver nanoparticle toxicity. *Advanced Biosystems*, 4(1):1900204.

Demelas, M., Lai, S., Spanu, A., Martinoia, S., Cosseddu, P., Barbaro, M., and Bonfiglio, A. (2013). Charge sensing by organic charge-modulated field effect transistors: application to the detection of bio-related effects. *Journal of Materials Chemistry B*, 1(31):3811–3819.

Desbief, S., di Lauro, M. znd Casalini, S., Guerin, D., Tortorella, S., Barbalinardo, M., ..., and Vuillaume, D. (2016). Electrolyte-gated organic synapse transistor interfaced with neurons. *Organic Electronics*, 38:21–28.

Didier, P., Lobato-Dauzier, N., Clément, N., Genot, A. J., Sasaki, Y., Leclerc, E., ..., and Minami, T. (2020). Microfluidic system with extended-gate-type organic transistor for real-time glucose monitoring. *ChemElectroChem*, 7(6):1801139.

Du Bois-Reymond, E. (1884). *Untersuchungen über thierische Elektricität. vol.2*. G. Reimer, Berlin.

Ecken, H.and Ingebrandt, S., Krause, M., Richter, D.and Hara, M., and Offenhäusser, A. (2003). 64-channel extended gate electrode arrays for extracellular signal recording. *Electrochimica acta*, 48(20-22):3355–3362.

Forrest, S. R. (2020). *Organic Electronics: Foundations to Applications.* Oxford University Press, USA.

Fromherz, P. (2008). Joining microelectronics and microionics: Nerve cells and brain tissue on semiconductor chips. *Solid-State Electronics*, 52(9):1364–1373.

Fromherz, P., Offenhausser, A.and Vetter, T., and Weis, J. (1991). A neuron-silicon junction: a retzius cell of the leech on an insulated-gate field-effect transistor. *Science*, 252(5010):1290–1293.

Fromherz, P. and Stett, A. (1995). Silicon-neuron junction: capacitive stimulation of an individual neuron on a silicon chip. *Physical Review Letters*, 75(8):1670.

Galvani, L. (1791). De viribus electricitatis in motu musculari. commentarius. *De Bonoiensi Scientiarum et Artium Intituo atque Academie Commentarii*, 7:363–418.

Gorter, E. and Grendel, F. (1925). On bimolecular layers of lipids on the chromocytes of the blood. *The Journal of experimental medicine*, 41(4):439–443.

Gross, G. W., Rieske, E., Kreutzberg, G. W., and Meyer, A. (1977). A new fixed-array multi-microelectrode system designed for long-term monitoring of extracellular single unit neuronal activity in vitro. *Neuroscience letters*, 6(2-3):101–105.

Gu, X., Yao, C., Liu, Y., and Hsing, I. M. (2016). 16-channel organic electrochemical transistor array for in vitro conduction mapping of cardiac action potential. *Advanced Healthcare Materials*, 5(18):2345–2351.

Gu, X., Yeung, S. Y., Chadda, A., Poon, E. N. Y., Boheler, K. R., and Hsing, I. M. (2019). Organic electrochemical transistor arrays for in vitro electrophysiology monitoring of 2d and 3d cardiac tissues. *Advanced Biosystems*, 3(2):1800248.

Hamill, O. P., Marty, A., Neher, E. Sakmann, B., and Sigworth, F. J. (1981). Improved patch-clamp techniques for high-resolution current recording from cells and cell-free membrane patches. *Pflügers Archiv*, 391(2):85–100.

Helmholtz, H. (1850). Note sur la vitesse de propagation de l'agent nerveux dans les nerfs rachidiens. *C R Acad Sci*, (30):204–206.

Helmholtz, H. (1852). Messungen über fortpflanzungsgeschwindigkeit der reizung in den nerven–zweite reihe. *Arch Anat Physiol Wiss Med*, page 199–216.

Hempel, F., Law, J. K. Y., Nguyen, T. C., Munief, W., Lu, X., Pachauri, V., ..., and Ingebrandt, S. (2017). Pedot: Pss organic electrochemical transistor arrays for extracellular electrophysiological sensing of cardiac cells. *Biosensors and Bioelectronics*, 93:132–138.

Hodgkin, A. L. and Huxley, A. F. (1952a). Currents carried by sodium and potassium ions through the membrane of the giant axon of loligo. *The Journal of physiology*, 116(4):449.

Hodgkin, A. L. and Huxley, A. F. (1952b). A quantitative description of membrane current and its application to conduction and excitation in nerve. *The Journal of physiology*, 117(4):500.

Hodgkin, A. L., Huxley, A. F., and Katz, B. (1952). Measurement of current-voltage relations in the membrane of the giant axon of loligo. *The Journal of physiology*, 116(4):424.

Hutzler, M. and Fromherz, P. (2004). Silicon chip with capacitors and transistors for interfacing organotypic brain slice of rat hippocampus. *European Journal of Neuroscience*, 19(8):2231–2238.

Jimison, L. H., Tria, S. A., Khodagholy, D., Gurfinkel, M., Lanzarini, E., Hama, A., ..., and Owens, R. M. (2012). Measurement of barrier tissue integrity with an organic electrochemical transistor. *Advanced materials*, 24(44):5919–5923.

Johnson, B., Peace, S. T., Cleland, T. A., and Molnar, A. (2013). A 50µm pitch, 1120-channel, 20khz frame rate microelectrode array for slice recording. *2013 IEEE Biomedical Circuits and Systems Conference (BioCAS). IEEE*, pages 109–112.

Kang, J.-W. and Cho, W.-J. (2019). Achieving enhanced ph sensitivity using capacitive coupling in extended gate fet sensors with various high-k sensing films. *Solid-State Electronics*, 152:29–32.

Kaul, R. A., Syed, N. I., and Fromherz, P. (2004). Neuron-semiconductor chip with chemical synapse between identified neurons. *Physical Review Letters*, 92(3):038102.

Kazutoshi, T. and Yamanaka, S. (2006). Induction of pluripotent stem cells from mouse embryonic and adult fibroblast cultures by defined factors. *Cell*, 126(4):663–676.

Kergoat, L., Piro, B., Berggren, M., Horowitz, G., and Pham, M. C. (2012). Advances in organic transistor-based biosensors: from organic electrochemical transistors to electrolyte-gated organic field-effect transistors. *Analytical and bioanalytical chemistry*, 402(5):1813–1826.

Krause, M., Ingebrandt, S., Richter, D., Denyer, M., Scholl, M., Sprössler, C., and Offenhäusser, A. (2000). Extended gate electrode arrays for extracellular signal recordings. *Sensors and Actuators B: Chemical*, 70(1-3):101–107.

Kuang, S. Y., Wang, Z., Huang, T., Wei, L., Xi, T., Kindy, M., and Gao, B. Z. (2015). Prolonging life in chick forebrain-neuron culture and acquiring spontaneous spiking activity on a microelectrode array. *Biotechnology letters*, 37(3):499–509.

Kyndiah, A., Leonardi, F., Tarantino, C., Cramer, T., Millan-Solsona, R., Garreta, E., ..., and Gomila, G. (2020). Bioelectronic recordings of cardiomyocytes with accumulation mode electrolyte gated organic field effect transistors. *Biosensors and Bioelectronics*, 150:111844.

Lai, S., Cosseddu, P., Gazzadi, G. C., Barbaro, M., and Bonfiglio, A. (2013). Towards high frequency performances of ultra-low voltage otfts: Combining self-alignment and hybrid, nanosized dielectrics. *Organic Electronics*, 14(3):754–761.

Law, J. K. Y., Yeung, C. K., Hofmann, B., Ingebrandt, S., Rudd, J. A., Offenhäusser, A., and Chan, M. (2009). The use of microelectrode array (mea) to study the protective effects of potassium channel openers on metabolically compromised hl-1 cardiomyocytes. *Physiological measurement*, 30(2):155–167.

Lehmann, M.and Baumann, W., Brischwein, M.and Gahle, H. J., Freund, I.and Ehret, R., ..., and Wolf, B. (2001). Simultaneous measurement of cellular respiration and acidification with a single cmos isfet. *Biosensors and Bioelectronics*, 16(3):195–203.

Lehmann, M.and Baumann, W., Brischwein, M., Ehret, R., Kraus, M., Schwinde, A., ..., and Wolf, B. (2000). Non-invasive measurement of cell membrane associated proton gradients by ion-sensitive field effect transistor arrays for microphysiological and bioelectronical applications. *Biosensors and Bioelectronics*, 15(3-4):117–124.

Liang, Y., Brings, F., Maybeck, V., Ingebrandt, S., Wolfrum, B., Pich, A., ..., and Mayer, D. (2019). Tuning channel architecture of interdigitated organic electrochemical transistors for recording the action potentials of electrogenic cells. *Advanced functional materials*, 29(29):1902085.

Liang, Y., Ernst, M., Brings, F., Kireev, D., Maybeck, V., Offenhäusser, A., and Mayer, D. (2018). High performance flexible organic electrochemical transistors for monitoring cardiac action potential. *Advanced healthcare materials*, 7(19):1800304.

Ling, G. and Gerard, R. (1949). The normal membrane potential of frog sartorius fibers. *Journal of cellular and comparative physiology*, 34(3):383–396.

Lorenzelli, L., Margesin, B., Martinoia, S., Tedesco, M. T., and Valle, M. (2003). Bio-electrochemical signal monitoring of in-vitro cultured cells by means of an automated microsystem based on solid state sensor-array. *Biosensors and Bioelectronics*, 18(5-6):621–626.

Marmont, G. (1949). Studies on the axon membrane. i. a new method. *Journal of cellular and comparative physiology*, 34(3):351–382.

Martinoia, S., Rosso, N., Grattarola, M., Lorenzelli, L., and Margesin, B.and Zen, M. (2001). Development of isfet array-based microsystems for bioelectrochemical measurements of cell populations. *Biosensors and Bioelectronics*, 16(9-12):1043–1050.

Matteucci, C. and Savi, P. (1844). *Traité des phénomènes électro-physiologiques des animaux.* Fortin, Masson.

Meyburg, S., Goryll, M., Moers, J., Ingebrandt, S., Böcker-Meffert, S., Lüth, H., and Offenhäusser, A. (2006). N-channel field-effect transistors with floating gates for extracellular recordings. *Biosensors and bioelectronics*, 21(7):1037–1044.

Minamiki, T., Minami, T., Kurita, R., Niwa, O., Wakida, S. I., Fukuda, K., Kumaki, D., and Tokito, S. (2014). Accurate and reproducible detection of proteins in water using an extended-gate type organic transistor biosensor. *Applied Physics Letters*, 104(24):243703.

Napoli, C., Lai, S., Giannetti, A., Tombelli, S., Baldini, F., Barbaro, M., and Bonfiglio, A. (2018). Electronic detection of dna hybridization by coupling organic field-effect transistor-based sensors and hairpin-shaped probes. *Sensors*, 18(4):990.

Neher, E. and Lux, H. D. (1969). Voltage clamp on helix pomatia neuronal membrane; current measurement over a limited area of the soma surface. *Pflügers Archiv*, 311(3):272–277.

Neher, E. and Sakmann, B. (1976). Single-channel currents recorded from membrane of denervated frog muscle fibres. *Nature*, 260(5554):799–802.

Nobili, L. (1828). Comparaison entre les deux galvanometres les plus sensibles, la grenouille et le moltiplicateur a deux aiguilles, suivie de quelques resultats noveaux. *Ann Chim Phys*, 38:225–245.

Obien, M. E. J., , and Frey, U. (2019). *In Vitro Neuronal Networks: Large-Scale, High-Resolution Microelectrode Arrays for Interrogation of Neurons and Networks.*, pages 83–123. Springer, Cham.

Obien, M. E. J., Deligkaris, K., Bullmann, T., Bakkum, D. J., and Frey, U. (2015). Revealing neuronal function through microelectrode array recordings. *Frontiers in neuroscience*, 8:423.

Odawara, A., Matsuda, N., Ishibashi, Y., Yokoi, R., and Suzuki, I. (2018). Toxicological evaluation of convulsant and anticonvulsant drugs in human induced pluripotent stem cell-derived cortical neuronal networks using an mea system. *Scientific reports*, 8(1):1–11.

Offenhäusser, A., Sprössler, C., Matsuzawa, M., and Knoll, W. (1997). Field-effect transistor array for monitoring electrical activity from mammalian neurons in culture. *Biosensors and Bioelectronics*, 12(8):819–826.

Overton, C. E. (1899). Über die allgemeinen osmotischen eigenschaften der zelle, ihre vermutlichen ursachen und ihre bedeutung für die physiologie. *Vierteljahrsschrift der Naturforschenden Gesellschaft in Zürich*, 44:88–135.

Overton, C. E. (1902). Betrage zur allgemaine muskel- und nervenphysiologie. ii uber die unentbehrlichkeit von natrium- (oder litium-) ionen fur den contractionsact des muskels. *Pflüger's Arch. ges. Physiol.*, 92:346–380.

Owicki, John C.an d Parce, J. W. (1992). Biosensors based on the energy metabolism of living cells: the physical chemistry and cell biology of extracellular acidification. *Biosensors and Bioelectronics*, 7(4):255–272.

Parkula, V., Berto, M., Diacci, C., Patrahau, B., Di Lauro, M., Kovtun, A., ..., and Biscarini, F. (2020). Harnessing selectivity and sensitivity in electronic biosensing: a novel lab-on-chip multigate organic transistor. *Analytical Chemistry*, 92(13):9330–9337.

Piccolino, M. (2006). Luigi galvani's path to animal electricity. *Comptes rendus biologies*, 329(5-6):303–318.

Pimashkin, A., Gladkov, A., Mukhina, I., and Kazantsev, V. (2013). Adaptive enhancement of learning protocol in hippocampal cultured networks grown on multielectrode arrays. *Frontiers in neural circuits*, 7:87.

Pine, J. (1980). Recording action potentials from cultured neurons with extracellular microcircuit electrodes. *Journal of neuroscience methods*, 2(1):19–31.

Piro, B., Mattana, G., and Reisberg, S. (2018). Transistors for chemical monitoring of living cells. *Biosensors*, 8(3):65.

Poghossian, A., Ingebrandt, S., Offenhäusser, A., and Schöning, M. J. (2009). Field-effect devices for detecting cellular signals. *Seminars in cell & developmental biology*, 20(1):41–48.

Ricci, S., Casalini, S., Parkula, V., Selvaraj, M., Saygin, G. D., Greco, P., ..., and Mas-Torrent, M. (2020). Label-free immunodetection of α-synuclein by using a microfluidics coplanar electrolyte-gated organic field-effect transistor. *Biosensors and Bioelectronics*, 167:112433.

Ritjareonwattu, S., Yun, Y. qnd Pearson, C., and Petty, M. C. (2010). Enhanced sensitivity of an organic field-effect transistor ph sensor using a fatty acid langmuir–blodgett film. *Organic Electronics*, 11(11):1792–1795.

Romeo, A., Tarabella, G., D'Angelo, P., Caffarra, C., Cretella, D., Alfieri, R., ..., and Iannotta, S. (2015). Drug-induced cellular death dynamics monitored by a highly sensitive organic electrochemical system. *Biosensors and Bioelectronics*, 68:791–797.

Sakata, T. (2019). Biologically coupled gate field-effect transistors meet in vitro diagnostics. *ACS omega*, 4(7):11852–11862.

Sallen, R. P. and Key, E. L. (1955). A practical method of designing rc active filters. *IRE Transactions on Circuit Theory*, 2(1):74–85.

Salyk, O., Víteček, J., Omasta, L., Šafaříková, E., Stříteský, S., Vala, M., and Weiter, M. (2017). Organic electrochemical transistor microplate for real-time cell culture monitoring. *Applied Sciences*, 7(10):998.

Schmoltner, K., Kofler, J., Klug, A., and List-Kratochvil, E. J. W. (2013). Electrolyte-gated organic field-effect transistors for sensing in aqueous media. *Proc. SPIE on Organic Field-Effect Transistors XII; and Organic Semiconductors in Sensors and Bioelectronics VI*, 8831, 88311N-1.

Schöning, M. J. and Poghossian, A. (2006). Bio feds (field-effect devices): state-of-the-art and new directions. *An International Journal Devoted to Fundamental and Practical Aspects of Electroanalysis*, 18(19-20):1893–1900.

Sekitani, T., Zschieschang, U., Klauk, H., and Someya, T. (2010). Flexible organic transistors and circuits with extreme bending stability. *Nature materials*, 9(12):1015–1022.

Seo, J., Song, M., Jeong, J., Nam, S., Heo, I., Park, S. Y., ..., and Kim, Y. (2016). Broadband ph-sensing organic transistors with polymeric sensing layers featuring liquid crystal microdomains encapsulated by di-block copolymer chains. *ACS Applied Materials & Interfaces*, 8(36):23862–23867.

Shirakawa, H., Louis, E. J., MacDiarmid, A. G., Chiang, C. K., and Heeger, A. J. (1977). Synthesis of electrically conducting organic polymers: halogen derivatives of polyacetylene,$(ch)_x$. *Journal of the Chemical Society, Chemical Communications*, (16):578–580.

Sigworth, F. J. and Neher, E. (1980). Single na+ channel currents observed in cultured rat muscle cells. *Nature*, 287(5781):447–449.

Someya, T., Dodabalapur, A., Gelperin, A., Katz, H. E., and Bao, Z. (2002). Integration and response of organic electronics with aqueous microfluidics. *Langmuir*, 18(13):5299–5302.

Spanu, A. (2016). *Organic transistor devices for in vitro electrophysiological applications.* Springer.

Spanu, A., Lai, S., Cosseddu, P., Bonfiglio, A., Tedesco, M., and Martinoia, S. (2013). Organic fet device as a novel sensor for cell bioelectrical and metabolic activity recordings. *6th International IEEE/EMBS Conference on Neural Engineering (NER)*, pages 937–940.

Spanu, A., Lai, S., Cosseddu, P., Tedesco, M., Martinoia, S., and Bonfiglio, A. (2015a). An organic transistor-based system for reference-less electrophysiological monitoring of excitable cells. *Scientific reports*, 5:8807.

Spanu, A., Pinna, L., Viola, F., Seminara, L., Valle, M., Bonfiglio, A., and Cosseddu, P. (2016). A high-sensitivity tactile sensor based on piezoelectric polymer pvdf coupled to an ultra-low voltage organic transistor. *Organic Electronics*, 36:57–60.

Spanu, A., Tedesco, M., Martinoia, S., Lai, S., Cosseddu, P., and Bonfiglio, A. (2015b). Bioelectrical and metabolic activity recordings by means of organic field effect transistors. *2015 XVIII AISEM Annual Conference*, pages 1–3.

Spanu, A., Tedesco, M. T., Martines, L., Martinoia, S., and Bonfiglio, A. (2018). An organic neurophysiological tool for neuronal metabolic activity monitoring. *APL bioengineering*, 2(4):046105.

Spanu, A., Viola, F., Lai, S., Cosseddu, P., Ricci, P. C., and Bonfiglio, A. (2017). A reference-less ph sensor based on an organic field effect transistor with tunable sensitivity. *Organic Electronics*, 48:188–193.

Strakosas, X., Huerta, M., Donahue, M. J., Hama, A., Pappa, A. M., Ferro, M., ..., and Owens, R. M. (2017). Catalytically enhanced organic transistors for in vitro toxicology monitoring through hydrogel entrapment of enzymes. *Journal of Applied Polymer Science*, 134(7):44483.

Surya, S. G., Raval, H. N., Ahmad, R., Sonar, P., Salama, K. N., and Rao, V. R. (2019). Organic field effect transistors (ofets) in environmental sensing and health monitoring: A review. *TrAC Trends in Analytical Chemistry*, 111:27–36.

Tang, C. W. (1986). Two-layer organic photovoltaic cell. *Applied physics letters*, 48(2):183–185.

Tang, C. W. and VanSlyke, S. A. (1987). Organic electroluminescent diodes. *Applied physics letters*, 51(12):913–915.

Thomas Jr, C. A., Springer, P. A., Loeb, G. E., Berwald-Netter, Y., and Okun, L. M. (1972). A miniature microelectrode array to monitor the bioelectric activity of cultured cells. *Experimental cell research*, 74(1):61–66.

Tixier-Mita, A., Ihida, S., Ségard, B. D., Cathcart, G. A., Takahashi, T., Fujita, H., and Toshiyoshi, H. (2016). Review on thin-film transistor technology, its applications, and possible new applications to biological cells. *Japanese Journal of Applied Physics*, 55(4S):04EA08.

Trantidou, T., Prodromakis, T., and Toumazou, C. (2012). Oxygen plasma induced hydrophilicity of parylene-c thin films. *Applied surface science*, 261:43–51.

Tsai, D., Sawyer, D., Bradd, A., Yuste, R., and Shepard, K. L. (2017). A very large-scale microelectrode array for cellular-resolution electrophysiology. *Nature Communications*, 8(1):1–11.

Tsumura, A., Koezuka, H., and Ando, T. J. A. P. L. (1986). Macromolecular electronic device: Field-effect transistor with a polythiophene thin film. *Applied physics letters*, 49(18):1210–1212.

Vassanelli, S. and Fromherz, P. (1999). Transistor probes local potassium conductances in the adhesion region of cultured rat hippocampal neurons. *Journal of Neuroscience*, 19(16):6767–6773.

Verkhratsky, A., Krishtal, O. A., and H., P. O. (2006). From galvani to patch clamp: the development of electrophysiology. *Pflügers Archiv*, 453(3):233–247.

Verkhratsky, A. and Parpura, V. (2014). *Patch-clamp methods and protocols. Chapter1: History of electrophysiology and the patch clamp. (pp. 1-19)*. Humana Press, New York.

Viola, F. A., Spanu, A., Ricci, P. C., Bonfiglio, A., and Cosseddu, P. (2018). Ultrathin, flexible and multimodal tactile sensors based on organic field-effect transistors. *Scientific reports*, 8(1):1–8.

Weimer, P. K. (1962). The tft a new thin-film transistor. *Proceedings of the IRE*, 50(6):1462–1469.

Wells, S. P., Waddell, H. M., Sim, C. B., Lim, S. Y., Bernasochi, G. B., Pavlovic, D., Kirchhof, P., Porrello, E., Delbridge, L., and Bell, J. (2019). Cardiomyocyte functional screening: interrogating comparative electrophysiology of high-throughput model cell systems. *American Journal of Physiology-Cell Physiology*, 317(6):C1256–C1267.

Wen, Y. and Xu, J. (2017). Scientific importance of water-processable pedot–pss and preparation, challenge and new application in sensors of its film electrode: A review. *Journal of Polymer Science Part A: Polymer Chemistry*, 55(7):1121–1150.

White, H. S., Kittlesen, G. P., and Wrighton, M. S. (1984). Chemical derivatization of an array of three gold microelectrodes with polypyrrole: fabrication of a molecule-based transistor. *Journal of the American Chemical Society*, 106(18):5375–5377.

Yao, C., Li, Q., Guo, J., Yan, F., and Hsing, I. M. (2015). Rigid and flexible organic electrochemical transistor arrays for monitoring action potentials from electrogenic cells. *Advanced healthcare materials*, 4(4):528–533.

Yeung, S. Y., Gu, X., Tsang, C. M., Tsao, S. W. G., and Hsing, I. M. (2019). Organic electrochemical transistor array for monitoring barrier integrity of epithelial cells invaded by nasopharyngeal carcinoma. *Sensors and Actuators B: Chemical*, 297:126761.

Zhang, Y., Li, J., Li, R., Sbircea, D. T., Giovannitti, A., Xu, J., ..., and Zhao, N. (2017). Liquid–solid dual-gate organic transistors with tunable threshold voltage for cell sensing. *ACS applied materials & interfaces*, 9(44):38687–38694.

Zschieschang, U., Weitz, R. T., Kern, K., and Klauk, H. (2009). Bias stress effect in low-voltage organic thin-film transistors. *Applied Physics A*, 95(1):139–145.

Zwartsen, A., de Korte, T., Nacken, P., de Lange, D. W., Westerink, R. H., and Hondebrink, L. (2019). Cardiotoxicity screening of illicit drugs and new psychoactive substances (nps) in human ipsc-derived cardiomyocytes using microelectrode array (mea) recordings. *Journal of molecular and cellular cardiology*, 136:102–112.